

NASA Technical Paper 1643

**Use of Nose Cap and Fuselage
Pressure Orifices for Determination
of Air Data for Space Shuttle
Orbiter Below Supersonic Speeds**

Terry J. Larson and Paul M. Siemers III

SEPTEMBER 1980

NASA

NASA Technical Paper 1643

Use of Nose Cap and Fuselage
Pressure Orifices for Determination
of Air Data for Space Shuttle
Orbiter Below Supersonic Speeds

Terry J. Larson
*Dryden Flight Research Center
Edwards, California*

Paul M. Siemers III
*Langley Research Center
Hampton, Virginia*



National Aeronautics
and Space Administration

**Scientific and Technical
Information Branch**

1980

USE OF NOSE CAP AND FUSELAGE PRESSURE
ORIFICES FOR DETERMINATION OF AIR DATA
FOR SPACE SHUTTLE ORBITER BELOW SUPERSONIC SPEEDS

Terry J. Larson
Dryden Flight Research Center

and

Paul M. Siemers III
Langley Research Center

INTRODUCTION

A shuttle entry air data system (SEADS) is being developed to support proposed orbiter experiments at supersonic and hypersonic speeds (refs. 1 and 2). The system consists of an array of 14 flush pressure orifices that is installed on the orbiter nose cap and is designed to permit the accurate determination of stagnation pressure, angle of attack, angle of sideslip, and other air data quantities at those speeds. Another air data system, which uses two probes that are mounted on the sides of the fuselage and deployed during entry at an altitude of about 30 kilometers, is used at Mach numbers of 3 and below. This system, which is designed for actual shuttle operations, does not, however, meet the accuracy requirements of the orbiter experiments program (ref. 2).

Because of the obvious advantages of extending the use of SEADS to subsonic and transonic speeds, wind tunnel tests of a preliminary design of SEADS were made at a Mach number of 0.4 (ref. 3) in the 10- by 10-Foot Supersonic Wind Tunnel at the NASA Lewis Research Center (ref. 4). To permit the accurate determination of all the air data provided by conventional air data systems, including Mach number and pressure altitude, additional flush static pressure orifices aft of the nose cap were investigated throughout the subsonic and transonic speed range (ref. 3). Because of the success of this investigation, it was decided that additional wind tunnel tests and flight tests of the system should be made. It was also concluded that the studies should investigate the feasibility of using similar systems for other aircraft.

As a result, nose cap (SEADS) and auxiliary flush static pressure measurements were made on a 0.1 scale shuttle forebody model at Mach numbers from 0.25 to 1.40 in the 16-Foot Transonic Tunnel at the Arnold Engineering Development Center (AEDC, ref. 5). The orifice array included static pressure orifices aft of the nose cap not investigated in reference 3. Data were obtained at angles of attack from -4° to 18° at both 0° and 2° of angle of sideslip. The test envelope was within the normal operating Mach number and flow angularity envelope of the orbiter during entry at pressure altitudes below approximately 20 kilometers.

The subsonic and transonic air data measuring capabilities of three orifice combinations were evaluated in detail. In two of the combinations, the orifices were confined to the region of the nose cap; the third included two auxiliary orifices. This paper outlines a data reduction method that permits the accurate determination of air data quantities from these orifice configurations. In contrast to the data reduction method described in reference 6, which uses all 14 of the pressure orifices on the nose cap, the method outlined herein uses only six or seven of the orifices investigated, six being the minimum that will provide all the conventional air data quantities that can be derived without temperature measurements.

SYMBOLS

h_p	pressure altitude, km
M	Mach number measured in wind tunnel
M_i	indicated Mach number
p	pressure, kPa
p_t	stagnation pressure measured in wind tunnel, kPa
p_{t_i}	indicated local stagnation pressure, kPa
p_∞	static pressure measured in wind tunnel, kPa
p_{∞_i}	indicated static pressure, kPa
q	dynamic pressure measured in wind tunnel, $0.7M^2p_\infty$, kPa
R	Reynolds number
x, y, z	longitudinal, lateral, and vertical model coordinates, respectively, cm
α	angle of attack measured in wind tunnel, deg

$\alpha_{\Delta p_\alpha=0}$	angle of attack at which the differential pressure between two pressure orifices is zero (fig. 11), deg
β	angle of sideslip measured in wind tunnel, deg
Δp_t	$= p_t - p_{t_i}$
Δp_α	pressure differential between two nose cap orifices in angle of attack plane, kPa
Δp_β	pressure differential between two nose cap orifices in angle of sideslip plane, kPa
Δp_∞	$= p_\infty - p_{\infty_i}$
τ_α	angle of attack parameter, $\frac{p_{50} - p_{45}}{(p_{48} - p_{50}) + 0.5(p_{50} - p_{45})}$
Subscripts:	
i, j, k	dummy variables for orifice location (fig. 2)

WIND TUNNEL MODEL

The wind tunnel model used to obtain the test data for this study (as well as the study reported in ref. 3) was a 0.1 scale model of the forebody of the space shuttle orbiter (fig. 1, table 1). The absence of wings on the model was not expected to affect the results of the investigation significantly. Unlike the model used for reference 7, the model used in this study did not simulate the thermal protection system (TPS) tiles to be used over parts of the orbiter or the sponge-like coated felt material to be used for heat shielding in the area aft of the cabin. The model used in reference 7 also had a slightly different fuselage mold line that corresponded to an earlier design of the orbiter.

Figure 2 shows the locations of the pressure orifices used in this study, and table 2 gives their coordinates. Orifices aft of the nose cap are referred to as auxiliary orifices to distinguish them from the SEADS orifices, which are restricted to the nose cap. The auxiliary orifices are located in regions that will be covered by TPS tiles on the actual vehicle. The orifice configuration used in this study is identical to that used in reference 3 except for the addition of orifices 111 and 112. All of the orifices not on the vertical centerline of the model's nose cap are paired with orifices in the same position on the other side of the fuselage.

Figure 3 shows the y-z coordinates of the nose cap orifices investigated in this study. Also shown in figure 3 are the orifices that make up what is considered to be the final SEADS configuration (which does not include any auxiliary orifices). In

both the test and final nose cap configurations, the orifices are located along the nose cap horizontal centerline and slightly displaced from, but parallel or nearly parallel to, the nose cap horizontal centerline. Orifices 55, 56, 57, and 58, which were part of the test configuration, were not close to the orifices used in the final system design; therefore, the data for those orifices are not included in this paper.

WIND TUNNEL TESTS

The tests were conducted in the 16-Foot Transonic Tunnel at the Arnold Engineering Development Center. This tunnel is a closed circuit flow wind tunnel capable of a Mach number range from 0.20 to 1.60. Stagnation pressure ranges from 7.7 kPa to 191.5 kPa, depending on the test Mach number. Detailed information about the tunnel is given in reference 5.

The sting-mounted model was tested at the conditions summarized in table 3. Angle of attack sweeps were made in 2° increments at 14 Mach numbers. Data were obtained at both 0° and 2° sideslip angles for most Mach numbers. The average values of unit Reynolds number, total pressure, static pressure, and dynamic pressure for the sweeps are given in the table.

Table 4 lists the estimated uncertainties in the wind tunnel test condition at each Mach number. The uncertainty in the measurement of local pressure is approximately ± 0.05 kPa. Repeat runs were made at the completion of the angle of attack sweeps to verify the data.

The data from these tests are compared in this paper with data reported in reference 3, which are for the same model but are from tests made in the 10- by 10-Foot Supersonic Wind Tunnel at the NASA Lewis Research Center (ref. 4) at a Mach number of 0.4. Comparisons are also made with the data in reference 7, which were obtained, as previously noted, from a different model. Those tests were made in the 14-Foot Transonic Wind Tunnel at the NASA Ames Research Center (ref. 8).

RESULTS AND DISCUSSION

Analysis of Pressure Data

The following sections describe the pressure relationships investigated for the determination of stagnation pressure, static pressure, angle of attack, and angle of sideslip using nose cap and auxiliary pressure orifices. From those measurements, all of the air data quantities supplied by conventional pitot-static and flow angularity (for example, vane sensor) systems can be derived. The pressure relationships, which are portrayed as calibration curves (for example, p_i/p_t versus angle of attack) do not completely define the desired quantity, but they do suggest the accuracy with which the quantity can be determined once other required quantities are known. The criteria for determining the adequacy of the relationships for calibration purposes are

linearity, the sensitivity of the measured pressure parameter to the air data quantity being determined, the lack of sensitivity of the parameter to other variables, the consistency of families of curves, and repeatability.

Stagnation pressure.—Figure 4 presents ratios of measured pressure to wind tunnel stagnation pressure plotted against angle of attack at constant Mach numbers for a sideslip angle of 0° . The model pressures were all measured on the vertical centerline of the nose cap. Figure 5 shows similar data for a sideslip angle of 2° . These data and fairings are presented to allow the selection of the most suitable orifices for the determination of stagnation pressure and also for an initial indication of the suitability of the various orifices for the determination of angle of attack.

The variations of pressure ratio with angle of attack resemble the variations of the cosine functions that are predicted by the various forms of Newtonian theory when it is applied to the determination of pressure distributions on hemispherical sensors.

A comparison of the fairings in figures 4 and 5 for the same Mach numbers shows that the variation of the pressure ratio as sideslip increases from 0° to 2° is small (less than 0.008). The difference generally increases slightly with Mach number. For example, the average difference for all of the orifices over the angle of attack range is near zero at a Mach number of 0.25. However, the average difference slightly exceeds 0.002 at a Mach number of 1.40.

Because figure 4 (and fig. 5) indicates a significant Mach number effect, the pressure ratios in figure 4 were plotted versus Mach number for selected values of angle of attack and presented in figure 6. The variations with Mach number are generally characterized by two inflection points, one near a Mach number of 0.6 and one near a Mach number of 1.0. This is especially evident for the higher numbered orifices in this group (orifices farther away from the horizontal centerline).

As expected, figures 4 to 6 reveal that all of the orifices exhibit angle of attack as well as Mach number effects. If the criterion for selecting orifices for stagnation pressure determination is the minimum variation of pressure ratio with changing angle of attack and Mach number, orifices 45 and 46 appear to be the most suitable. The same conclusion was reached in reference 3 for the measurement of stagnation pressure at Mach 0.4. Corrections of less than 3 percent would be necessary for pressure measurement for angles of attack from -2° to 16° throughout the Mach number range investigated (0.25 to 1.40). Furthermore, the corrections would vary only slightly with Mach number (fig. 6).

The significant variation of pressure ratio with angle of attack demonstrated by some of the orifices indicates the desirability of using orifice pairs for the determination of angle of attack, as discussed below.

Angle of attack.—The same nose cap orifices along the vertical centerline that were investigated for stagnation pressure measurement (orifices 45 to 50) were evaluated for angle of attack determination. As in reference 3, the orifices were evaluated by examining the variation of angle of attack with $\Delta p_a/q$, the ratio of the difference in pressure between the members of a pair of nose cap orifices to dynamic pressure. The results are shown in figures 7 and 8 at constant Mach numbers for

sideslip angles of 0° and 2° , respectively. Orifice 45 was used as one of the orifices in each pair in order to achieve large differences in pressure for a number of orifice pairs. Straight line slopes (which denote sensitivity) were calculated for each orifice pair in each figure (except fig. 8(d), for which data were limited) by using the ordinate values at -2° and 16° of angle of attack.

The same comments made in reference 3 regarding curve behavior at the investigated Mach number of 0.4 apply to the curves in figures 7 and 8 throughout the Mach number range. That is, regardless of Mach number, the linearity of the curves decreases slightly as the distance between the orifice pairs increases, but the sensitivity of the curves increases with orifice separation. Orifice pairs 45, 47 and 45, 48 were judged to provide the best combinations of linearity and sensitivity for angle of attack determination.

Figure 9 shows the percentage of change in the slopes of the curves in figures 7 and 8 as sideslip angle increases from 0° to 2° . It would have been better to have had data at a higher sideslip angle to define the effects more accurately. However, the effect of sideslip on the slopes seems to be small for most orifice pairs and at most Mach numbers.

Figure 10 shows the slopes of the curves in figure 7 plotted against Mach number for a sideslip angle of 0° . Also shown, for comparison, is the corresponding curve for the hemispherical probe sensor used for angle of attack measurements in the YF-12 airplane (ref. 9). The variations with Mach number for all of the orifice pairs are similar and gradual. In general, the curves are invariant with Mach number, except for the transonic Mach numbers between approximately 0.70 and 1.20. The similarity of the nose cap curves to the YF-12 curve shows that the pressure distribution on the shuttle nose cap closely approximates that on a true hemisphere. Because of the larger angle between the orifices of the YF-12 sensor (90°), the slope values for that sensor are larger than for any of the shuttle orifice pairs.

The curves in figures 7 and 8 could be used directly for angle of attack determination. However, a more accurate method is to determine angle of attack by using the slope and intercept values as shown in figures 10 and 11, respectively, for the selected orifice pair. The accuracy of this preferred method depends on how linear the variation of $\Delta p_\alpha/q$ is with changing angle of attack and how accurately the intercept of $\Delta p_\alpha/q$ with angle of attack (that is, the value of α at which $\Delta p_\alpha/q$ equals zero) can be defined. For a hemispherical probe, the intercept should be constant with Mach number. However, for a nonspherical surface, such as that of the shuttle nose cap, this is not necessarily true.

Figure 11 shows a plot of the intercepts of the investigated orifice pairs plotted against Mach number for 0° of sideslip. These values were obtained from the curves in figure 7. Again, the curves for orifice pairs 45, 47 and 45, 48 demonstrate the best potential for accuracy. The data in figure 11 suggest that a constant intercept value of 7.8° could be used for orifice pair 45, 47 throughout the Mach number range without introducing an error in angle of attack larger than 0.1° .

Whichever of the above methods is used for angle of attack determination, Mach number and dynamic pressure must be determined. Since both quantities depend on

the measurement of stagnation and static pressure, which are themselves affected by angle of attack, an iterative data reduction method is usually employed for all three quantities, as discussed in the section entitled Derivation of Air Data.

Another parameter that can be used for the determination of angle of attack from the pressure differences between members of orifice pairs is τ_α (fig. 12), which is defined as $\frac{p_{50} - p_{45}}{(p_{48} - p_{50}) + 0.5(p_{50} - p_{45})}$. This parameter is similar to the RAX parameter of reference 7, which was developed for a configuration consisting of three equally spaced orifices on the vertical centerline of a hemisphere. The central orifice, which was on the horizontal centerline, was used for measuring stagnation pressure. Obviously, orifices other than orifices 45, 48, and 50 could be used for τ_α . Those particular orifices were chosen because they maximized the sensitivity of τ_α to changes in angle of attack.

Figure 12(a) illustrates two advantages of the use of this parameter over the sensitivity parameters shown in figures 10 and 11. First, τ_α requires in addition to the basic orifice pressure measurements only a knowledge of Mach number. The denominator of τ_α performs the normalization accomplished by the use of dynamic pressure in the other method. In addition, for the same angle of attack the parameter is insensitive to Mach number, as shown by figure 12(b), in which τ_α is plotted against Mach number. A possible disadvantage of this parameter is that three pressure measurements must be used rather than the two needed to determine angle of attack. However, since there is an identical term in the numerator and the denominator, the errors compensate for each other in the τ_α measurement. Other, but not necessarily serious, disadvantages of the parameter when used with orifices 45, 48, and 50 are its nonlinearity and its changing sensitivity with angle of attack (fig. 12(a)). Another disadvantage of this parameter is that its denominator can go to zero for certain flow conditions (that is, $p_{48} - p_{50} = -0.5(p_{50} - p_{45})$). Because of the position of the upper orifice in the subject configuration, this condition occurs near an angle of attack of 1° . To extend the angle of attack measuring capability to the lower angles of attack, the upper orifice should be located farther up on the surface of the nose.

Angle of sideslip.—Angle of sideslip can be determined, like angle of attack, by using orifices located in a horizontal plane of the nose cap (that is, orifice pairs 51, 52; 53, 54; 55, 56; or 57, 58 (fig. 3)). Since angle of sideslip test data are restricted to 0° and 2° , the usefulness of the calibration curves is limited for purposes of sideslip determination. Therefore, of the methods discussed for the determination of angle of attack, only the method that uses sensitivity and incorporates dynamic pressure (fig. 10) was investigated. Figure 13 shows the variation of the sensitivity values (slopes) with angle of attack for two orifice pairs at constant Mach number. The sensitivity values were calculated by assuming that the variation of $\Delta p_\beta/q$ was linear with changes in sideslip angle, and they were, of course, based only on data for 0° and 2° of sideslip.

The sensitivity values vary somewhat differently with Mach number, but all of the curves show maximum sensitivity for angles of attack in the range from 6° to 8° . Figure 14 shows a crossplot of the data from figure 13. The curves for an angle of attack of 0° are analogous to those of the corresponding figure for angle of attack determination at 0° of sideslip (fig. 10). The spacing of orifices 51, 52 is similar to that of orifices 45, 47 (fig. 3), so it is not surprising that the corresponding sensitivity is nearly the same. From the curves in figures 13 and 14, this orifice pair appears to be suitable for angle of sideslip determination.

Static pressure.—As shown, pressure measurements on the nose cap are suitable for the determination of stagnation pressure and flow angularity. However, because the nose cap is in a region of high pressure, pressures from auxiliary flush orifices (orifices behind the nose cap) were analyzed to find a source suitable for the accurate determination of static pressure. The correction for static pressure position error (that is, the difference between ambient pressure and local pressure) for any pressure orifice measurement was expected to vary appreciably with both Mach number and flow angularity for the range of the tests discussed in this paper. The major criterion chosen for selecting orifices was minimum sensitivity of the measured pressure to angle of attack.

Of the orifices located on the surfaces of the orbiter to be covered by the thermal protection system tiles, data analysis indicated that the six best orifices were orifices 19, 20, 23, 24, 25, and 26. Those orifices can be thought of as being members of three pairs, in which each orifice is in a position diametrically opposed to that of its partner (fig. 2). Figure 15 shows the variation of the pressure correction for position error with changing angle of attack at constant Mach numbers for orifices 19, 23, and 26, each of which represents an orifice pair. If it is assumed that the magnitude of the required correction is of no consequence (that only the variation of the correction with angle of attack and Mach number matters), the performance of the three orifices is similar up to a Mach number of approximately 1.10. For these Mach numbers, the correction generally increases smoothly with angle of attack for each orifice, and the shapes of the respective curves are similar. However, at Mach numbers of 1.15 and above, the pressure corrections from orifices 23 and 26 behave erratically with changes in angle of attack, whereas the curve of the pressure corrections for orifice 19 is relatively smooth. Hence, the orifice believed to be best for the measurement of static pressure for the Mach number range investigated is orifice 19.

The pressure corrections derived from orifice 19 were averaged with those from its companion, orifice 20, to simulate the pressure corrections that would result if the data from orifices 19 and 20 were manifolded in order to minimize sideslip effects. Figure 16 shows the resulting corrections plotted against angle of attack at constant Mach numbers for both the 0° and the 2° angle of sideslip data. There are no discernible differences between the corrections for the two angles of sideslip until Mach number rises above 0.80. At Mach numbers of 0.90 and 1.05 and at angles of attack below 4° , the differences are as large as 3 percent. At Mach numbers from 1.20 to 1.40, the differences are smaller but cover a wider range of angles of attack. An inspection of the data showed that the variations in the pressure corrections from orifices 19 and 20 were larger when considered individually (without being averaged; that is, without simulated manifolded).

Figure 17 shows a crossplot of the data in figure 16 for 0° of sideslip. As the figure shows, over the angle of attack range from 0° to 16° the variation of the pressure correction with changes in angle of attack does not exceed 3 percent at any Mach number. Position error corrections are less than 1 percent up to a Mach number of 0.60, regardless of angle of attack. For all angles of attack, a large Mach number effect appears in the transonic range.

Pressures not presented in this paper were measured from orifices in the surfaces to be covered by felt material (fig. 2), and they were found to be more sensitive to changes in angle of attack than orifices on the nose section. These orifices were thus considered to be unsuitable as sources of static pressure. Of several orifices that were installed in areas to be covered by thermal protection system tiles and installed on the model after the tests reported in reference 3, orifices 111 and 112 were found to perform the best. The variation of the pressure correction with changing angle of attack for orifice 112 (fig. 18) is small up to and including a Mach number of 0.80. The wing leading edge glove (fig. 1) evidently affects the flow at Mach numbers of 0.90 and above, causing the large sensitivity of the measured pressure to changes in angle of attack.

Of all the orifices investigated for the measurement of static pressure, orifices 19 and 20 performed best over the test Mach number range (0.25 to 1.40).

Comparisons With Other Tunnels

Pressure ratios from the present tests from the nose cap orifices on the vertical centerline are compared in figure 19 with those from the NASA Lewis Research Center wind tunnel data reported in reference 3. The accuracy of the latter data, which were obtained only at a Mach number of 0.40, was considered somewhat questionable because the data were obtained at subsonic test conditions for which the tunnel was not fully calibrated. The tests reported in reference 3 were made at angles of attack up to 20° , whereas the present tests were limited to 16° at the same Mach number. As already noted, the same model was used for both tests. Figure 19 shows that the agreement of the pressure ratios from the two tests is within 1 percent for both 0° and 2° of sideslip.

An additional comparison between these tests is made in figure 20, which contains plots of $\Delta p_\alpha / q$ versus angle of attack for the same measurements. Also tabulated in the figure are the slopes of the curves calculated from the data. The agreement of the two sets of data is good. The slopes of all of the orifice pairs except orifices 45 and 46, which have the lowest sensitivities (slope values), agree within 3 percent for both angles of sideslip. The comparisons in figures 19 and 20 serve to validate the data of both wind tunnel tests.

Comparisons of the static pressure position error corrections for orifices 19, 23, and 26 as determined from the present tests and those in reference 7 are shown in figure 21 for Mach numbers from 0.40 to 1.10. The differences are generally within 1 percent up to a Mach number of 0.90. Substantially larger discrepancies appear at the higher transonic speeds; however, they are probably due primarily to differences between the wind tunnel models.

Derivation of Air Data

The pressure measurements reveal that several combinations of pressure orifices are potentially capable of providing accurate air data measurements. The analysis shows that (1) orifices on the nose cap can provide the measurements needed for the determination of stagnation pressure and flow angularity and (2) orifices aft of the nose cap can provide the measurements needed to determine static pressure. The following section outlines two ways to combine the measurements from optimum orifice arrays to determine all the air data provided by conventional air data systems (Mach number, pressure altitude, airspeed, angle of attack, angle of sideslip, and so forth). The discussion also includes a discussion of the potential of orifice arrays that use only orifices in the region of the nose cap for providing all of the air data quantities.

Description of orifice arrays and data reduction.—Three orifice arrays, termed A, B, and C (table 5) were selected for analysis. Array A is made up of both nose cap orifices and auxiliary orifices on the sides of the fuselage. This array was judged from a review of the data to have the most potential for accurate air data measurements over the Mach number range from 0.25 to 1.40. Arrays B and C use the same orifices as array A for the measurement of stagnation pressure, angle of attack, and angle of sideslip, but use only one fuselage pressure measurement (orifice 9, which is in the region of the nose cap (fig. 2)), in addition to a nose cap pressure measurement (p_{45} or p_{46}), to derive a Mach number measurement. The only difference between arrays B and C is the source of the stagnation pressure measurement.

Two data reduction schemes, referred to as methods I and II, are considered. Figure 22 presents the calibration curves and steps required for both methods. Method I (fig. 22(a)) is conventional; an indicated static pressure and indicated stagnation pressure are corrected for position error. The position errors for both measurements are assumed to be functions of both Mach number and angle of attack. By defining the position errors as a function of indicated Mach number rather than true Mach number, the iteration of only one variable, angle of attack, is required. For simplicity, the calibration curves and calculations used for the determination of angle of sideslip are not included in figure 22. The procedure would be similar to that used to determine angle of attack (ref. 9).

Method II, outlined in figure 22(b), differs from method I in the way in which Mach number is determined. In this method, Mach number is derived from the ratio of two suitable local pressure measurements. Unlike method I, method II does not correct these pressures for stagnation and static pressure position errors. The suitability of the pressures, therefore, is decided not by how closely these pressures approximate stagnation pressure or static pressure, but rather by the magnitude of the slope when the ratio of the two pressures is plotted against Mach number and by the expected accuracies and degree of repeatability of the ratio.

Table 6 lists the figures that pertain to the calibration curves required for deriving air data from the three pressure orifice arrays (A, B, and C) by the two data reduction methods (I and II). Both methods are considered for array A, but not for arrays B and C. Rapid convergence occurs for both of the data reduction methods by using the data in the figures listed in table 6.

Array A: Figures 23, 24, and 25(a) present calibration curves 1 and 2 as required for array A by method I (fig. 22(a)). Figure 10 provides calibration curve 3 for array A, as well as for arrays B and C. The static pressure position error correction curves in figure 23 are similar to those in figure 17 except that they are functions of indicated Mach number instead of true Mach number. The curves in figure 23 for angles of attack between -2° and 16° are reproduced in figure 24. The overall variation in the correction due to angle of attack for angles between 0° and 16° ranges from 0 percent to 4 percent, depending on Mach number. The stagnation pressure correction (fig. 25(a)) is small and is practically constant with Mach number for angles of attack between 4° and 8° . Indicated Mach number is determined from the ratio of measured stagnation pressure to measured static pressure, using the well known pitot-static formula relating Mach number to the pressure ratio.

Figures 25(b) and 26 present calibration curves 1 and 2 as required for array A by method II (fig. 22(b)). The stagnation pressure correction curve shown in figure 25(b) is plotted against true Mach number, rather than indicated Mach number as in method I. The curves in figures 25(a) and 25(b) are similar, since the corrections do not vary greatly with Mach number.

Calibration curve 2 for method II, shown in figure 26, illustrates an advantage of method II over method I: Method II defines the direct effect of angle of attack on the determination of Mach number. In method I, the effect of angle of attack must be calculated from the calibration curves (figs. 24 and 25(a)). An additional advantage in regard to the subject data is that it can be shown that in general there is a smaller angle of attack effect on Mach number if the curves in figure 26 are used than if those in either figure 24 or figure 25(a) are. What this means is that there are

compensating errors when the ratio $\frac{p_{46}}{\frac{p_{19} + p_{20}}{2}}$ is used to determine Mach number

instead of the values of p_{46} and $\frac{p_{19} + p_{20}}{2}$ individually.

Arrays B and C: Orifice 9 was selected as the optimum orifice of those investigated for the measurement of the lower-valued pressure in the ratio of $\frac{p_j}{p_k}$ (curve 2, method II). Because the orifice is in the vertical plane of symmetry, pressures measured at this orifice are less sensitive to sideslip angle than pressures measured at side fuselage orifices, which are often manifolded to decrease sideslip sensitivity. The location of orifice 9 is especially interesting in that similar pressure values would be expected if measurements were made with an orifice on the upper surface of the nose cap near its trailing edge.

Figure 27 shows the ratios of p_{45}/p_9 and p_{46}/p_9 as a function of Mach number for arrays B and C, respectively. In comparison with figure 26, the pressure ratios show great sensitivity to angle of attack, especially at the higher Mach numbers. However, the variations with angle of attack are systematic and predictable, and it was concluded that an all nose cap orifice array could be used as a complete air data sensor system.

Mach number accuracy.—The relative accuracy with which Mach number could be calculated with the three orifice arrays using method II is shown in figures 28 to 30 for angles of attack of 0° , 8° , and 16° . In this study, it was assumed that the only variation in error between the three arrays occurred in the quantities used to determine calibration curve 2 (figs. 26 and 27); the errors in the other calibration curves would be about the same for all three orifice arrays. Errors in pressure of ± 0.005 kPa, which are typical of high quality flight test instrumentation, were assumed. The signs of the errors were selected that maximized the errors in the pressure ratios. The resulting errors in Mach number due to instrumentation are shown in figure 28 for both high altitude and low altitude entry profiles (fig. 31).

The errors in Mach number resulting from an angle of attack error of 1° are shown in figure 29. The uncertainty due to angle of attack for array A is small in comparison to the other arrays; for array A the maximum Mach number error due to angle of attack is only 0.002, whereas for arrays B and C the uncertainties are as large as 0.05.

Primarily because of this, the total Mach number errors (fig. 30) for array A are smaller than those of the other two arrays. For array A, the maximum total Mach number error is 0.021, whereas for arrays B and C the errors are 0.076 and 0.082, respectively. All the maximum uncertainties occur at a Mach number of 1 and an angle of attack of 0° . Errors are smaller at subsonic Mach numbers and higher angles of attack. At Mach numbers of 0.80 and less, the maximum errors are 0.009, 0.021, and 0.030 for arrays A, B, and C, respectively. Array B performs more accurately than array C because of its smaller sensitivity to angle of attack error.

From the results portrayed in these figures, it seems clear that an array of orifices on the shuttle nose cap could provide adequate accuracy for the determination of basic air data quantities at subsonic speeds. For verification, of course, such a configuration would have to be flight tested. Array A, which consists of both nose cap and fuselage orifices, would provide an accurate air data system throughout the subsonic and transonic speed ranges. However, additional uncertainties would result from the steps and gaps in the thermal protection system tiles (which were not simulated in the tests discussed in this paper). The results also suggest that flush pressure measurements, without the use of probes or boom-mounted sensors, could be used to determine basic air data for other aircraft at subsonic and transonic speeds.

CONCLUDING REMARKS

Wind tunnel pressure data were acquired from pressure orifices on a 0.1 scale model of the space shuttle forebody that were arranged in a preliminary configuration of the shuttle entry air data system (SEADS). Pressures from those and auxiliary pressure orifices were evaluated for their ability to provide subsonic and transonic air data for space shuttle flights. This study, which is an extension of a wind tunnel study made at a Mach number of 0.40, covered a Mach number range from 0.25 to 1.40 and an angle of attack range from -4° to 18° . The following conclusions were drawn from the study:

An air data system comprising orifices on the nose cap and on the sides of the forebody forward of the cabin constitutes a complete and accurate air data system at subsonic and transonic speeds. In this system, the orifices on the nose cap provide stagnation pressure and flow angularity measurements, and the auxiliary orifices provide static pressure measurements. For Mach numbers less than approximately 0.80, orifices on the nose cap can be used as a complete and accurate air data system for the determination of Mach number, airspeed, pressure altitude, flow angles, and so forth.

An air data reduction method designed for flush pressure orifice systems was developed that defines the effects of angle of attack on the determination of Mach number more clearly than the described conventional method.

Air data systems comprised only of flush pressure orifices, which would eliminate the need for probes or boom-mounted sensors, could be used to determine basic air data on other aircraft at subsonic and transonic speeds.

*Dryden Flight Research Center
National Aeronautics and Space Administration
Edwards, Calif., September 24, 1979*

REFERENCES

1. Siemers, Paul M. III: Shuttle Entry Technology Payloads. AAS Paper 75-251, Am. Astronaut. Soc., Aug. 1975.
2. Siemers, Paul M. III; and Larson, Terry J.: Space Shuttle Orbiter and Aerodynamic Testing. J. Spacecraft and Rockets, vol. 16, no. 4, July-Aug. 1979, pp. 223-231.
3. Larson, Terry J.; and Schweikhard, William G.: Use of the Shuttle Entry Air Data Pressure System at Subsonic Speeds. Proc. 1978 Air Data Systems Conference, May 1978. (Available from Dept. Aeronaut., U. S. Air Force Academy, Colorado Springs, Colo.)
4. Aiello, Robert A.: NASA Lewis 10- by 10-Foot Supersonic Wind Tunnel. NASA TM X-71625, 1974.
5. Test Facilities Handbook. Tenth ed. Vol. IV. Propulsion Wind Tunnel Facility. Arnold Eng. Dev. Center, May 1974.
6. Wolf, H.; and Eades, J. B., Jr.: Analysis of the Shuttle Air Data System. NASA CR-145279, Oct. 1977.
7. Esparza, V.; and Thornton, D. E.: Results of an Air Data Probe Investigation Utilizing a 0.10 Scale Orbiter Forebody (Model 57-0) in the Ames Research Center 14 Foot Wind Tunnel (0A220). NASA CR-147,625, 1976.
8. Ames Research Facilities Summary—1974. NASA/Ames Research Center, 1974.
9. Johnson, Harold J.; and Montoya, Earl J.: Local Flow Measurements at the Inlet Spike Tip of a Mach 3 Supersonic Cruise Airplane. NASA TN D-6987, 1973.

TABLE 1.—PHYSICAL DIMENSIONS OF FULL SCALE AND
0.1 SCALE SHUTTLE FOREBODY

	Full scale	Model
Length, cm	1897.4	189.74
Maximum width, cm	538.5	53.85
Maximum depth, cm	575.3	57.53
Fineness ratio	3.524	3.524
Maximum cross-sectional area, cm ²	2131.0	21.31

TABLE 2.—PRESSURE ORIFICE COORDINATES
(a) Nose cap orifices

Orifice ^a	0.1 scale model coordinates, cm		
	x	y	z
45	59.94	0	85.78
46	60.02	0	85.04
47	60.27	0	84.10
48	60.73	0	83.08
49	61.49	0	82.04
50	62.76	0	80.77
51	60.05	-1.02	85.22
52	60.05	1.02	85.22
53	60.73	-2.90	85.22
54	60.73	2.90	85.22
55	60.73	-1.72	83.49
56	60.73	1.72	83.49
57	61.49	-2.56	82.63
58	61.49	2.56	82.63
1	60.49	0	88.32
2	60.09	0	87.18
3	59.94	0	85.98
4	60.07	0	84.80
5	60.46	0	83.64
6	60.06	0	82.59
7	61.84	0	81.64
8	62.74	0	80.79
9	61.08	-3.43	84.94
10	60.52	-2.34	84.86
11	60.18	-1.21	84.81
12	60.18	1.21	84.81
13	60.52	2.34	84.86
14	61.08	3.43	84.94

^aOrifices 45 to 58 are used in the configuration for this study; orifices 1 to 14 are used in the final SEADS configuration.

TABLE 2.—Concluded

(b) Auxiliary orifices

Orifice	x, cm	y, cm	z, cm
9	70.10	0	-----
19	85.34	-16.08	85.57
20	85.34	16.08	85.57
23	105.66	-----	87.78
24	105.66	-----	87.78
25	115.82	-----	90.83
26	115.82	-----	90.83
111	136.40	-----	95.00
112	136.40	-----	95.00

TABLE 3.—AVERAGE TEST CONDITIONS FOR ANGLE OF ATTACK SWEEPS

[Angle of attack sweeps were made in 2° increments;
there was some variation around the test condition values]

M	α , deg	β , deg	R, per m	p_t , kPa	p_∞ , kPa	q, kPa
0.252	-4.0 to 16.0	0	5.978×10^6	114.24	109.31	4.86
0.251	-2.0 to 15.9	2.0	5.998	114.24	109.33	4.83
0.400	-1.9 to 16.0	0	7.060	88.64	79.40	8.88
0.400	-2.0 to 15.9	2.0	7.047	88.58	79.33	8.89
0.601	-1.9 to 16.0	0	10.637	101.36	79.41	20.08
0.600	-2.0 to 17.9	2.0	10.637	101.38	79.45	20.05
0.700	-2.1 to 16.0	0	11.736	101.29	73.02	25.05
0.702	-1.9 to 6.2	2.0	11.752	101.31	72.95	25.12
0.800	-4.0 to 16.0	0	12.651	101.29	66.46	29.76
0.800	-3.9 to 19.0	2.0	12.654	101.36	66.52	29.77
0.900	-3.9 to 17.9	0	13.303	101.30	59.90	33.96
0.900	-1.9 to 18.0	2.0	13.461	102.57	60.65	34.38
0.950	-4.0 to 18.0	0	13.589	101.37	56.71	35.83
0.950	-4.0 to 17.9	2.0	13.579	101.34	56.69	35.82
0.979	-2.0 to 18.0	0	13.773	102.01	55.23	37.04
1.050	-4.0 to 18.0	0	12.513	91.00	45.31	34.97
1.050	-4.0 to 17.9	2.0	12.510	90.98	45.31	34.96
1.100	-2.0 to 18.0	0	12.719	91.59	42.96	36.35
1.100	-2.0 to 19.9	2.0	12.795	92.07	43.20	36.55
1.149	-4.0 to 18.0	0	12.690	90.67	40.07	37.03
1.199	-1.9 to 18.0	0	12.801	91.03	37.83	38.08
1.199	-2.0 to 18.0	2.0	12.795	91.07	37.89	38.11
1.300	-2.1 to 18.0	0	11.817	82.92	30.57	36.15
1.300	-2.0 to 17.9	2.0	11.814	83.06	30.62	36.20
1.400	-2.0 to 18.0	0	11.479	80.06	26.27	36.02
1.400	-3.9 to 18.0	2.0	11.483	80.09	26.27	36.03

TABLE 4.—UNCERTAINTIES IN WIND TUNNEL TEST CONDITIONS

M	Uncertainties					
	M	p_{∞} , N/cm ²	q, N/cm ²	R, per m	α , deg	β , deg
0.25	±0.006	±0.14	±0.20	±3.8 × 10 ⁴	±0.1	±0.1
0.40	±0.005	±0.13	±0.18	±2.6	±0.1	±0.1
0.60	±0.003	±0.13	±0.17	±2.9	±0.1	±0.1
0.70	±0.003	±0.13	±0.15	±3.1	±0.1	±0.1
0.80	±0.003	±0.13	±0.14	±3.2	±0.1	±0.1
0.90	±0.004	±0.13	±0.12	±3.5	±0.1	±0.1
0.95	±0.003	±0.13	±0.11	±3.5	±0.1	±0.1
0.98	±0.003	±0.13	±0.11	±3.6	±0.1	±0.1
1.05	±0.003	±0.13	±0.10	±3.4	±0.1	±0.1
1.10	±0.003	±0.12	±0.10	±3.5	±0.1	±0.1
1.15	±0.003	±0.11	±0.09	±3.5	±0.1	±0.1
1.20	±0.003	±0.11	±0.08	±3.5	±0.1	±0.1
1.30	±0.003	±0.11	±0.07	±3.4	±0.1	±0.1
1.40	±0.004	±0.11	±0.06	±3.6	±0.1	±0.1

TABLE 5.—PRESSURE ORIFICE ARRAYS A, B, AND C

Air data quantity	Orifice array		
	A	B	C
	Orifices used		
Stagnation pressure	p_{46}	p_{46}	p_{46}
Mach number	p_{19}, p_{20} ¹	p_9, p_{45}	p_9, p_{46}
Angle of attack	p_{45}, p_{47}	p_{45}, p_{47}	p_{45}, p_{47}
Angle of sideslip	p_{53}, p_{54}	p_{53}, p_{54}	p_{53}, p_{54}

¹Orifices listed under Mach number are used in conjunction with stagnation pressure orifice for measurement of pressure ratio for determination of Mach number.

TABLE 6.—FIGURES SHOWING CALIBRATION CURVES
REQUIRED FOR APPLYING DATA REDUCTION
METHODS I AND II TO ORIFICE ARRAYS A, B, C

Orifice array	Data reduction method	
	I	II
A	10, 23, 24, 25(a)	10, 25(b), 26
B	-----	10, 25(b), 27(a)
C	-----	10, 25(b), 27(b)

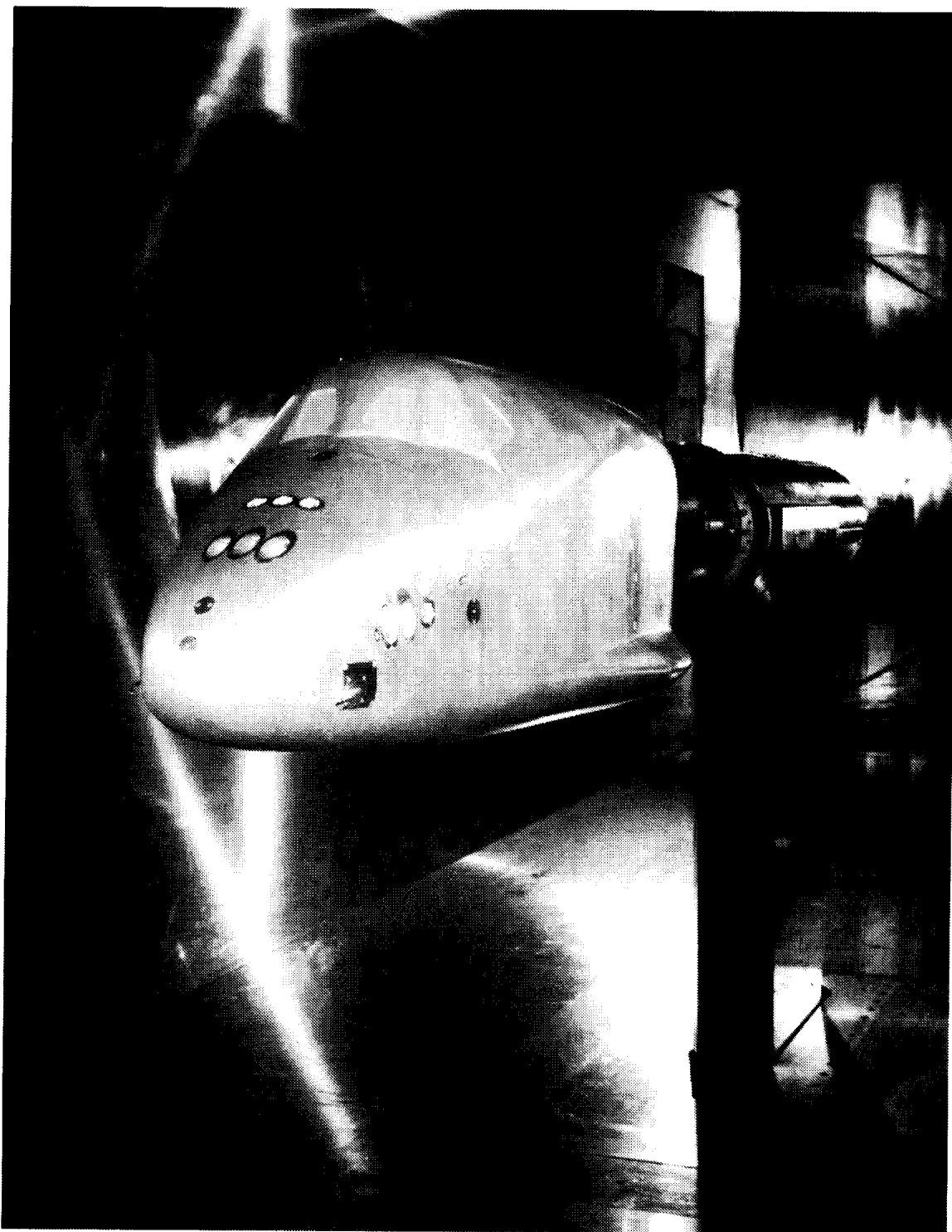


Figure 1. Shuttle forebody model.

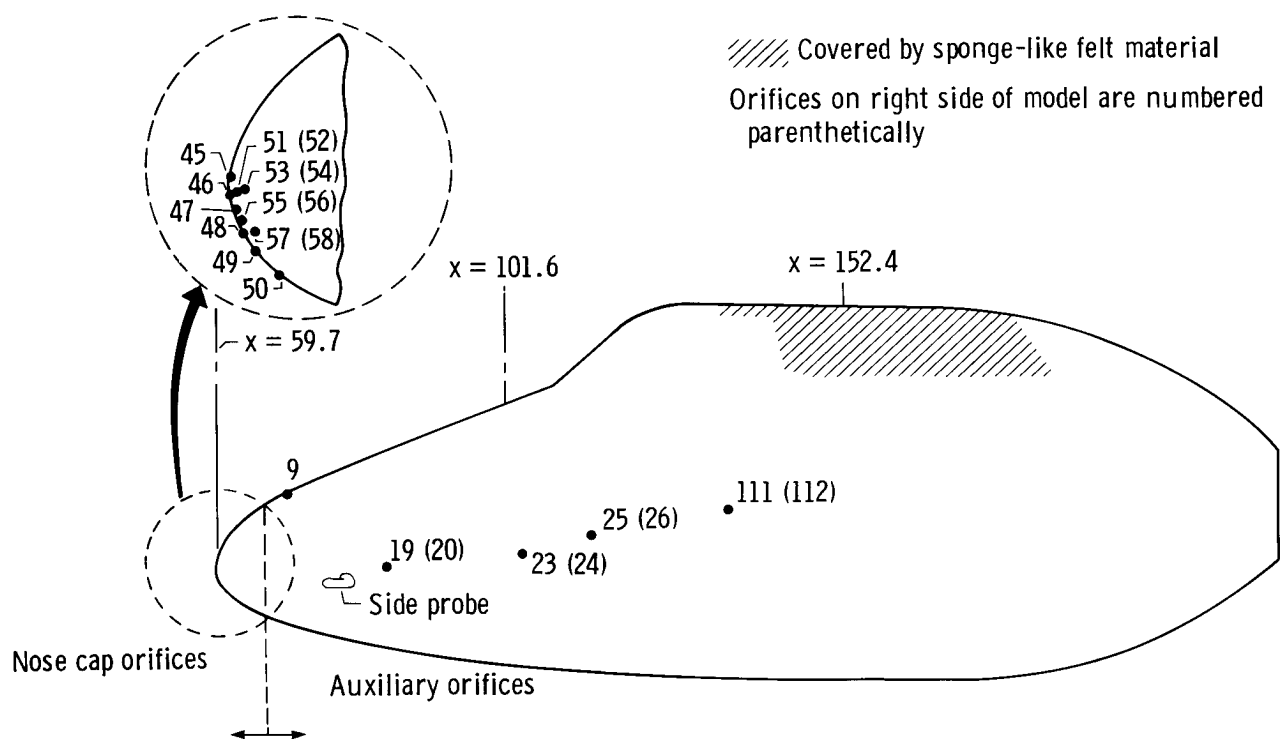


Figure 2. Pressure orifice locations on 0.1 scale wind tunnel model. Fuselage stations are in centimeters.

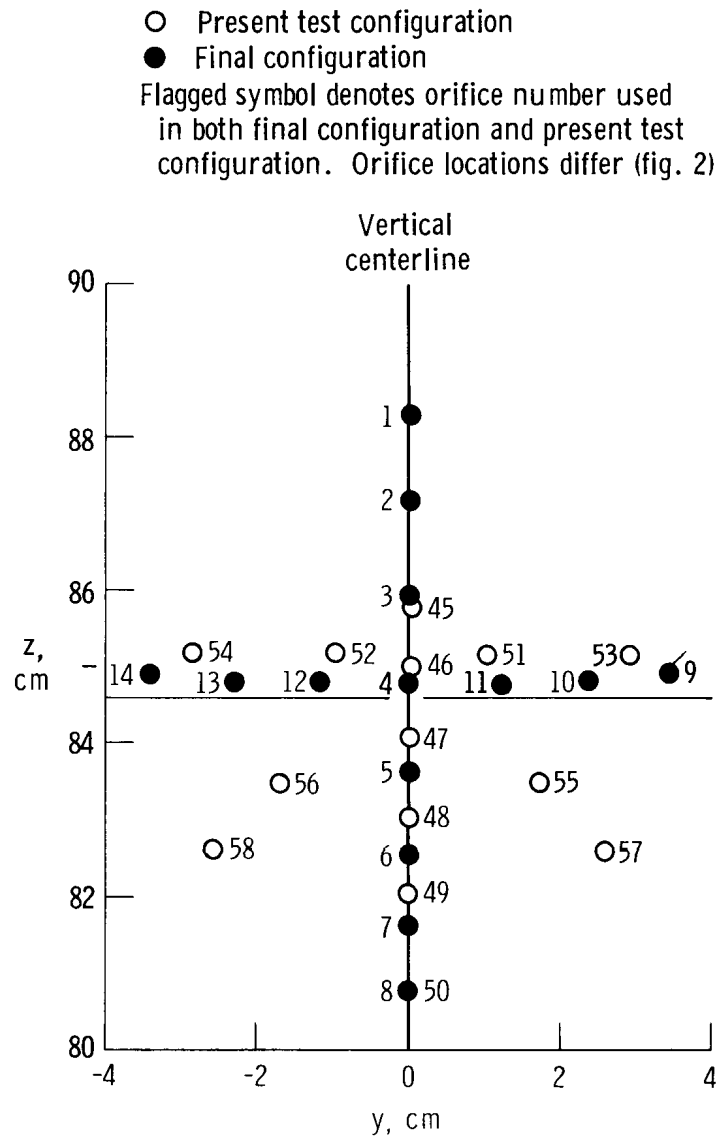
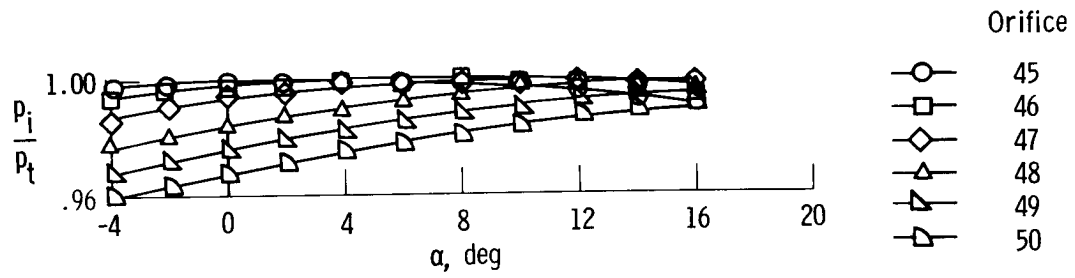
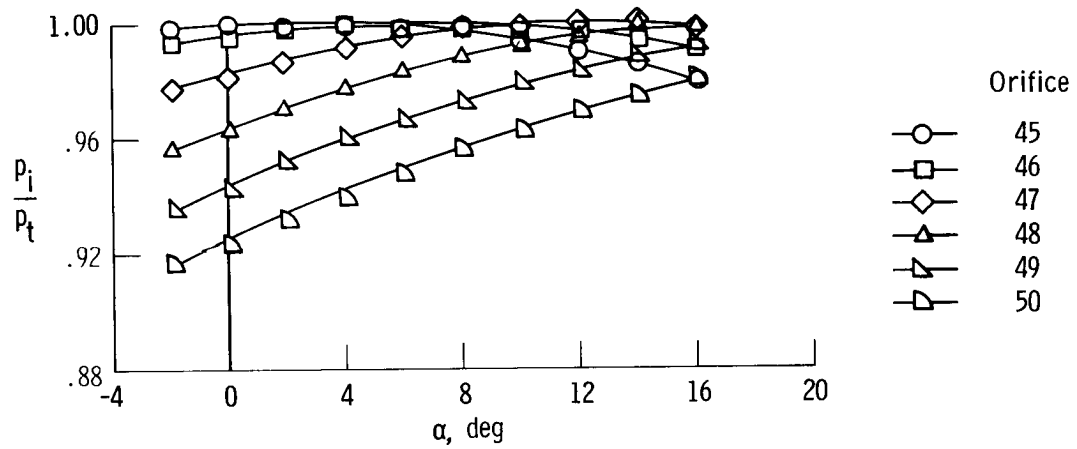


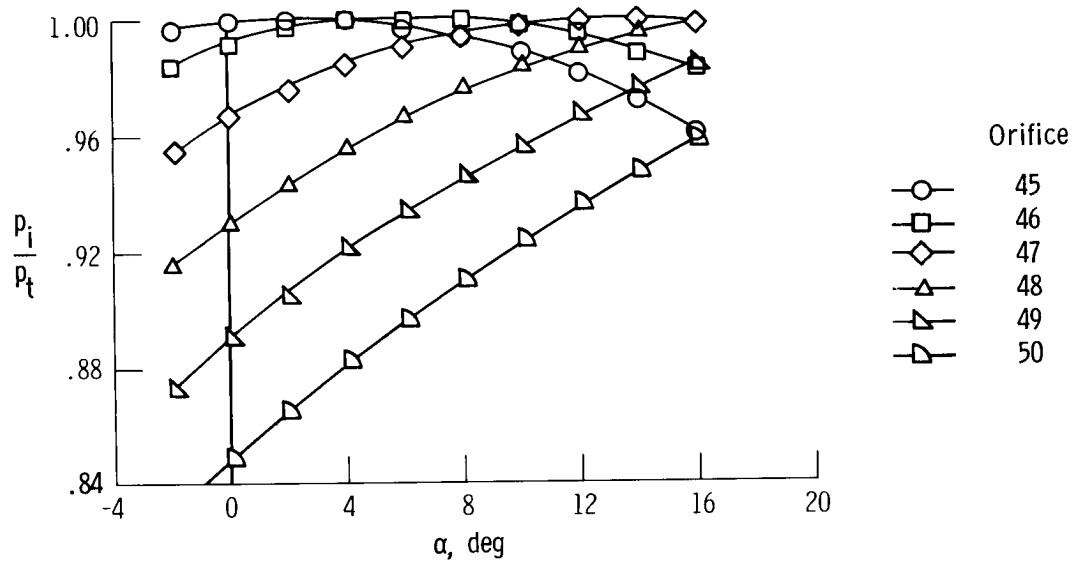
Figure 3. *y-z* coordinates of nose cap orifices. Present tests and final configuration viewed from front.



(a) $M = 0.25$.

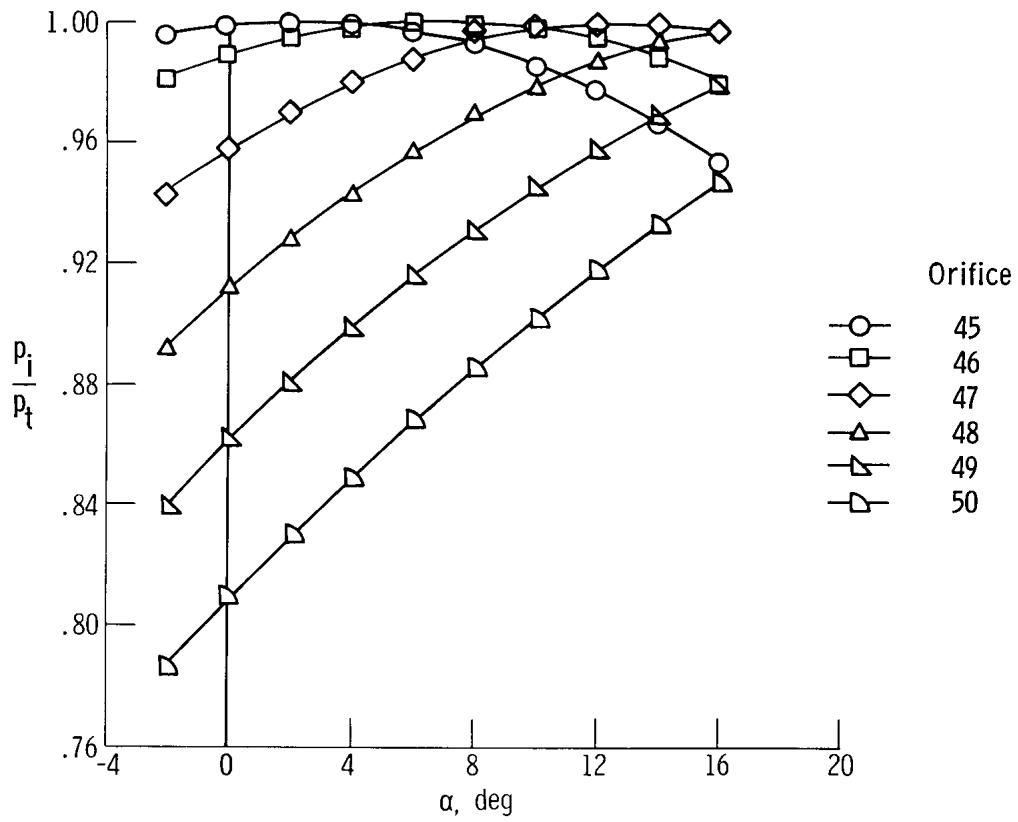


(b) $M = 0.40$.



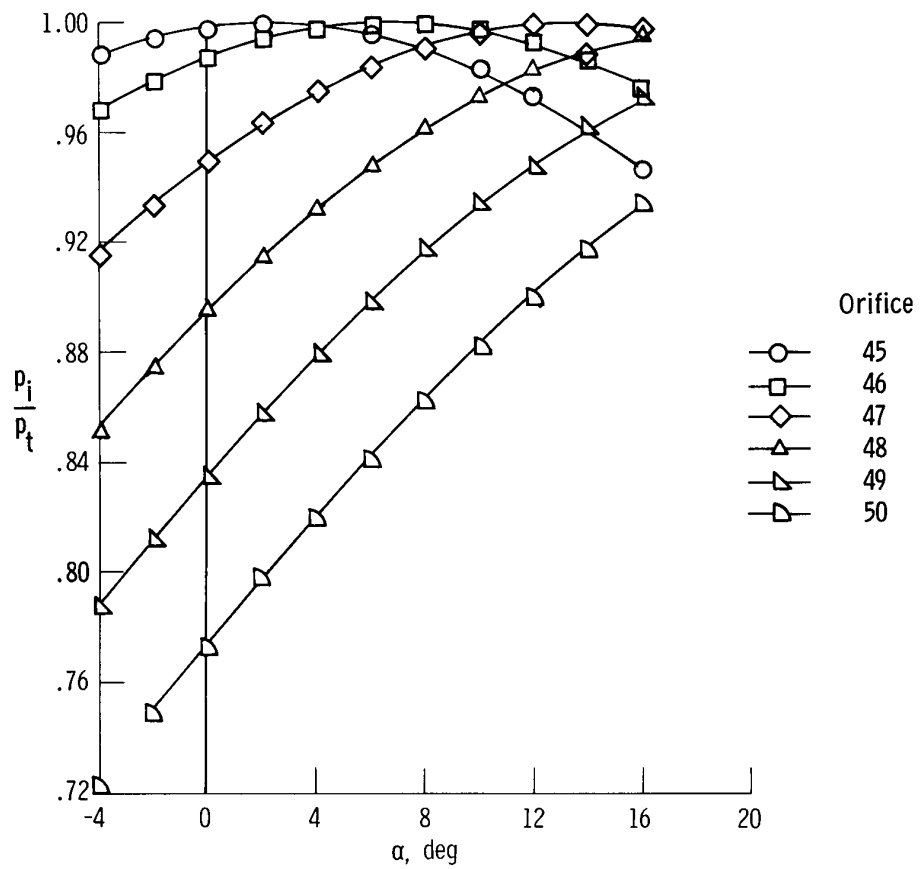
(c) $M = 0.60$.

Figure 4. Ratio of nose cap pressures measured on vertical centerline to total pressure plotted against angle of attack. $\beta = 0^\circ$.



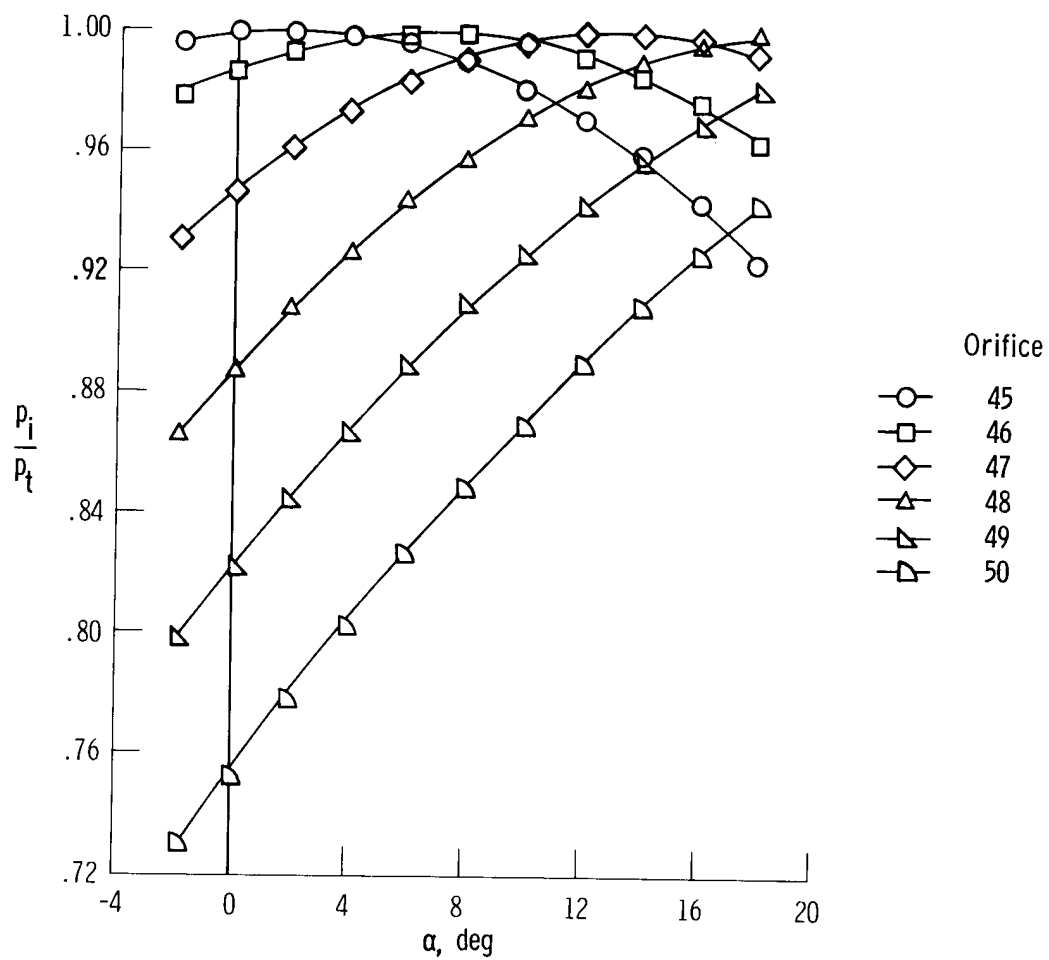
(d) $M = 0.70$.

Figure 4. Continued.



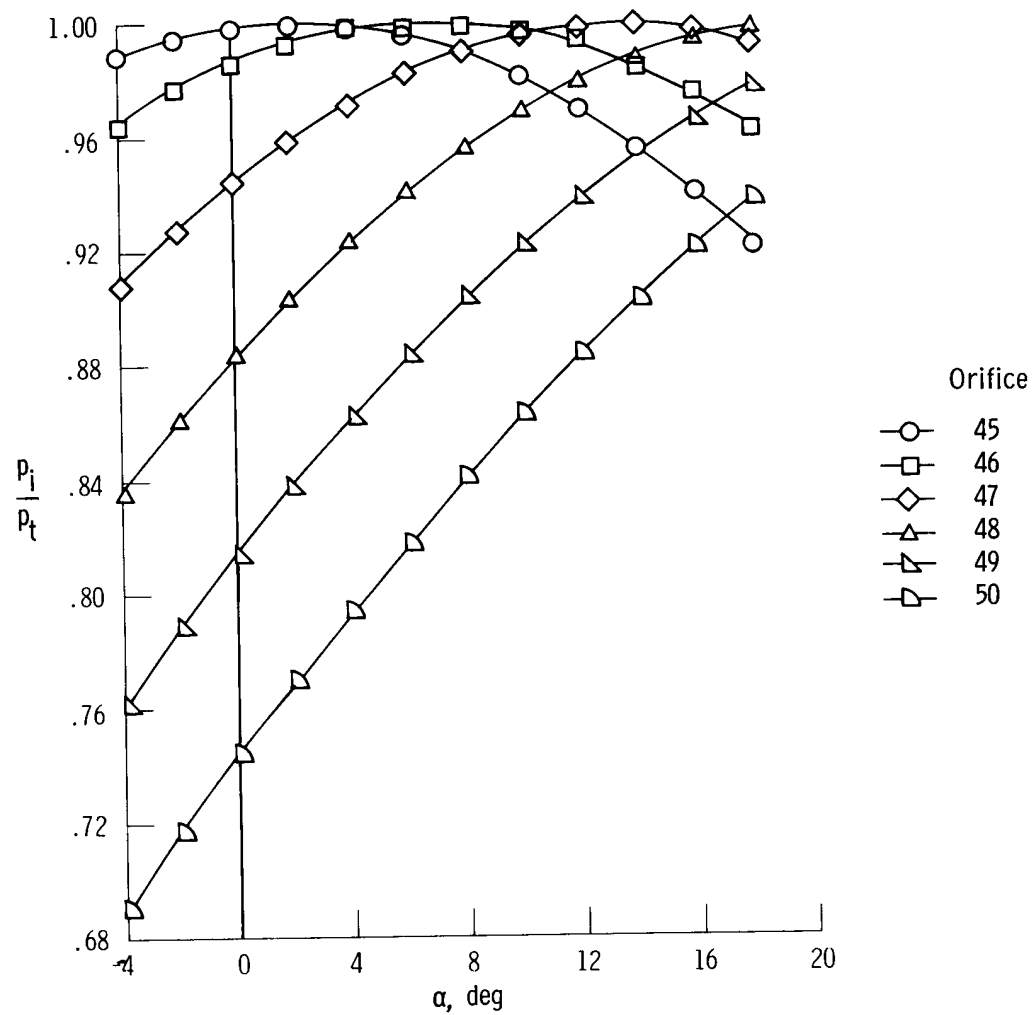
(e) $M = 0.80$.

Figure 4. Continued.



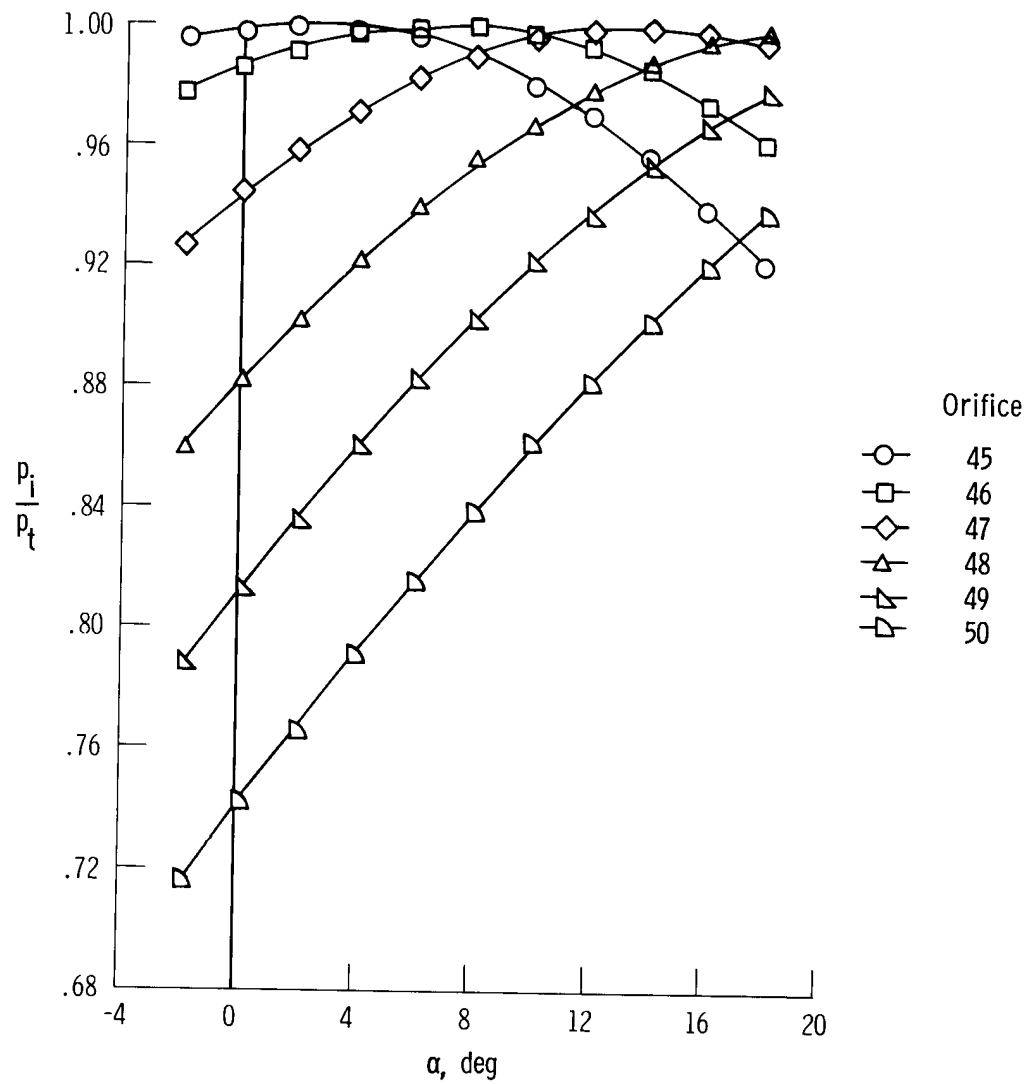
(f) $M = 0.90$.

Figure 4. Continued.



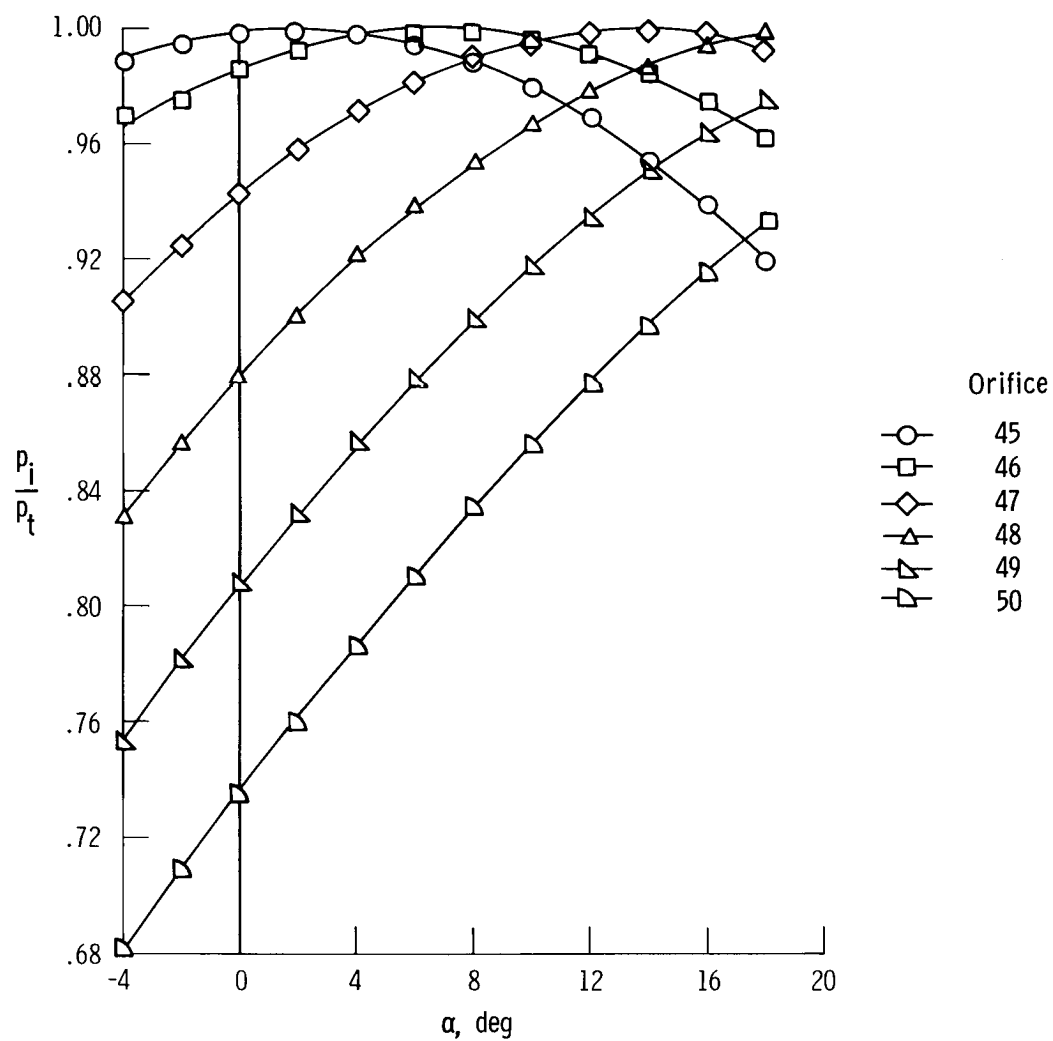
(g) $M = 0.95$.

Figure 4. Continued.



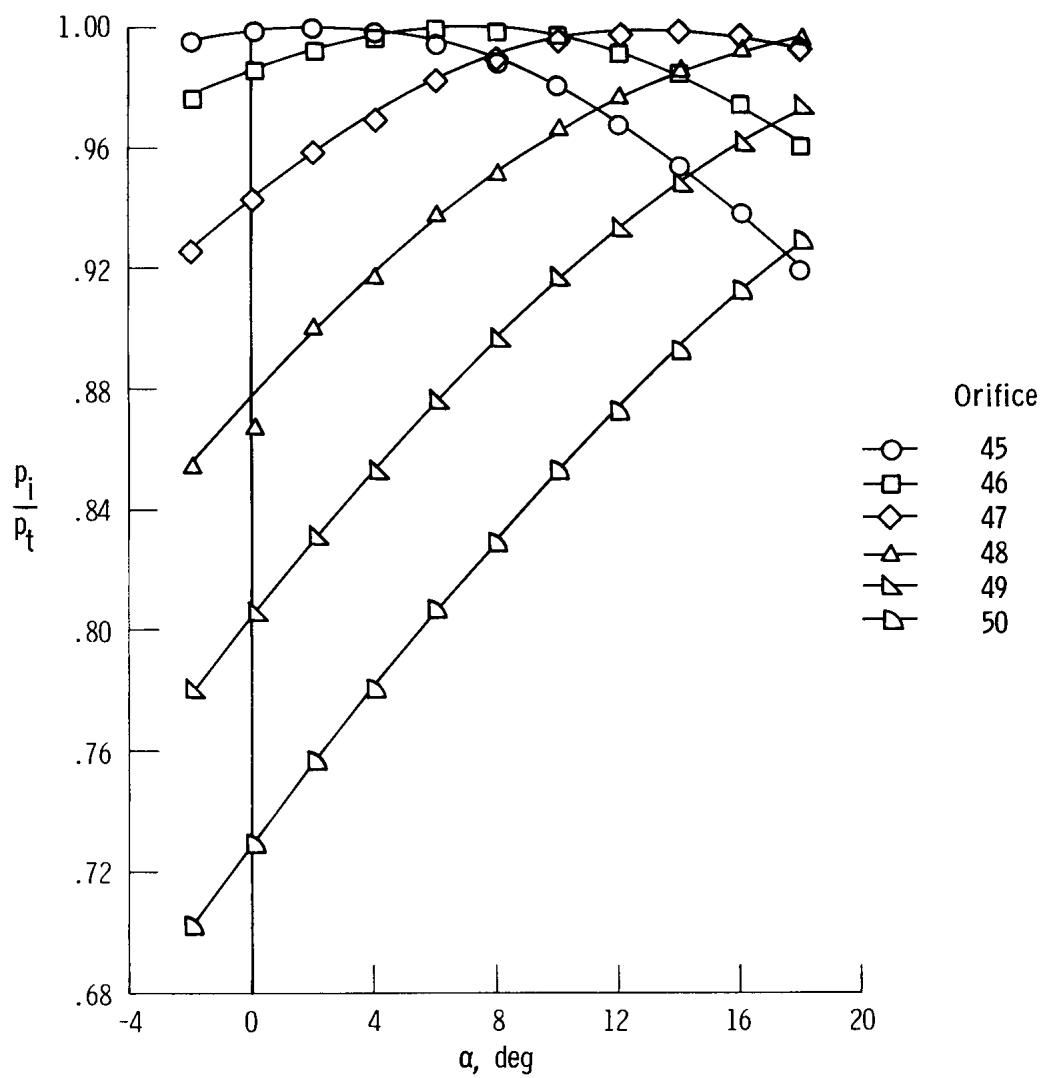
(h) $M = 0.98$.

Figure 4. Continued.



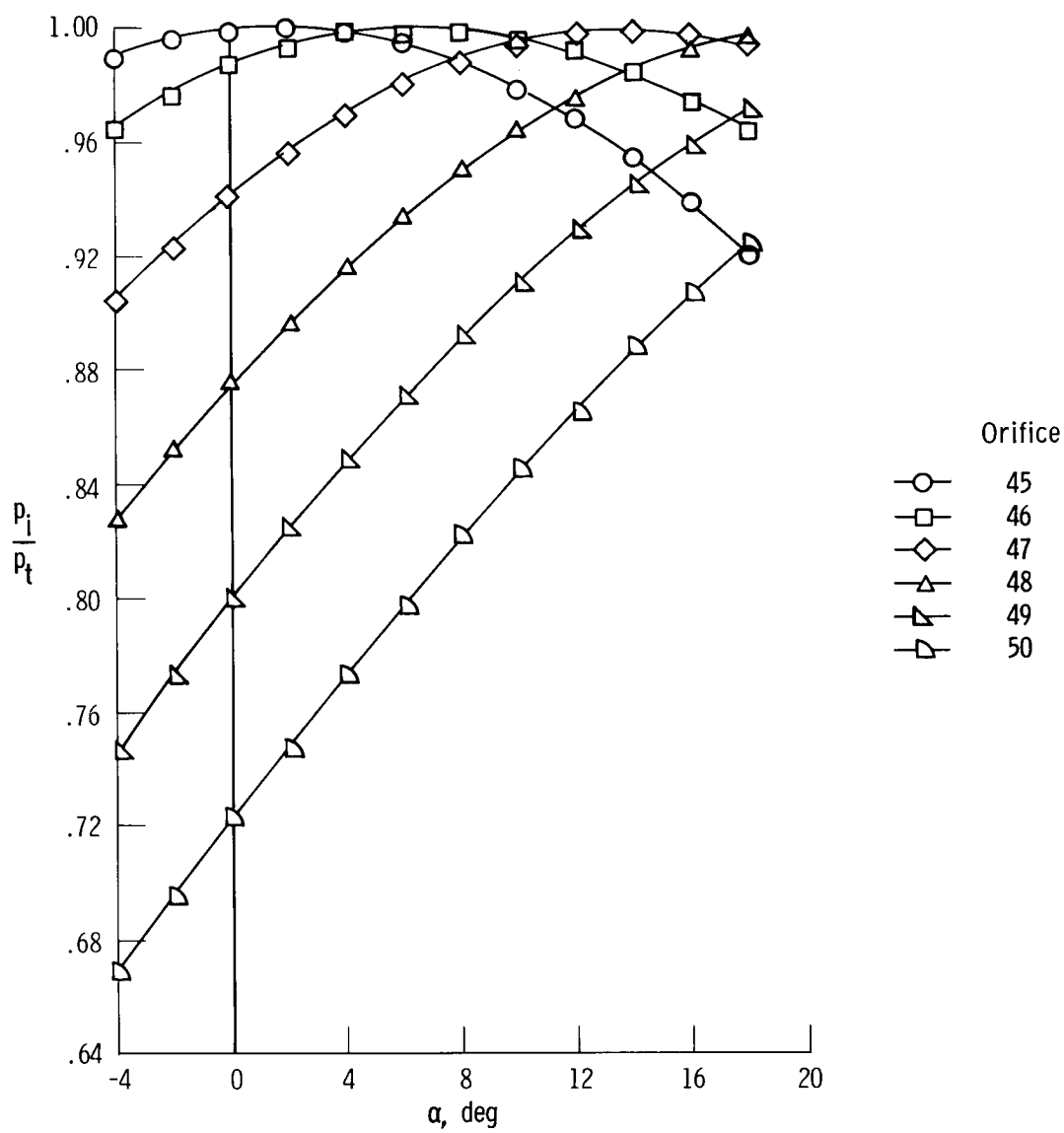
(i) $M = 1.05$.

Figure 4. Continued.



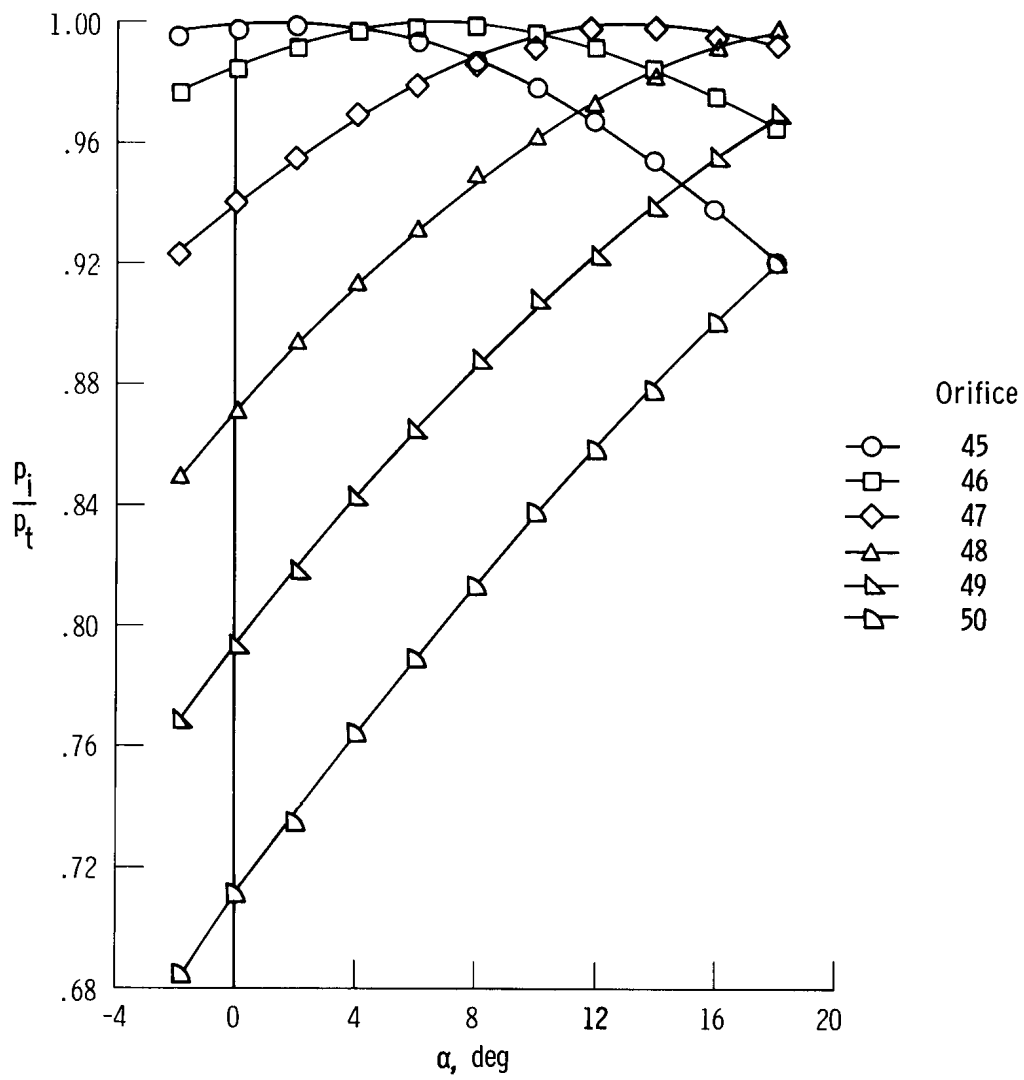
(j) $M = 1.10$.

Figure 4. Continued.



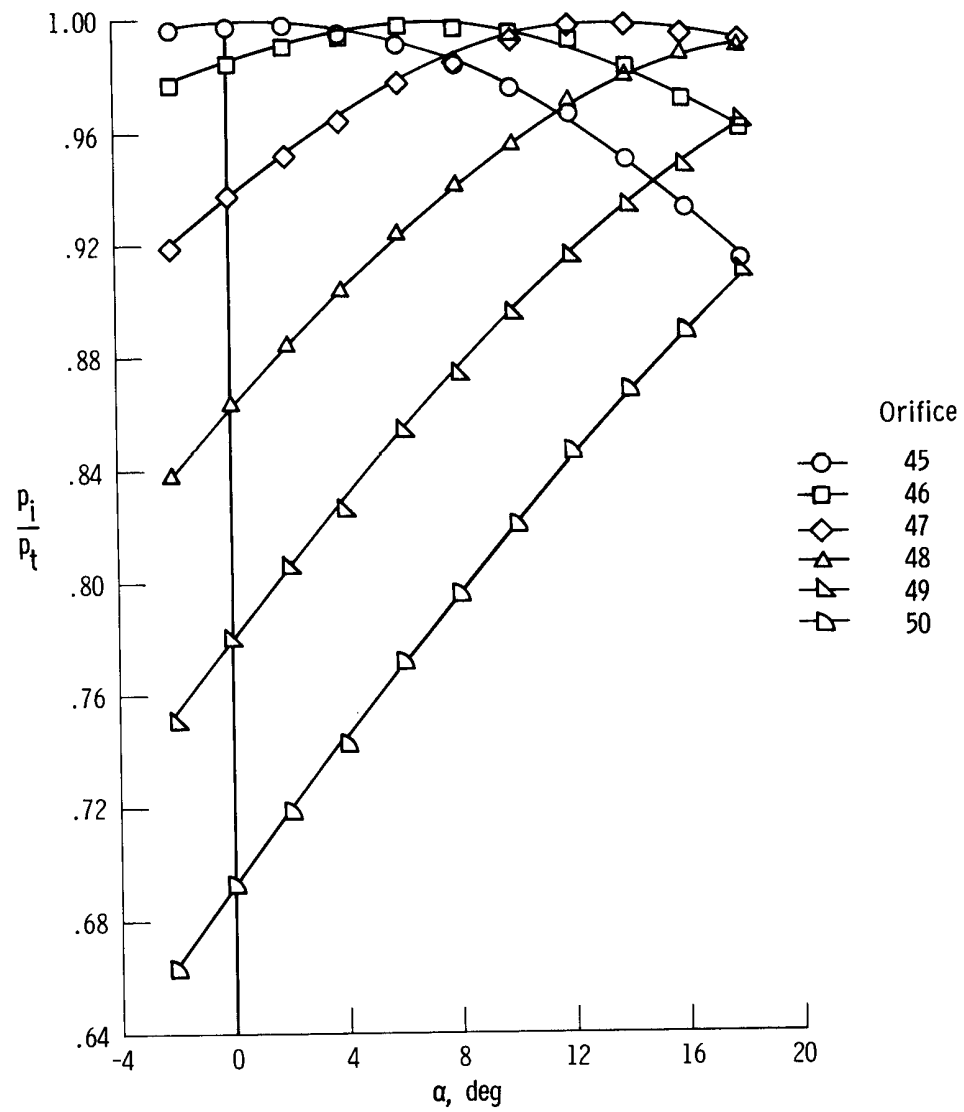
(k) $M = 1.15$.

Figure 4. Continued.



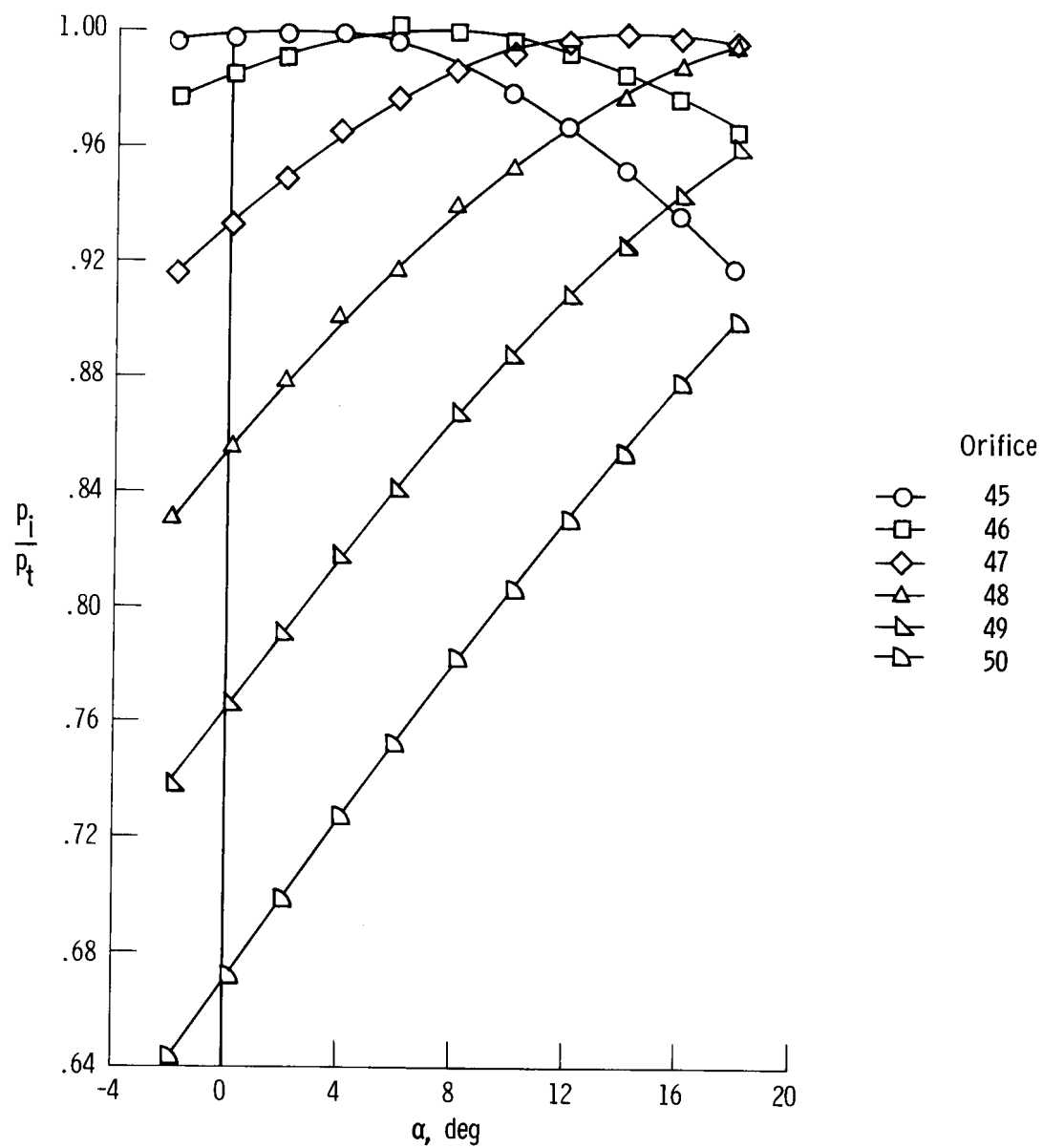
(1) $M = 1.20$.

Figure 4. Continued.



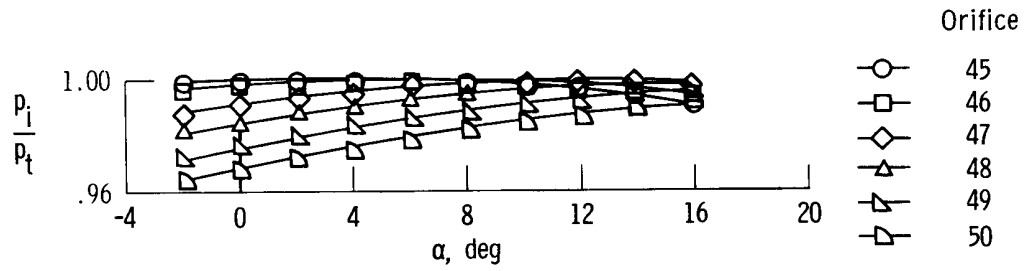
(m) $M = 1.30$.

Figure 4. Continued.

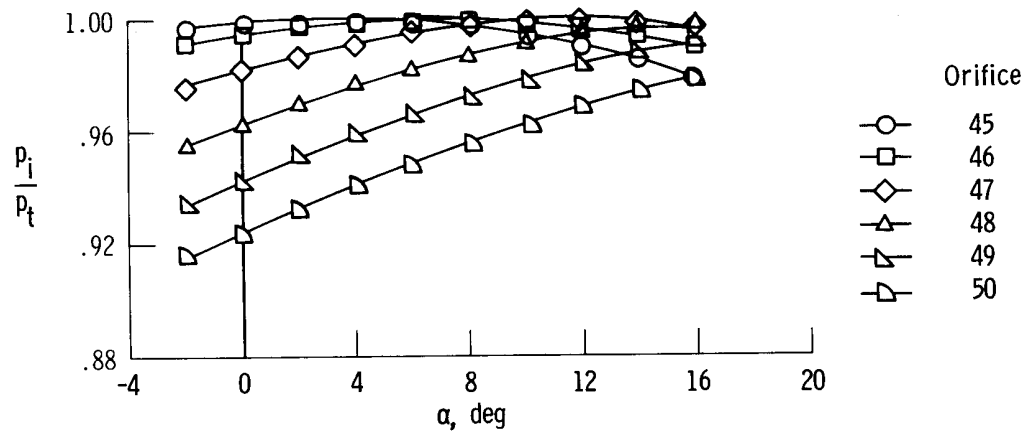


(n) $M = 1.40$.

Figure 4. Concluded.

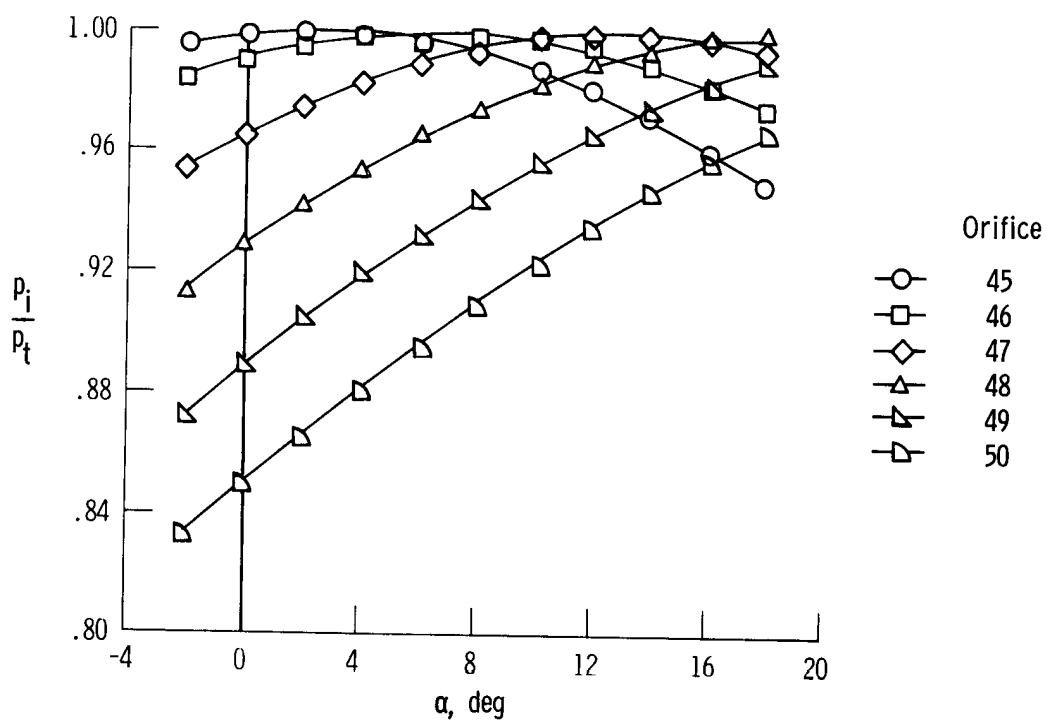


(a) $M = 0.25$.



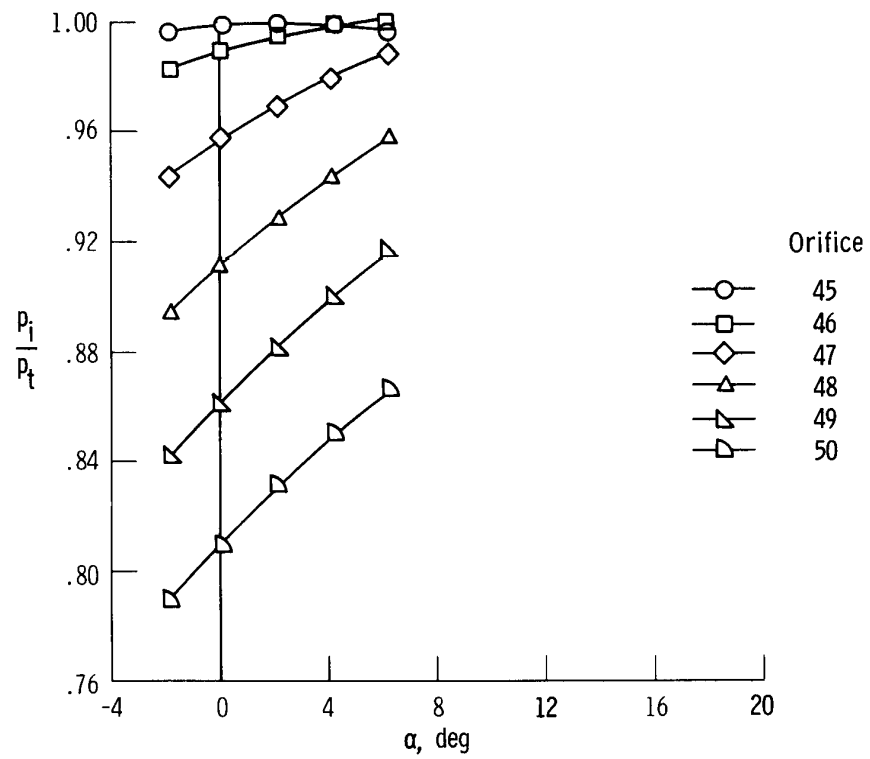
(b) $M = 0.40$.

Figure 5. Ratio of nose cap pressures measured on vertical centerline to total pressure plotted against angle of attack. $\beta = 2^\circ$.



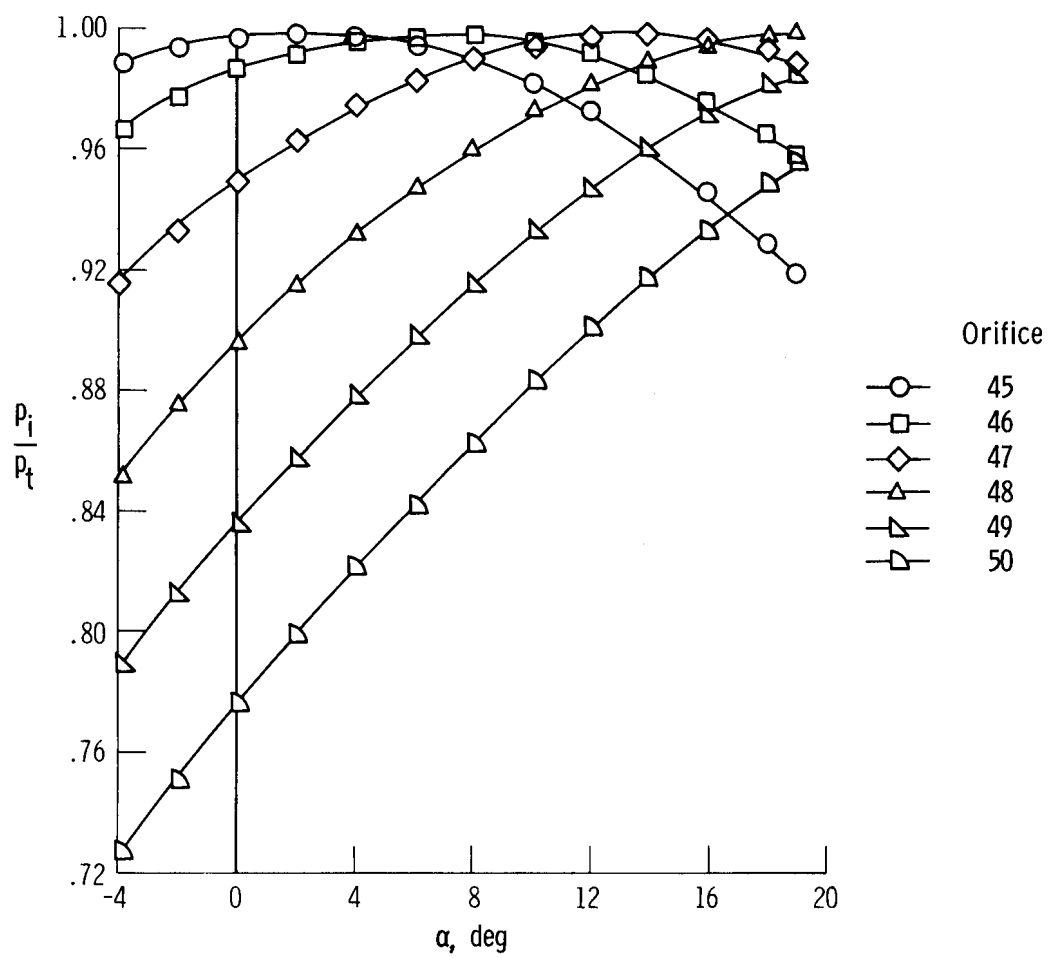
(c) $M = 0.60$.

Figure 5. Continued.



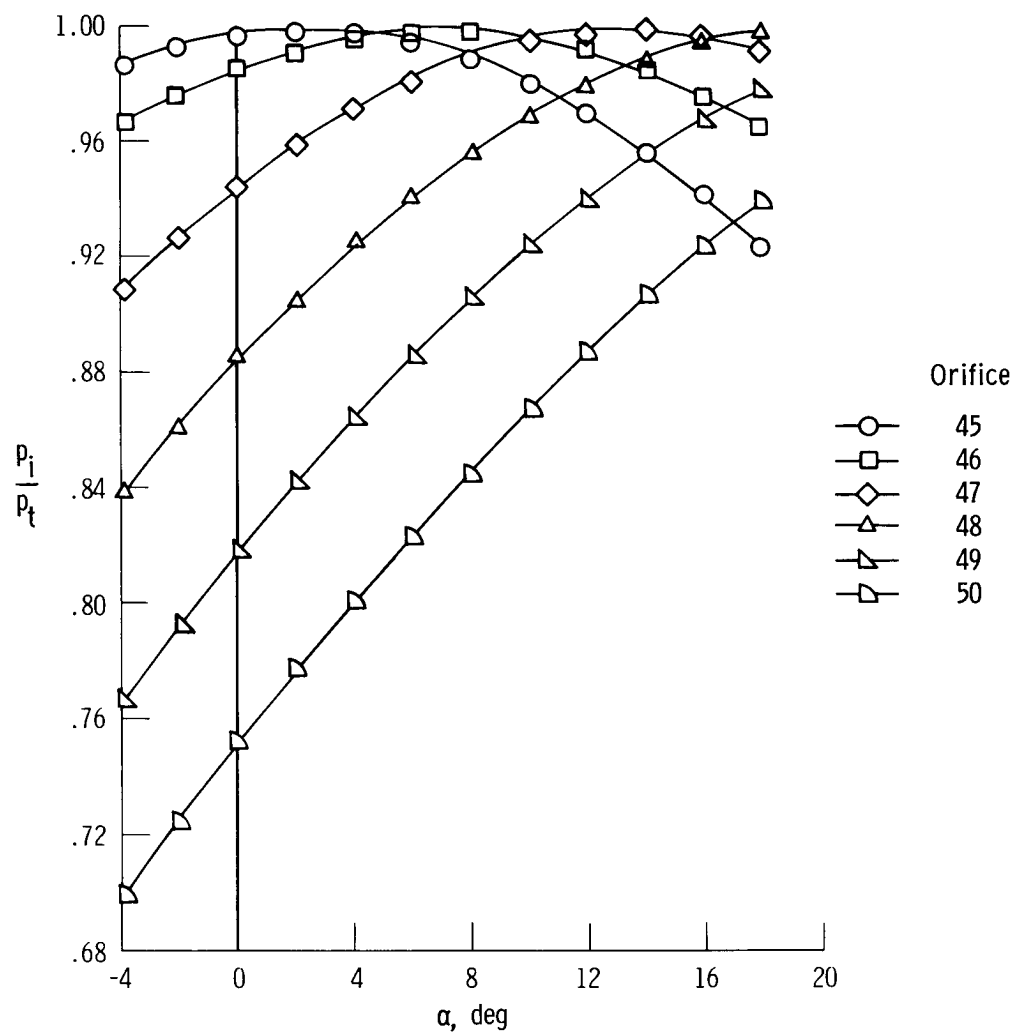
(d) $M = 0.70$.

Figure 5. Continued.



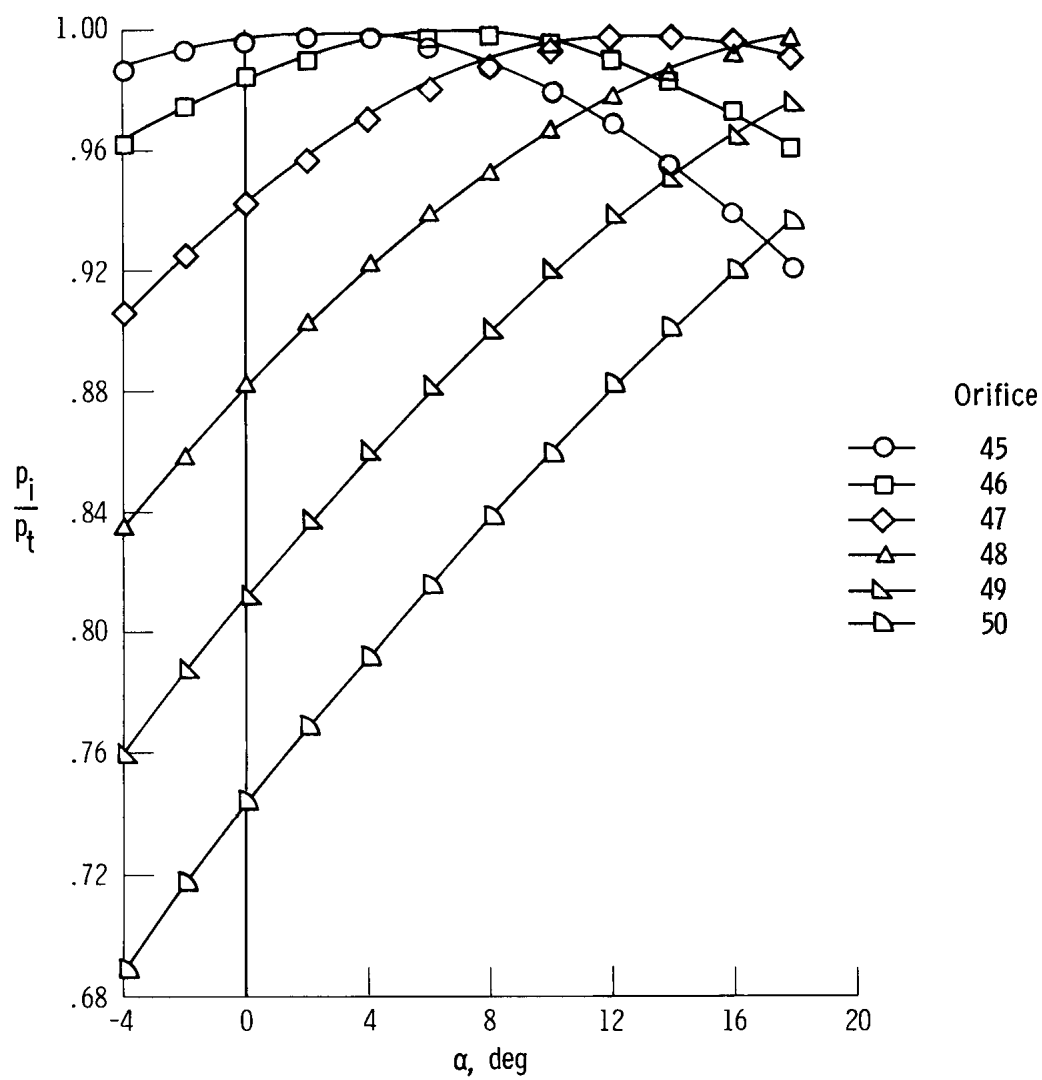
(e) $M = 0.80$.

Figure 5. Continued.



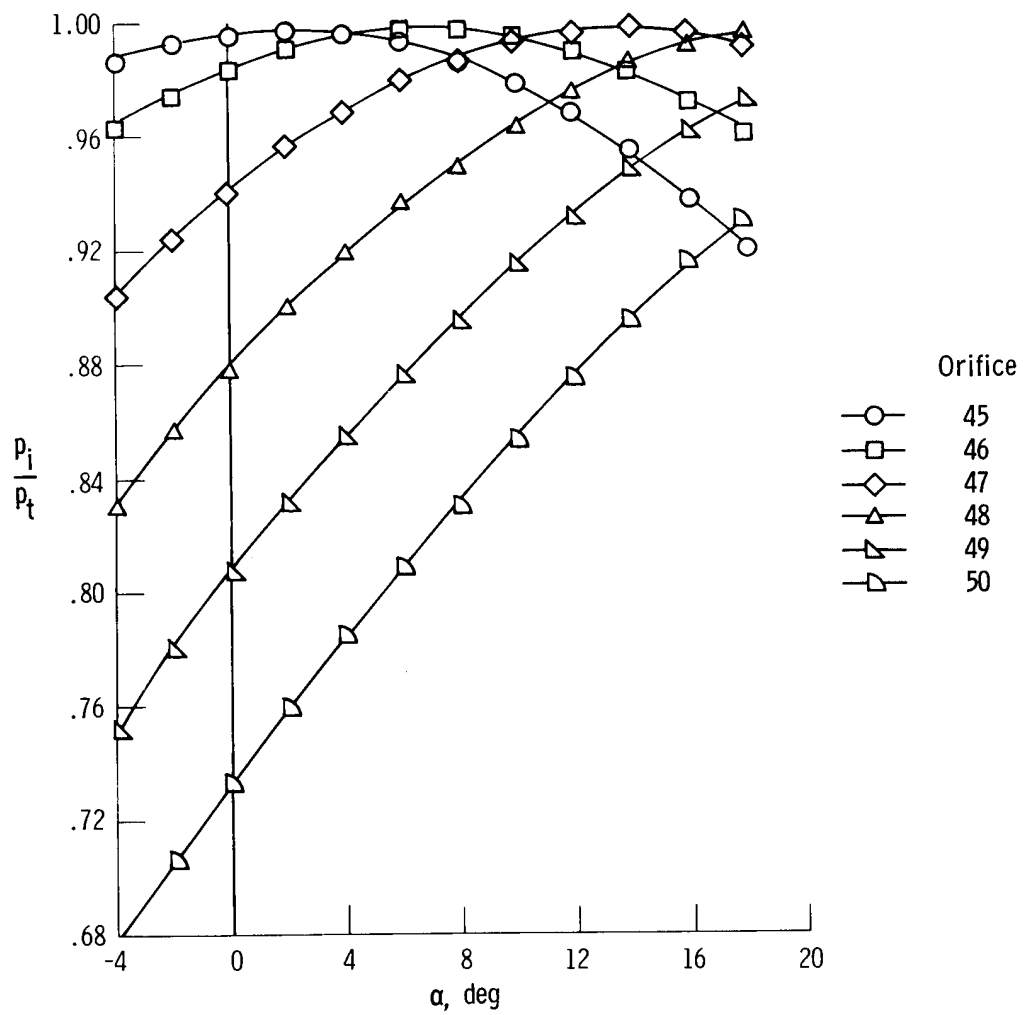
(f) $M = 0.90$.

Figure 5. Continued.



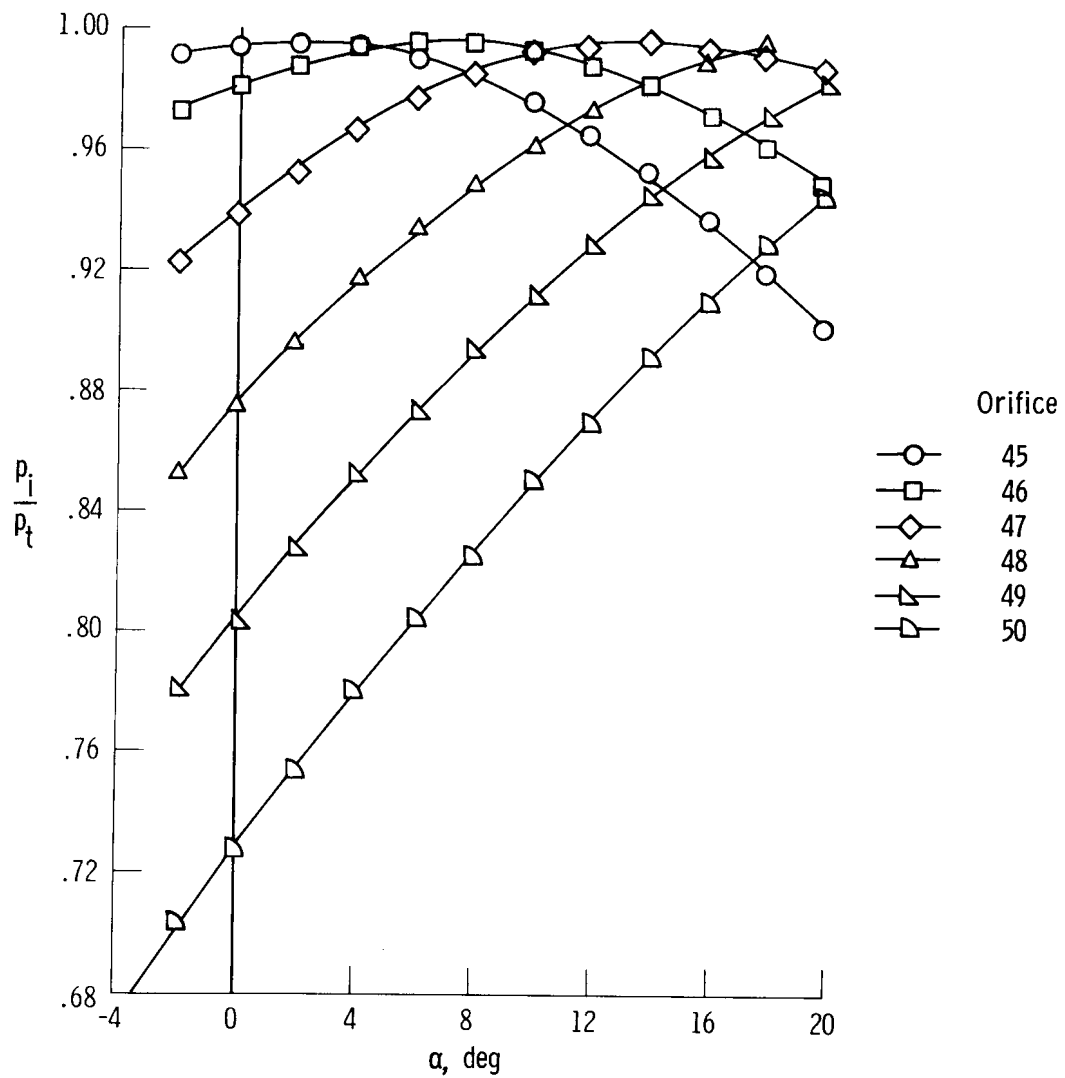
(g) $M = 0.95$.

Figure 5. Continued.



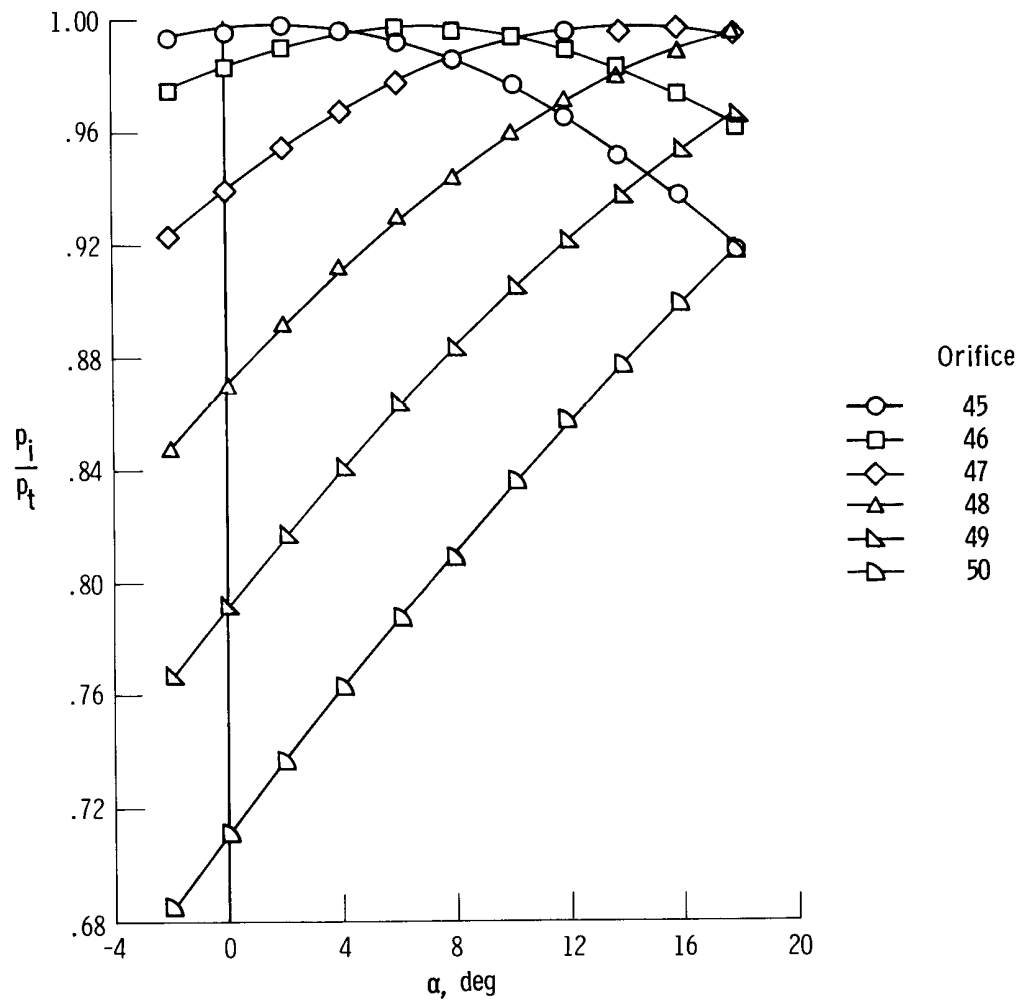
(h) $M = 1.05$.

Figure 5. Continued.



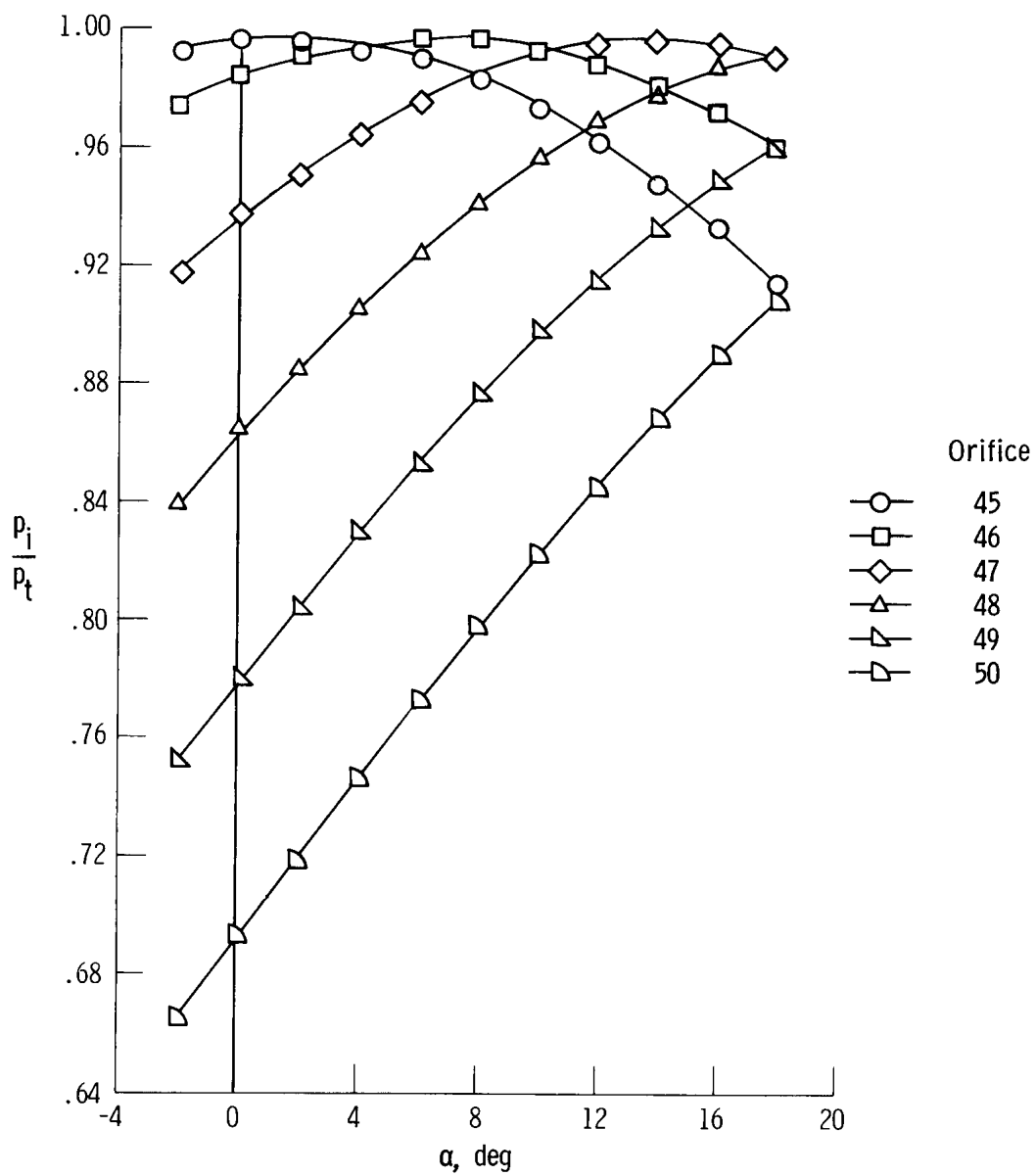
(i) $M = 1.10$.

Figure 5. Continued.



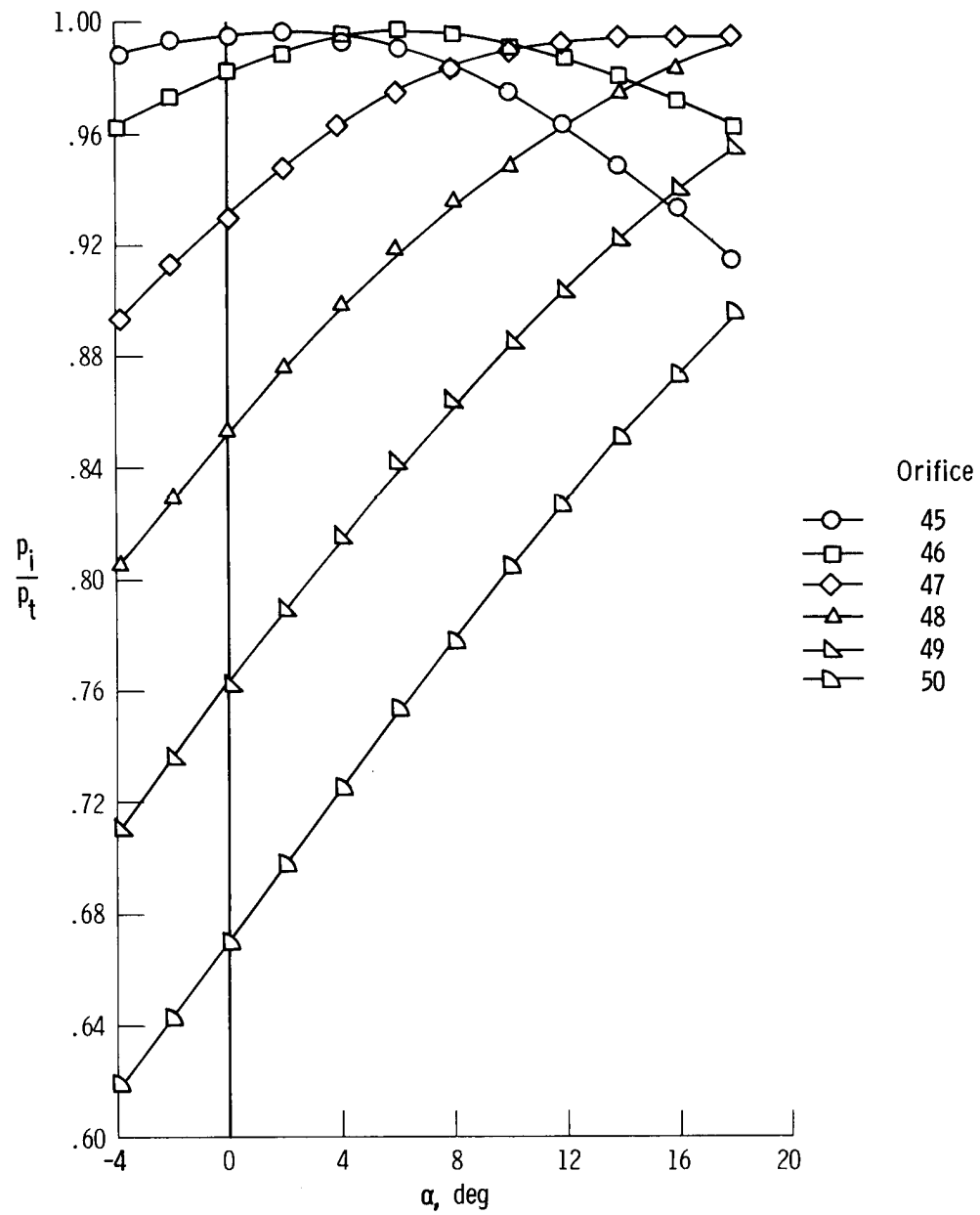
(j) $M = 1.20$.

Figure 5. Continued.



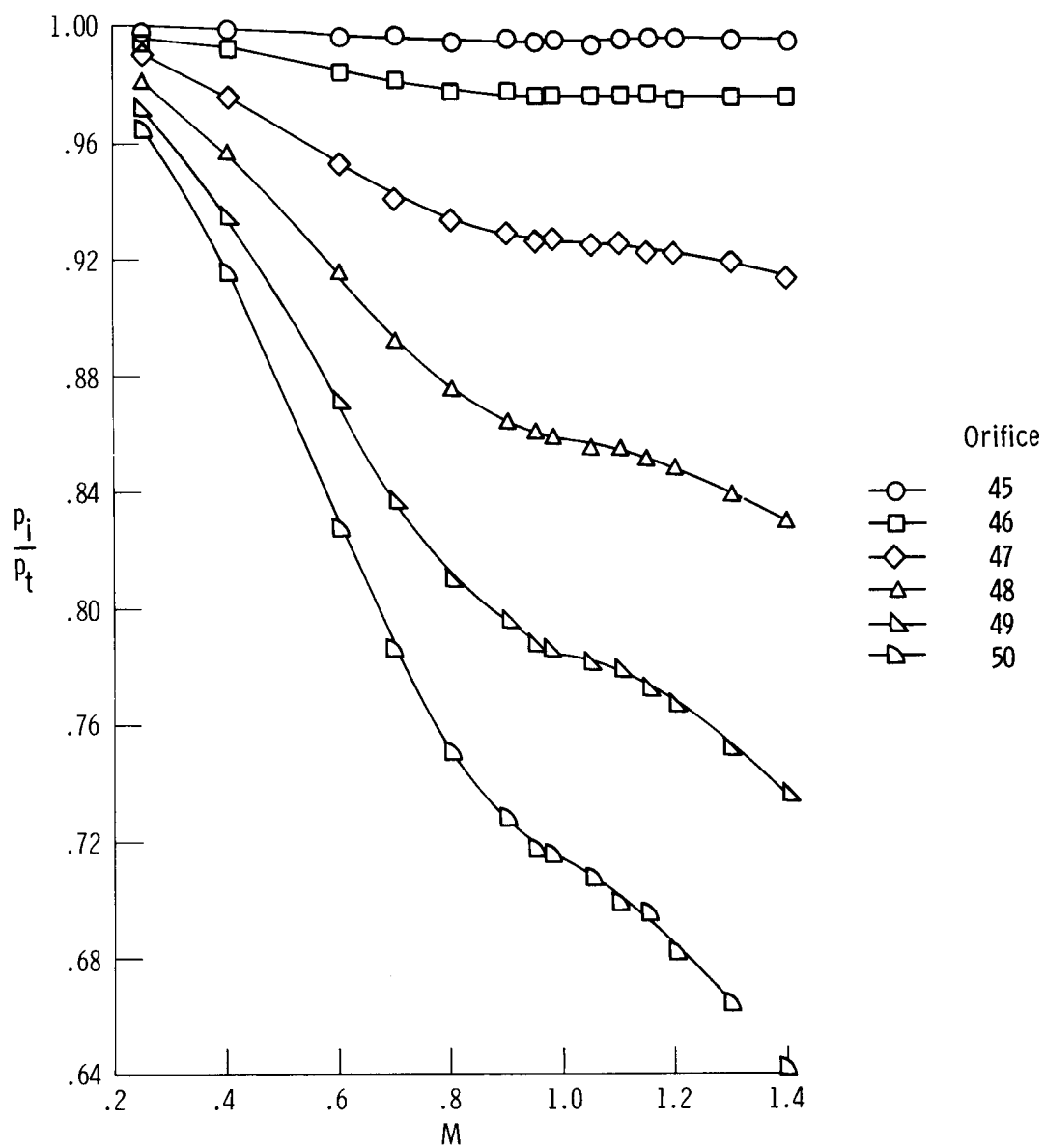
(k) $M = 1.30$.

Figure 5. Continued.



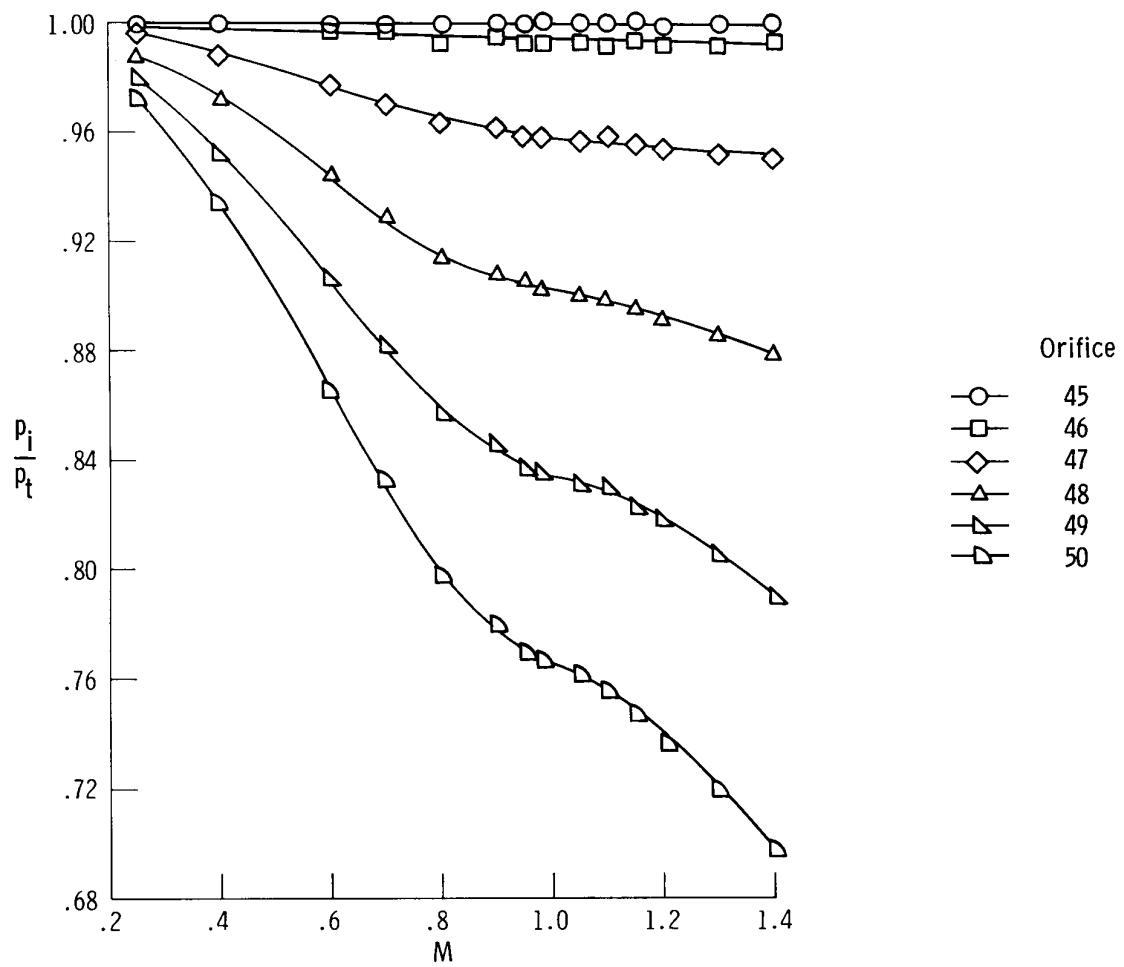
(1) $M = 1.40$.

Figure 5. Concluded.



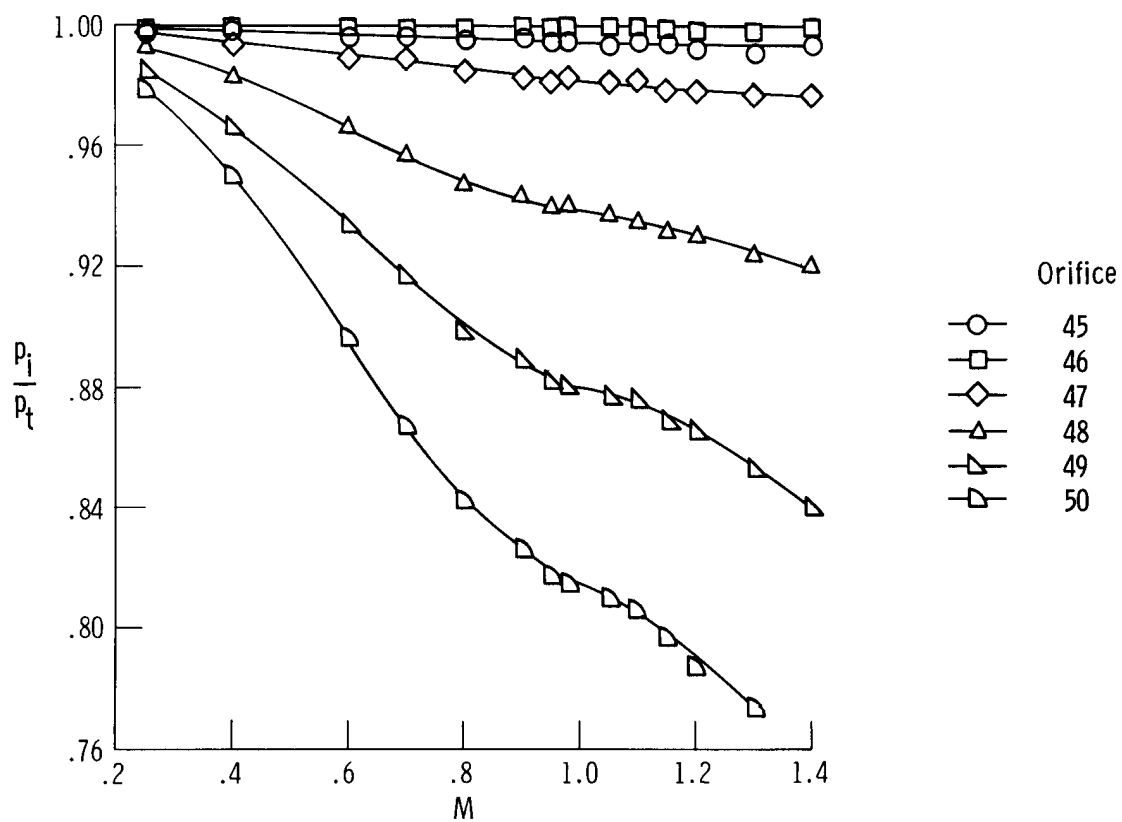
(a) $\alpha = -2^\circ$.

Figure 6. Ratio of nose cap pressures measured on vertical centerline to total pressure plotted against Mach number. $\beta = 0^\circ$.



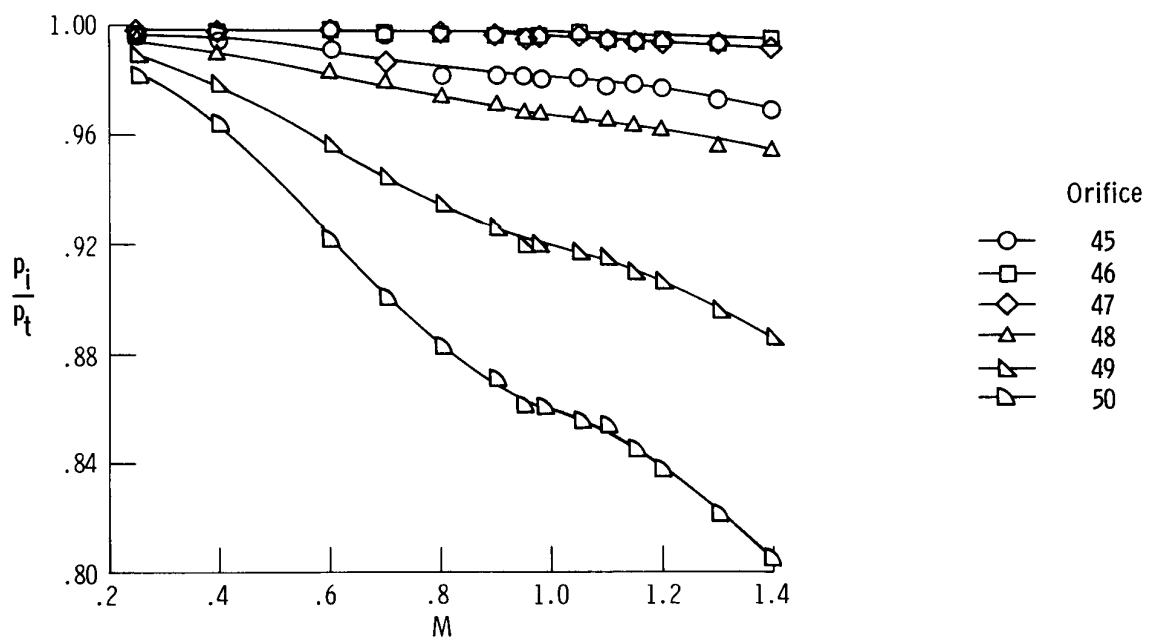
(b) $\alpha = 2^\circ$.

Figure 6. Continued.



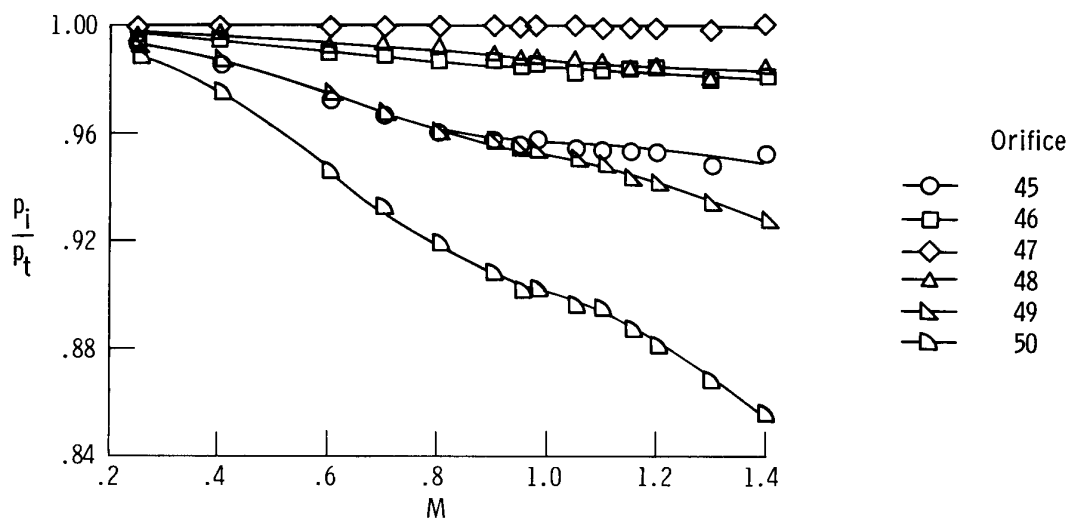
(c) $\alpha = 6^\circ$.

Figure 6. Continued.



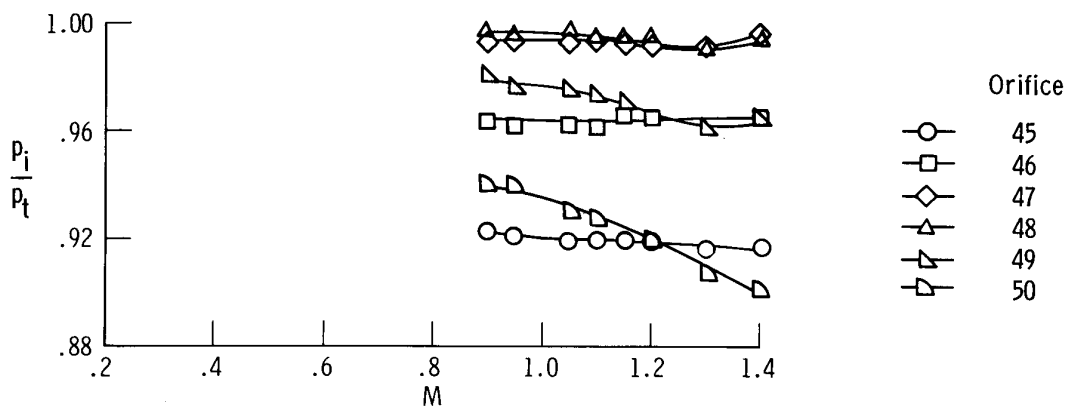
(d) $\alpha = 10^\circ$.

Figure 6. Continued.



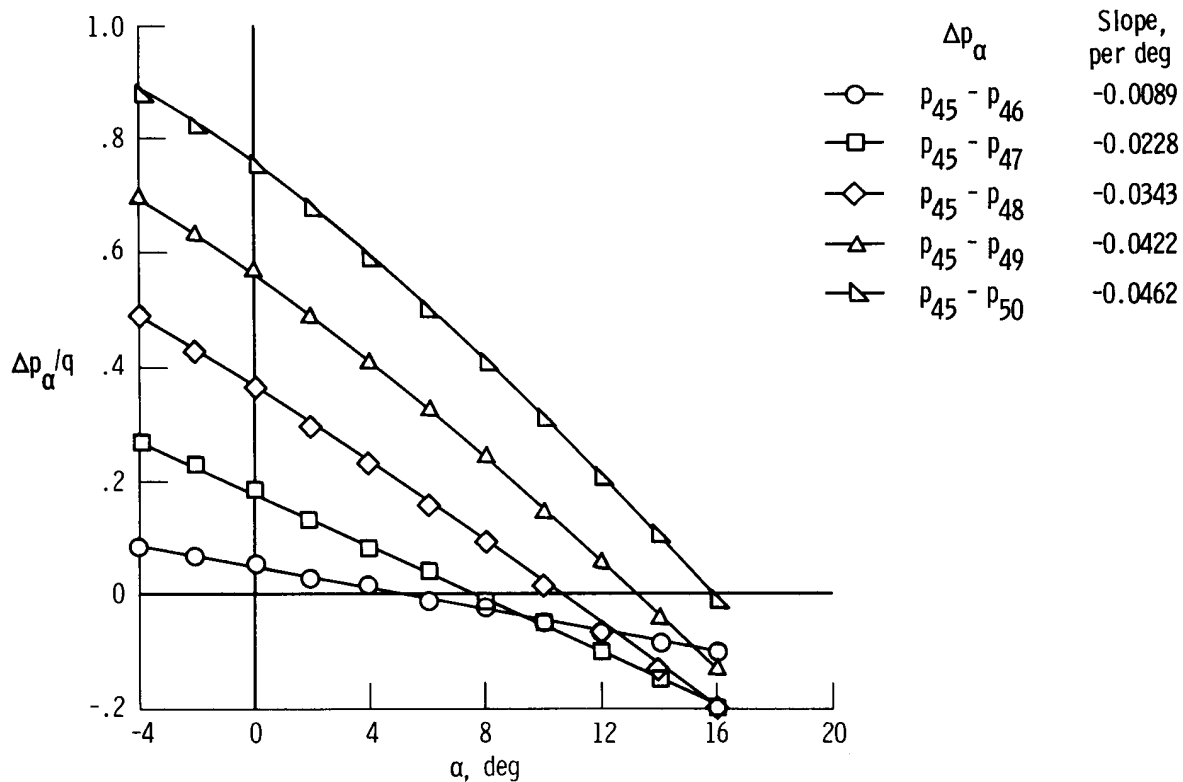
(e) $\alpha = 14^\circ$.

Figure 6. Continued.



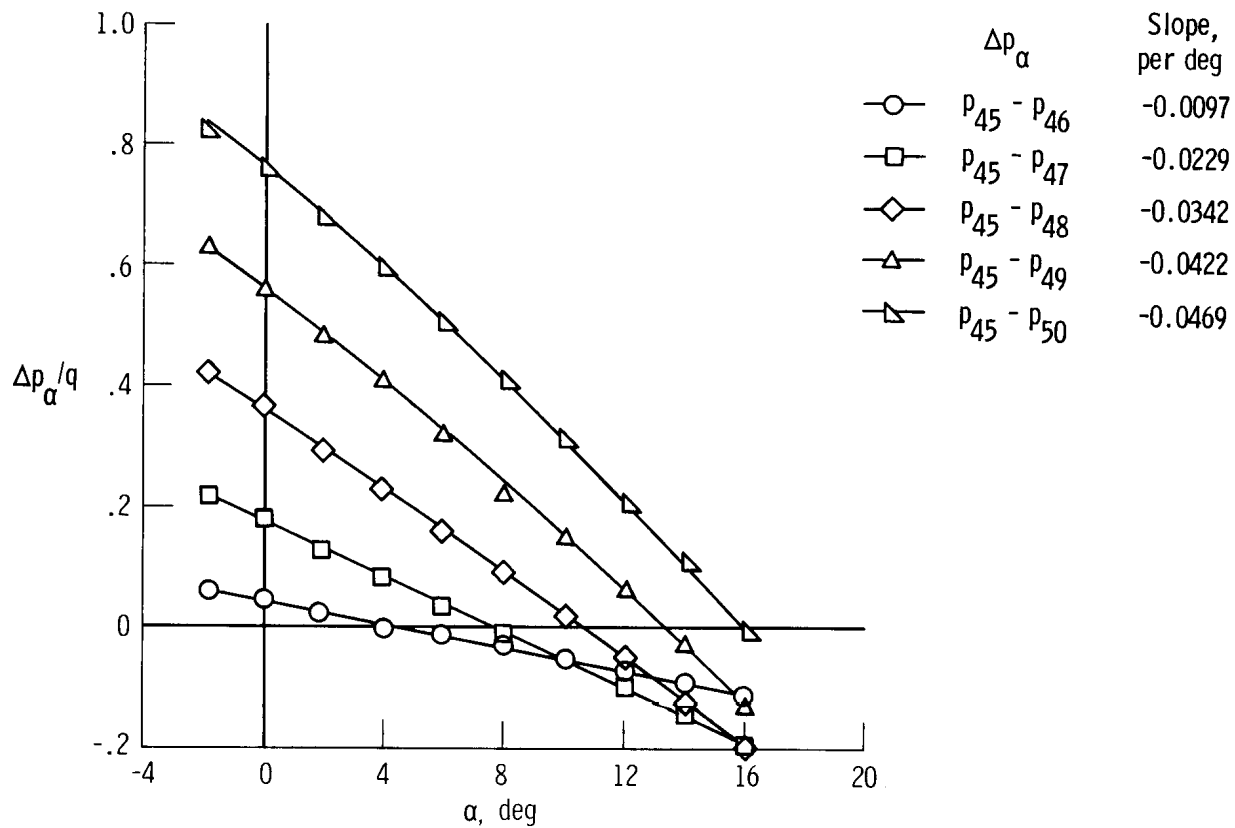
(f) $\alpha = 18^\circ$.

Figure 6. Concluded.



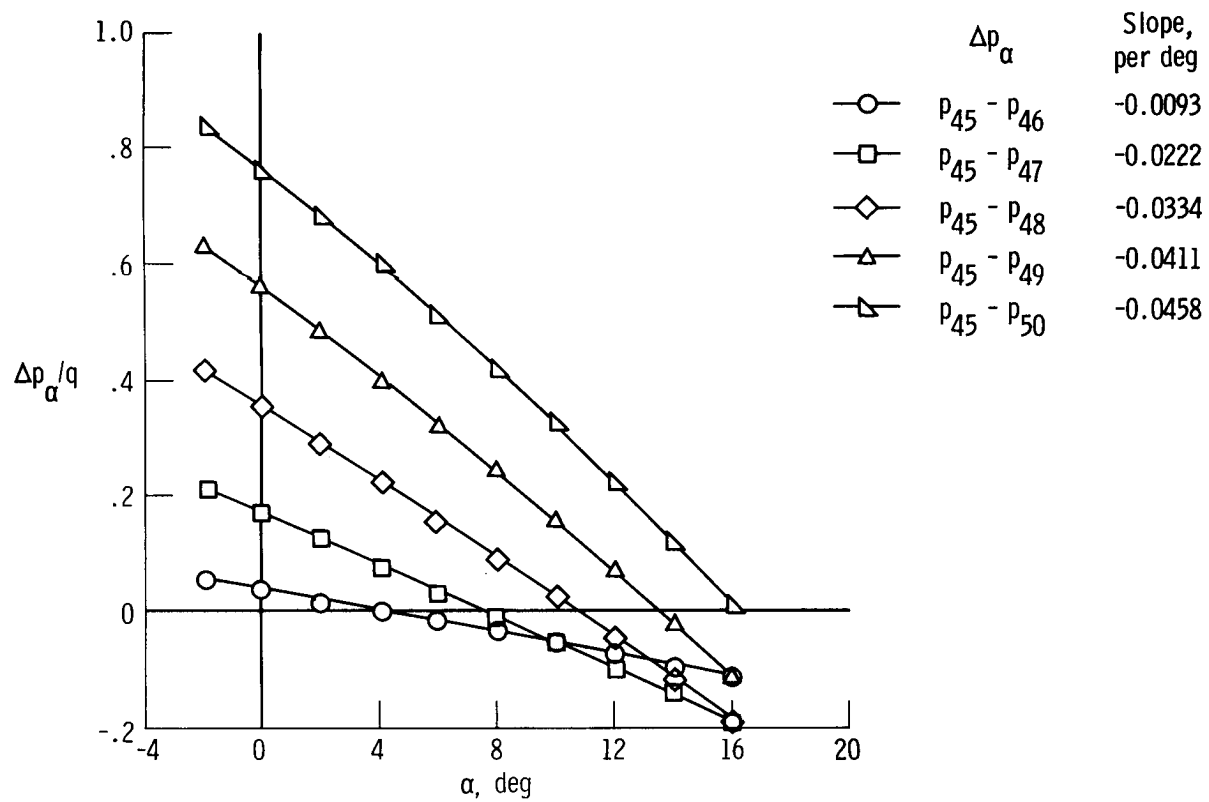
(a) $M = 0.25$.

Figure 7. Pressure parameter for selected nose cap orifices plotted against angle of attack. $\beta = 0^\circ$; orifice 45 reference.



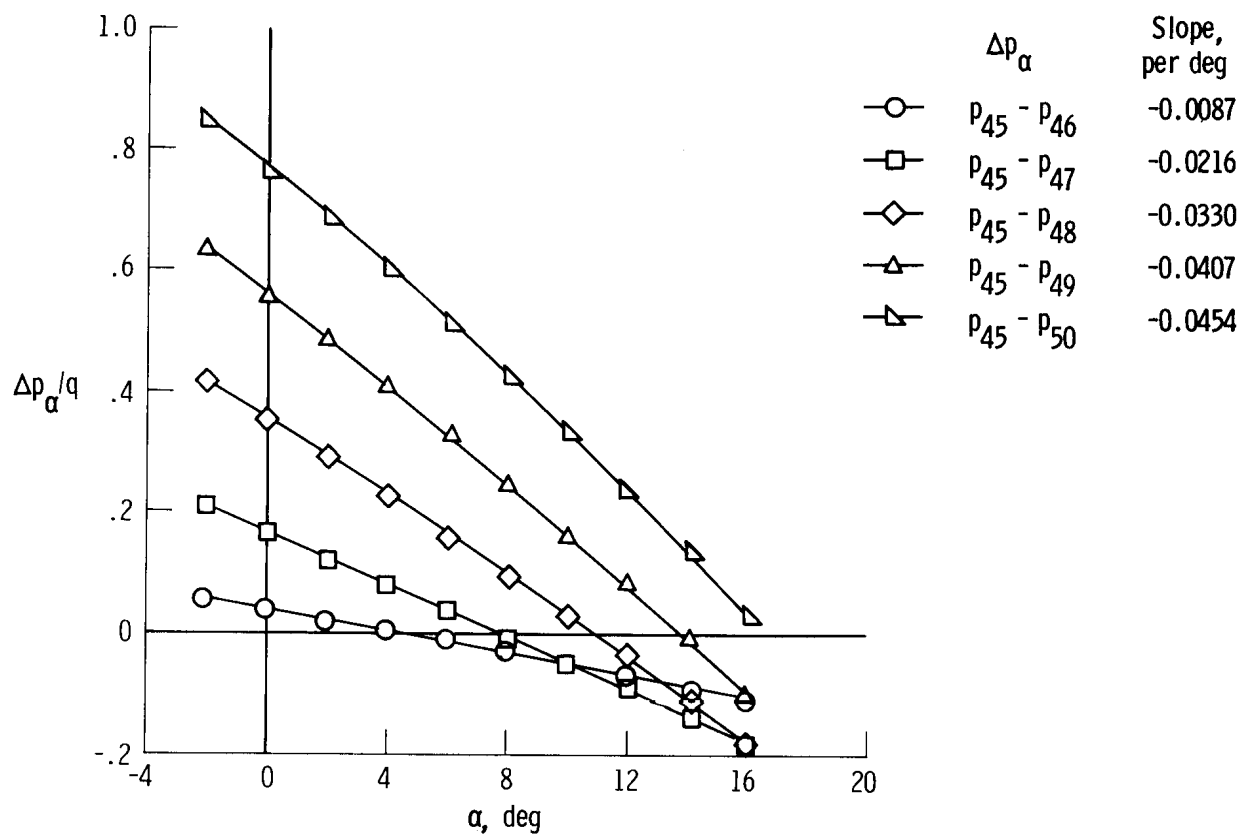
(b) $M = 0.40$.

Figure 7. Continued.



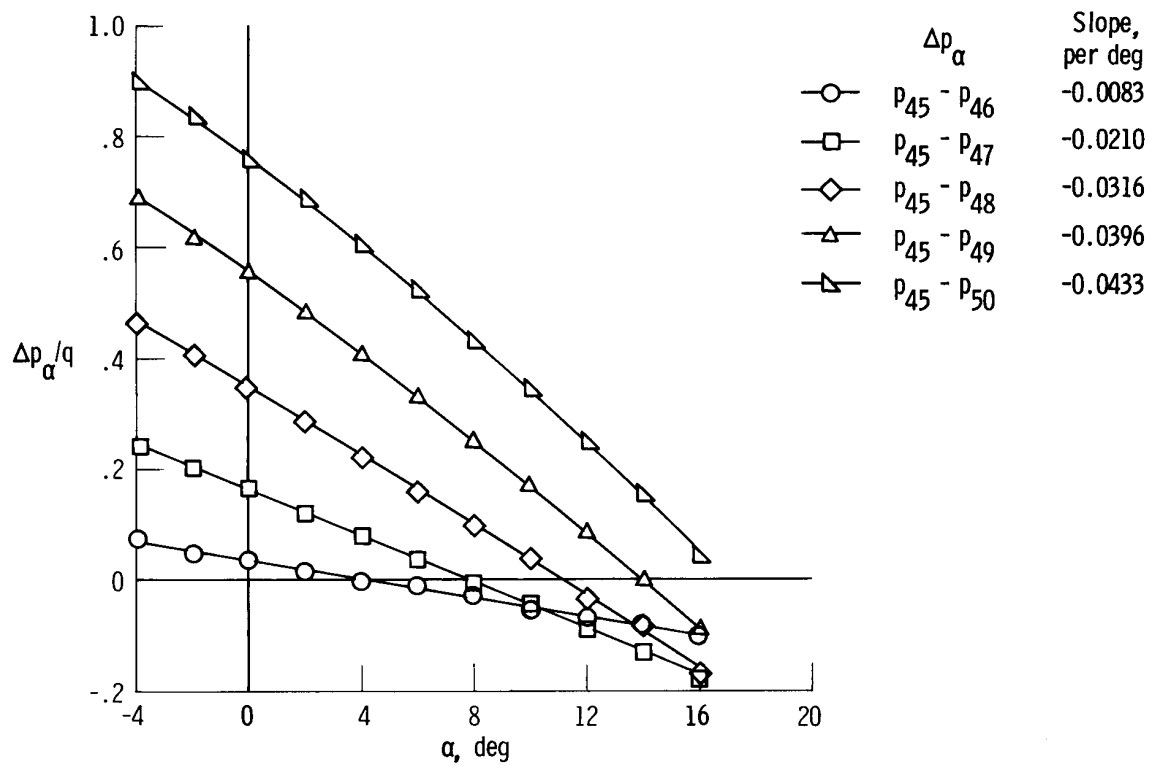
(c) $M = 0.60$.

Figure 7. Continued.



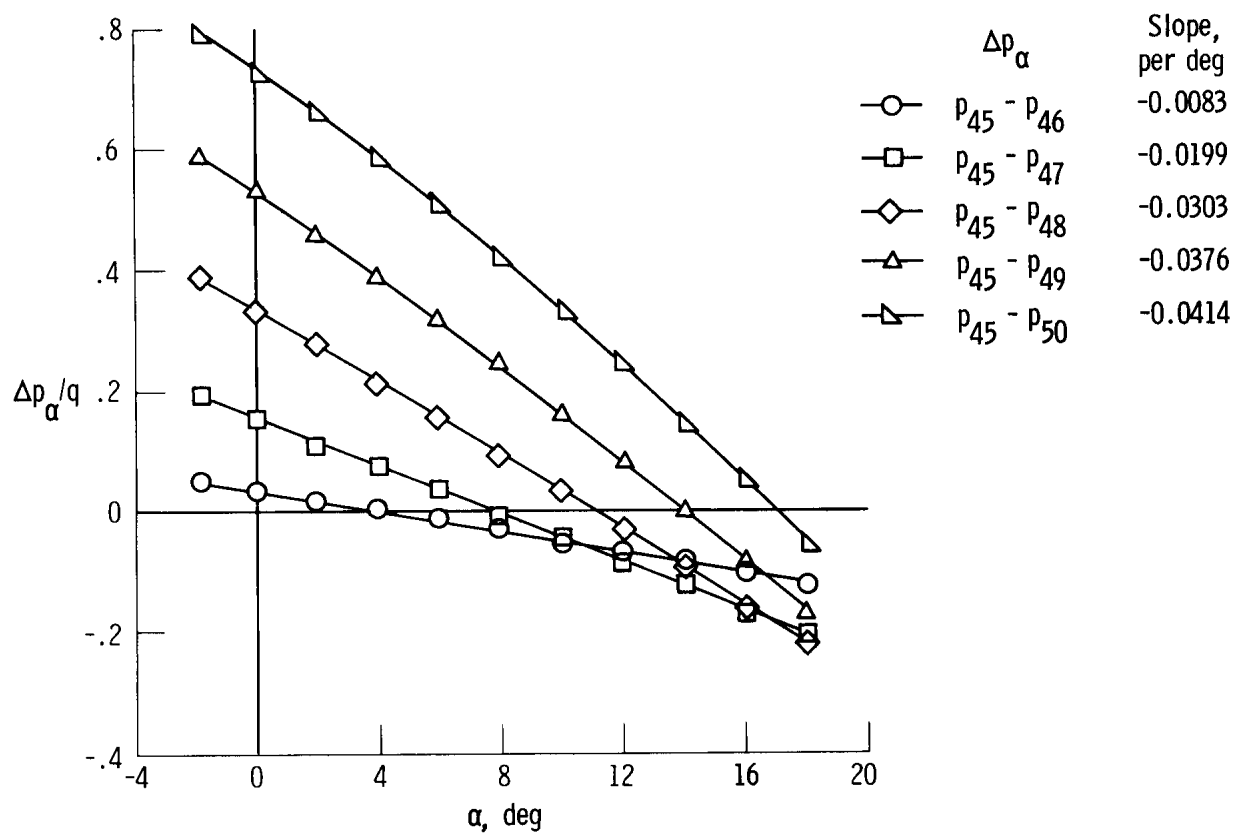
(d) $M = 0.70$.

Figure 7. Continued.



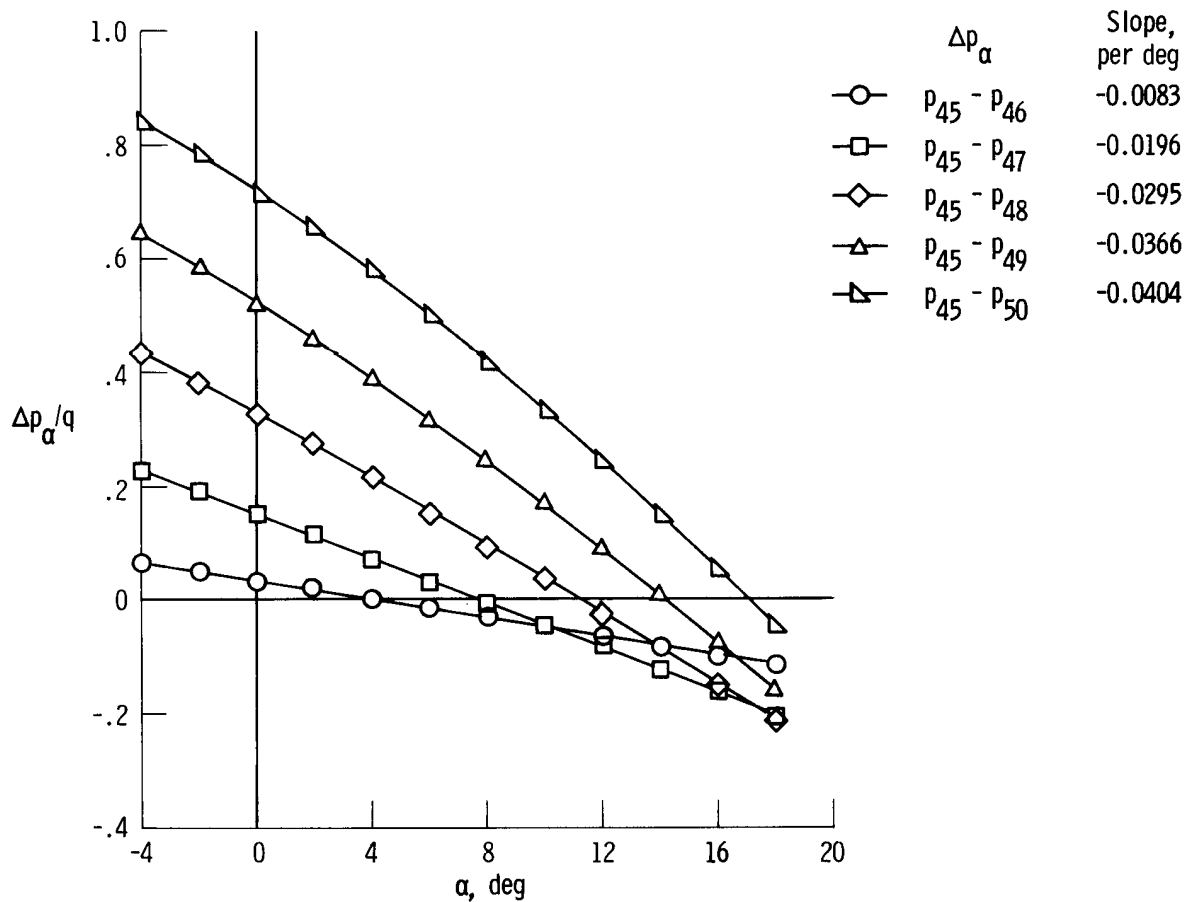
(e) $M = 0.80$.

Figure 7. Continued.



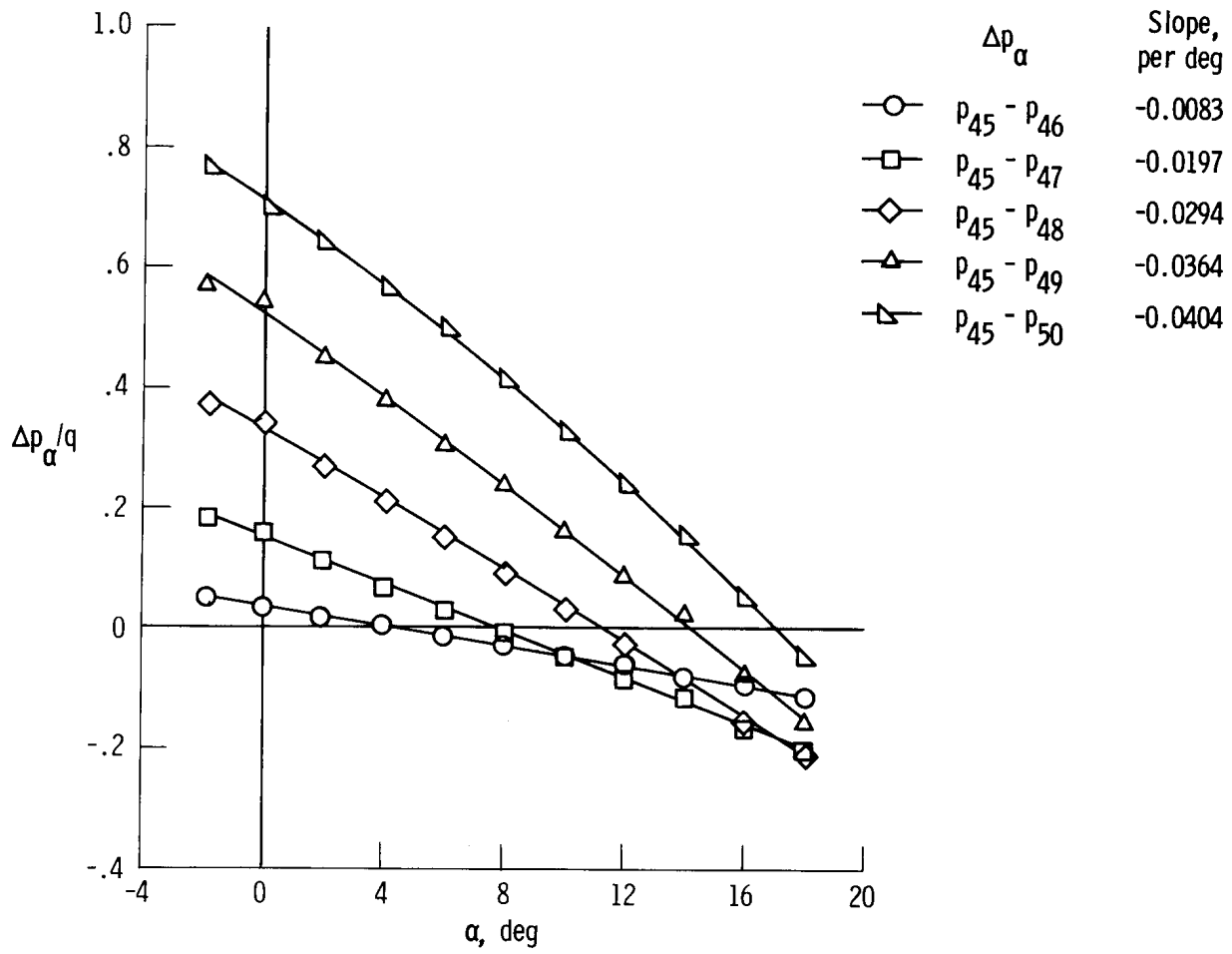
(f) $M = 0.90$.

Figure 7. Continued.



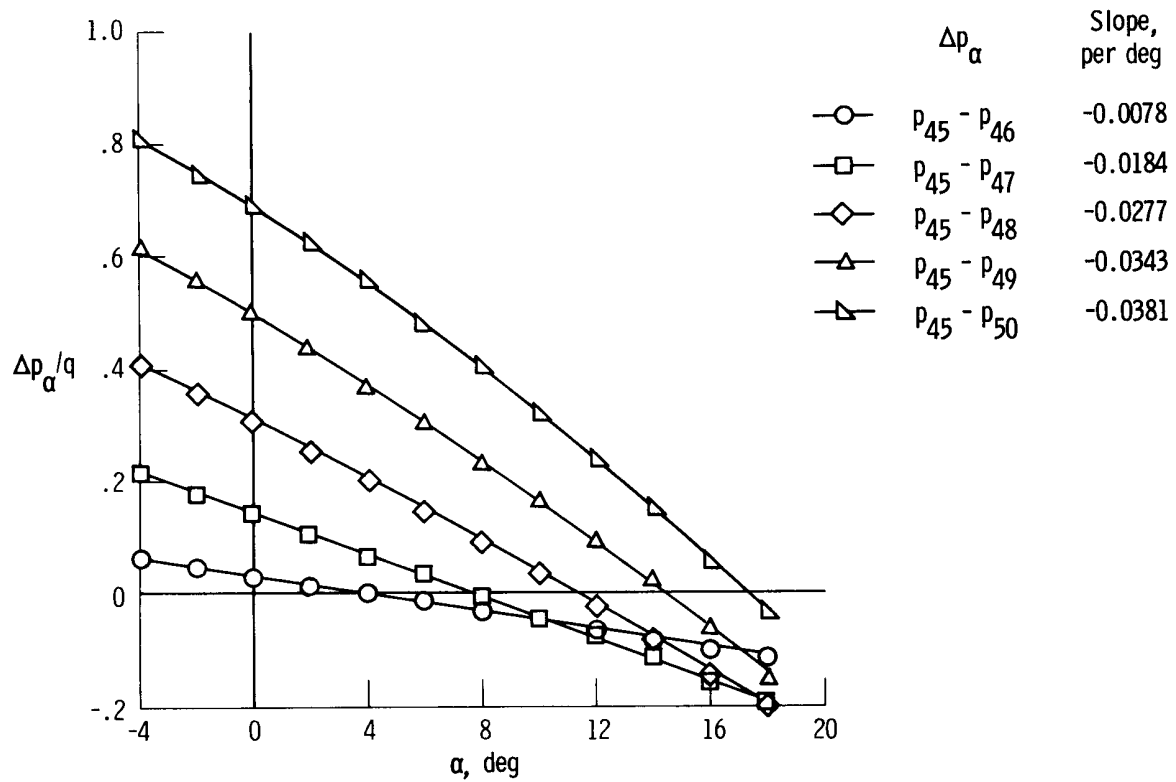
(g) $M = 0.95$.

Figure 7. Continued.



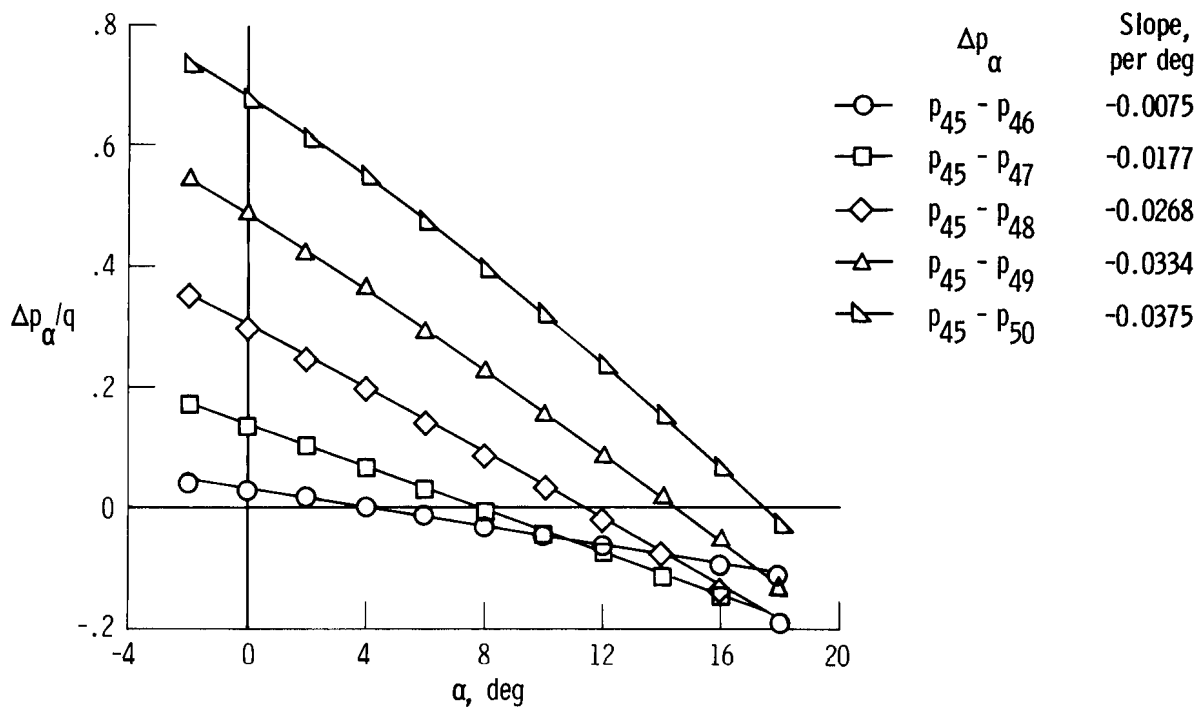
(h) $M = 0.98$.

Figure 7. Continued.



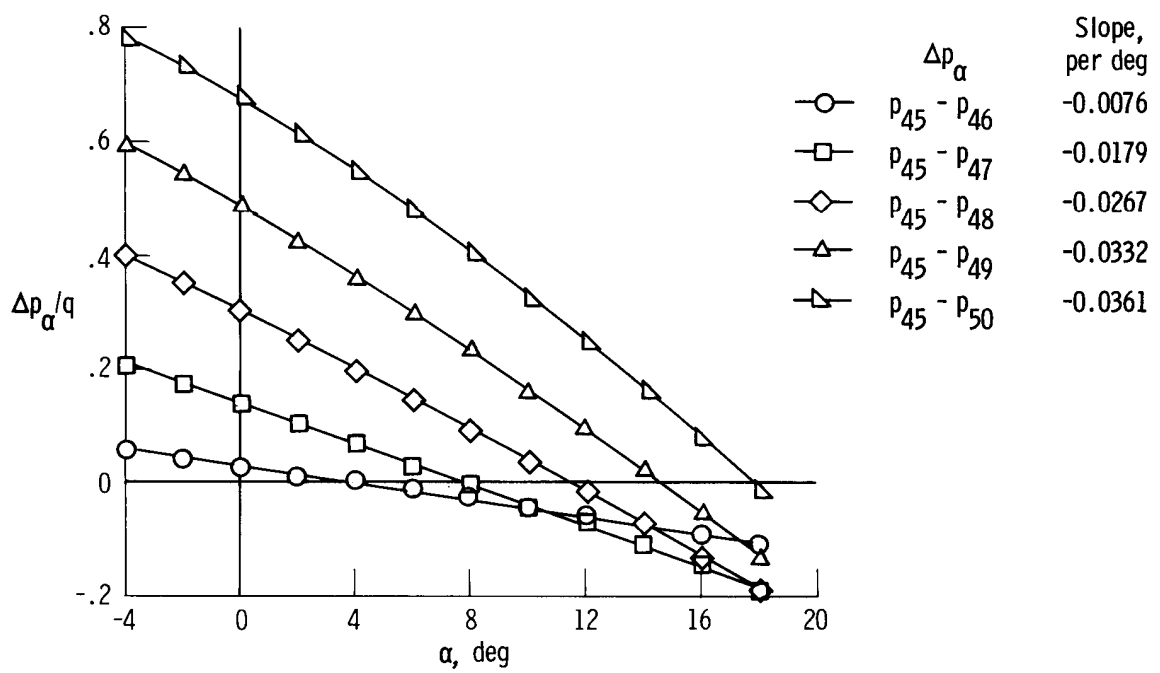
(i) $M = 1.05$.

Figure 7. Continued.



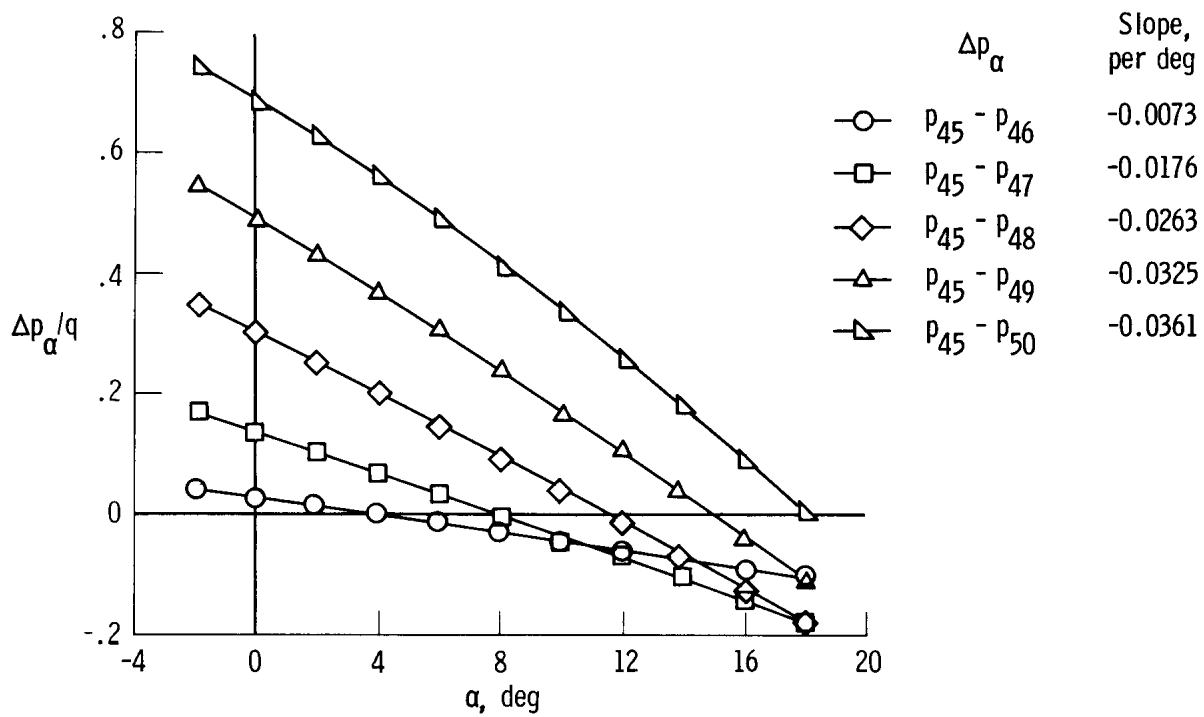
(j) $M = 1.10$.

Figure 7. Continued.



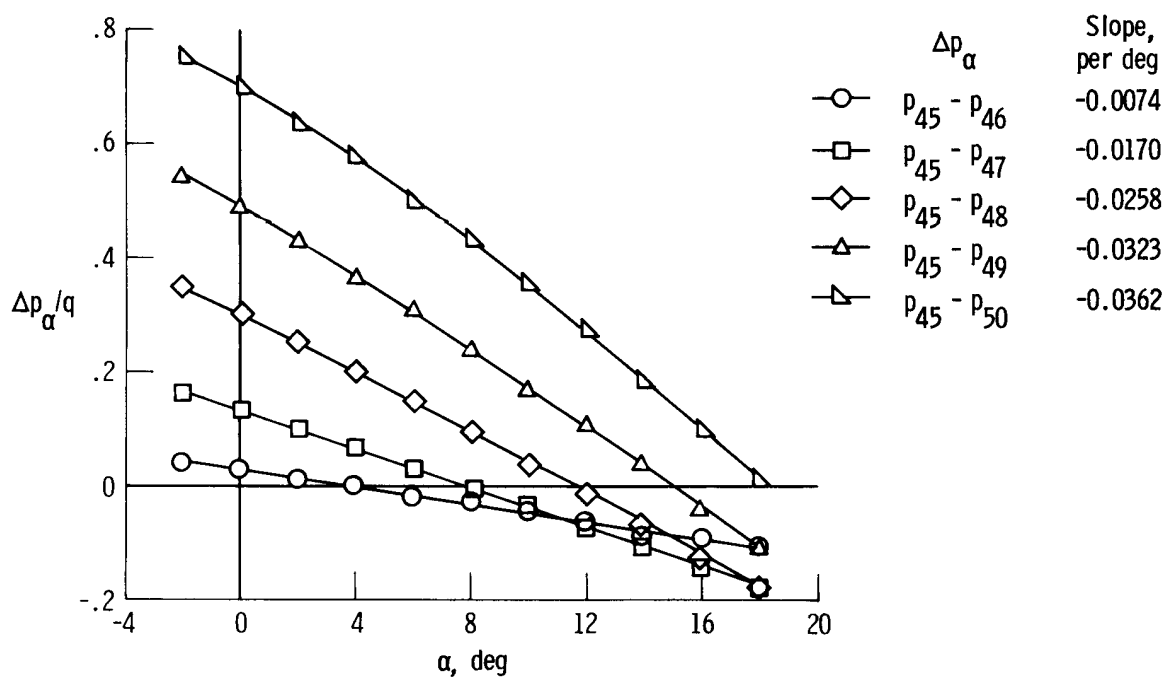
(k) $M = 1, 15.$

Figure 7. Continued.



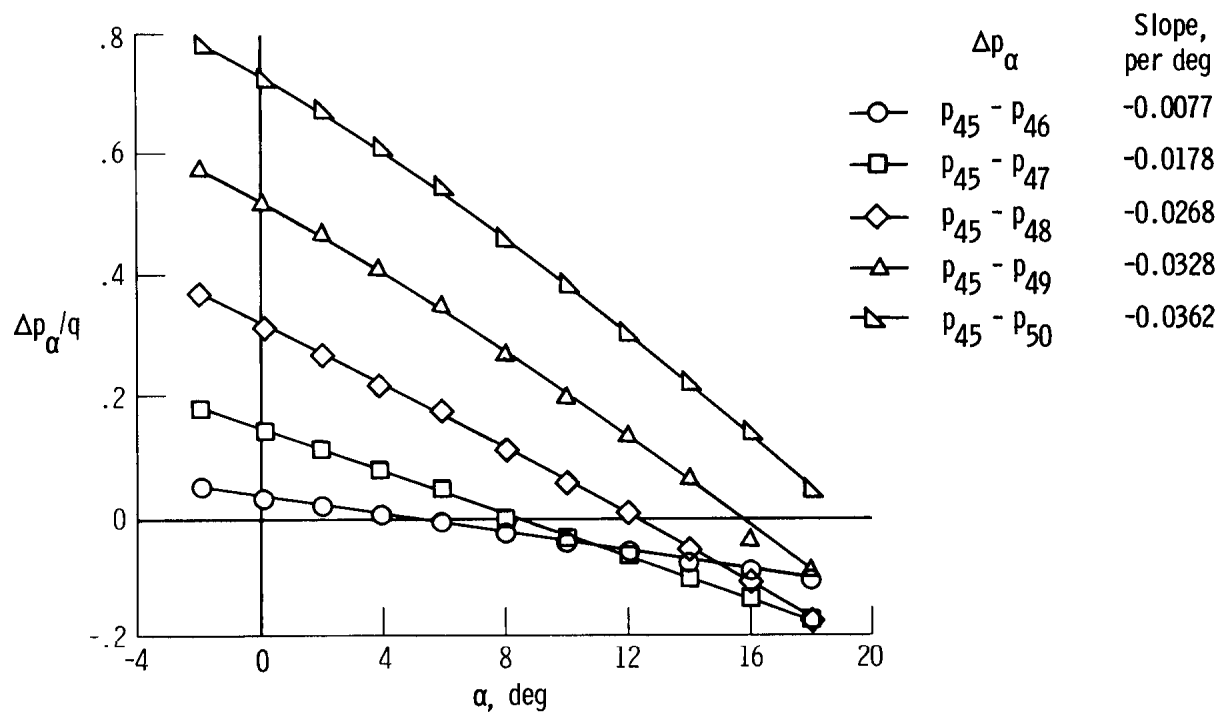
(1) $M = 1.20$.

Figure 7. Continued.



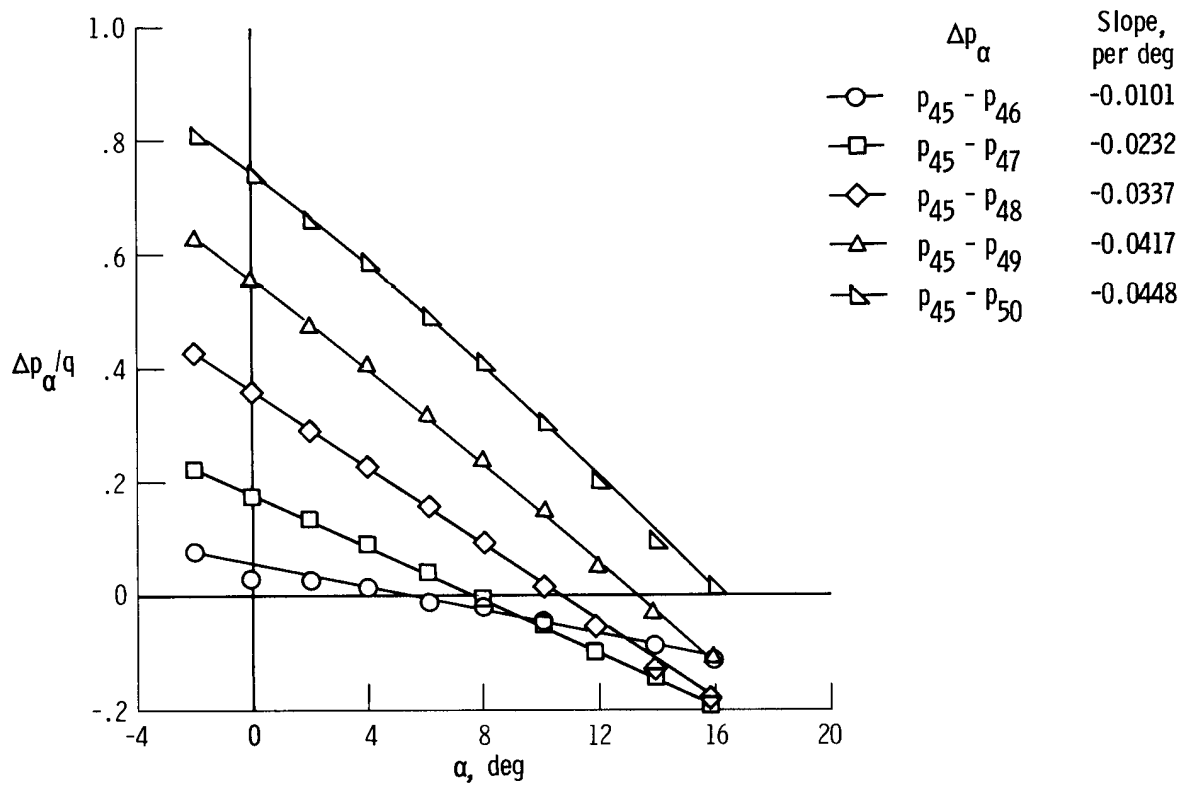
(m) $M = 1.30$.

Figure 7. Continued.



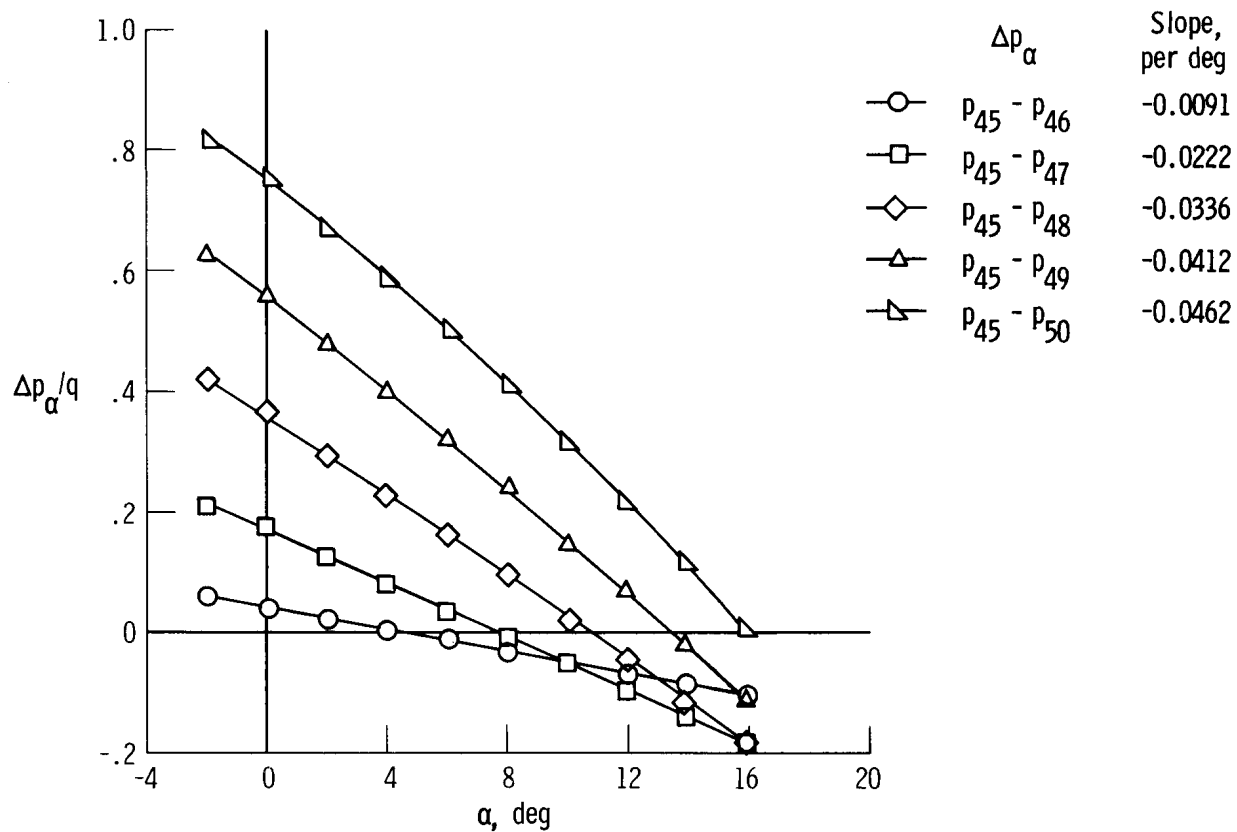
(n) $M = 1.40$.

Figure 7. Concluded.



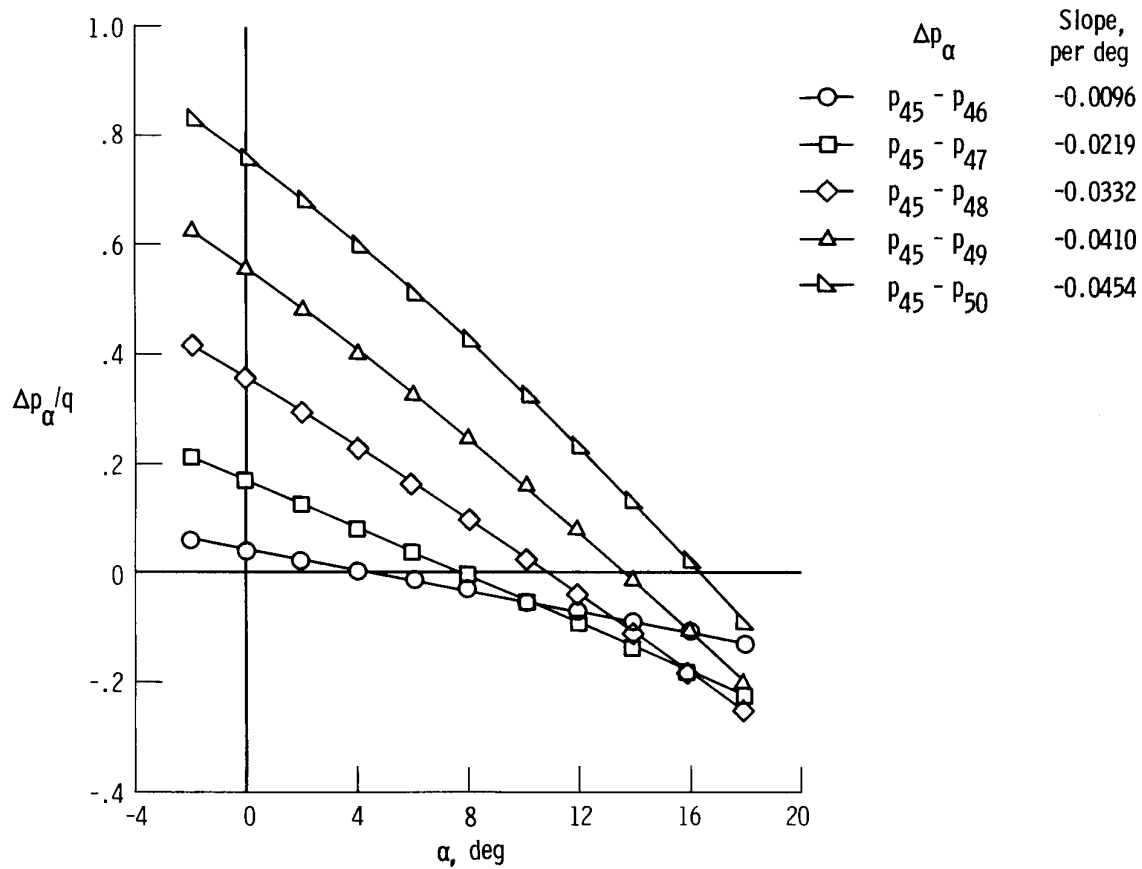
(a) $M = 0.25$.

Figure 8. Pressure parameter for selected nose cap orifices plotted against angle of attack. $\beta = 2^\circ$; orifice 45 reference.



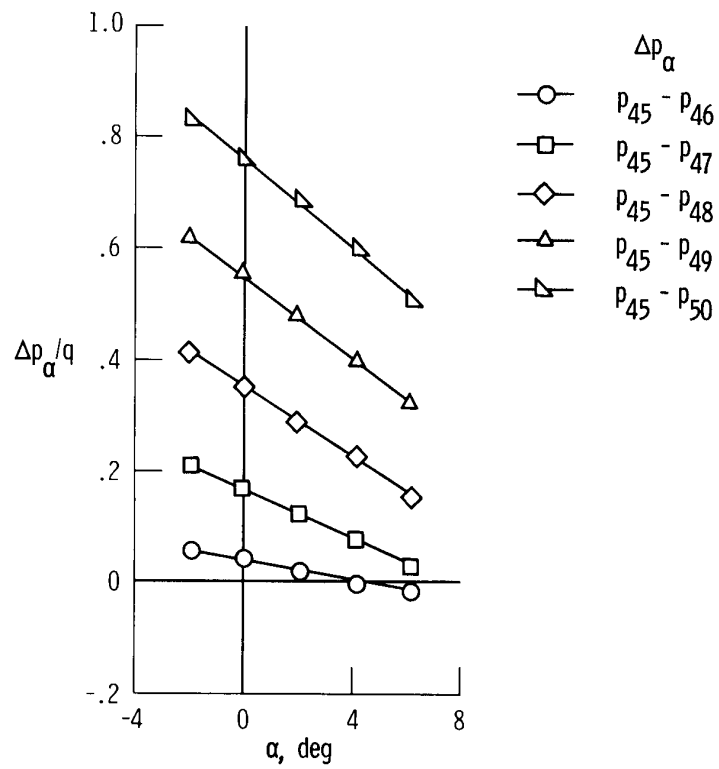
(b) $M = 0.40$.

Figure 8. Continued.



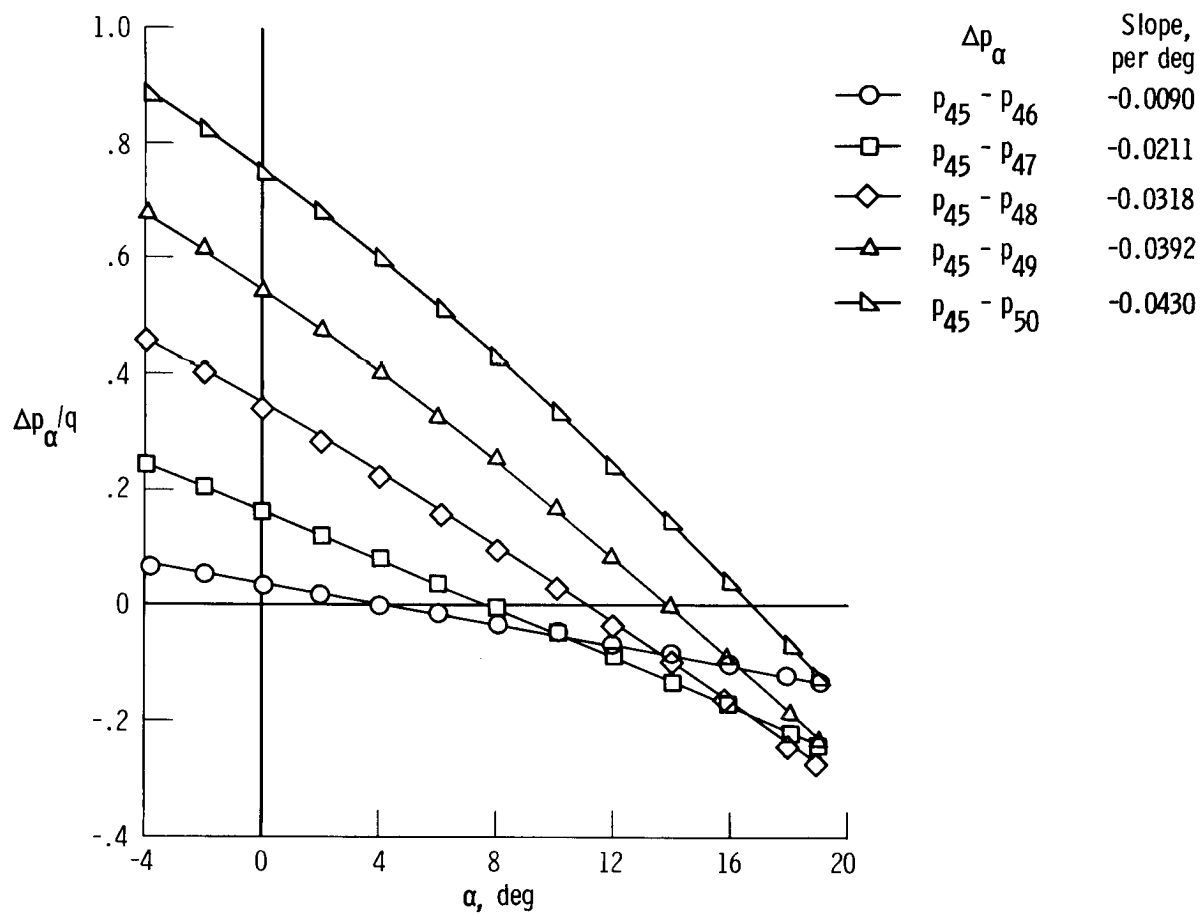
(c) $M = 0.60$.

Figure 8. Continued.



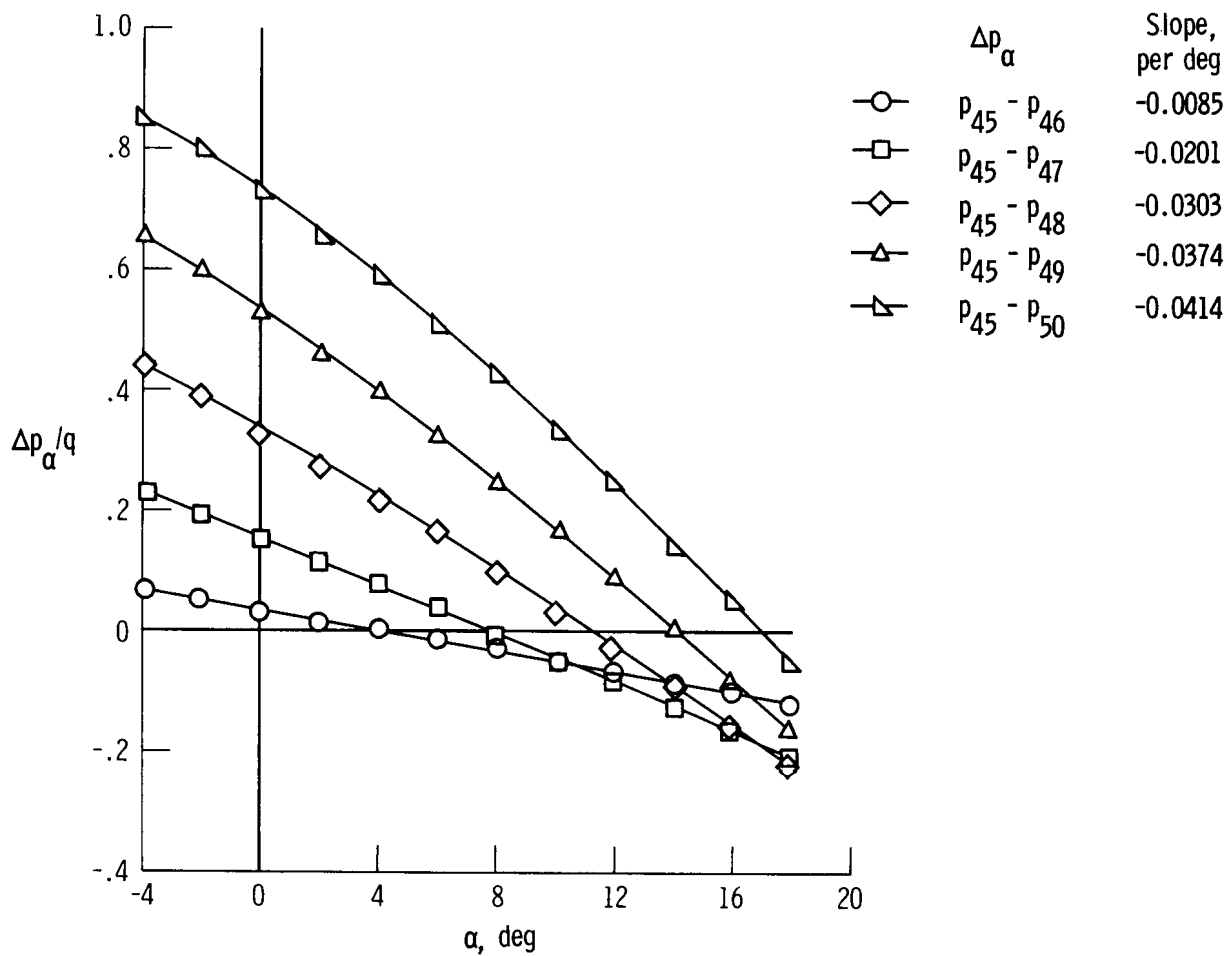
(d) $M = 0.70$.

Figure 8. Continued.



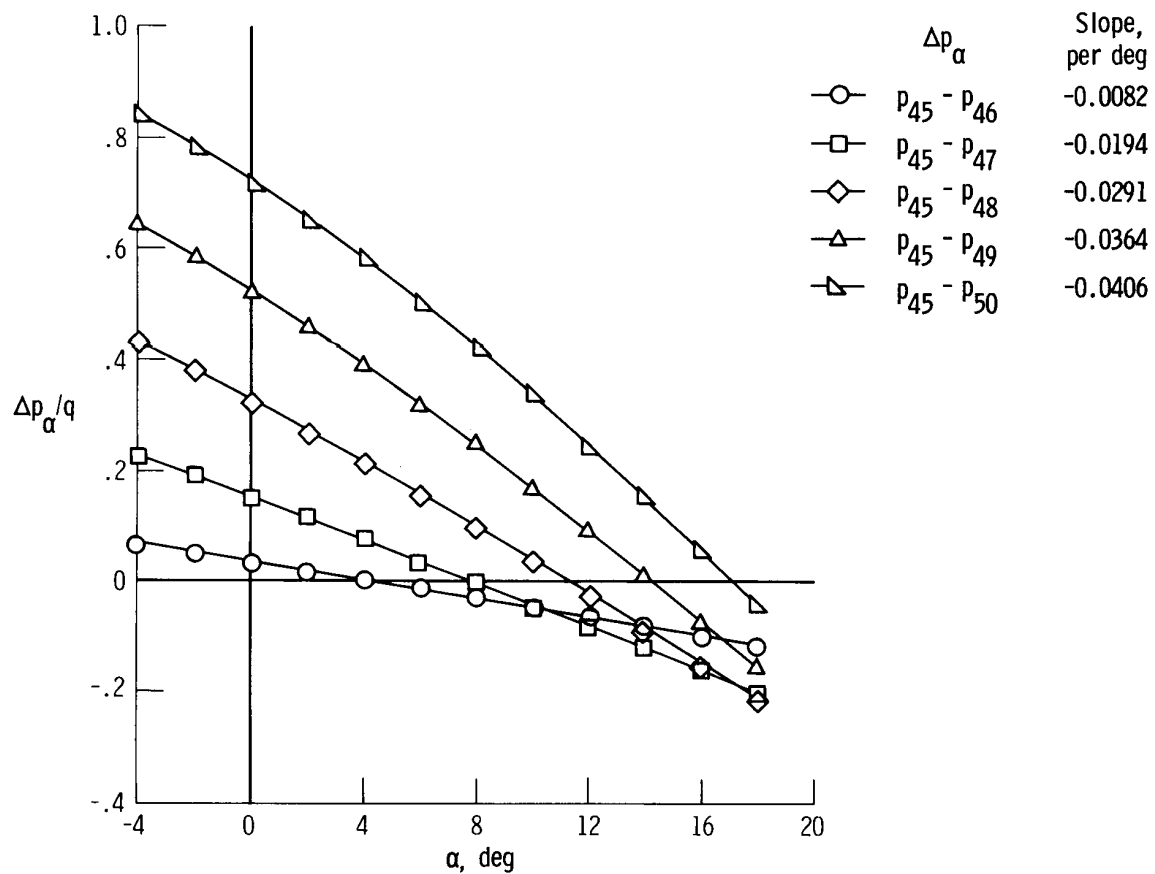
(e) $M = 0.80$.

Figure 8. Continued.



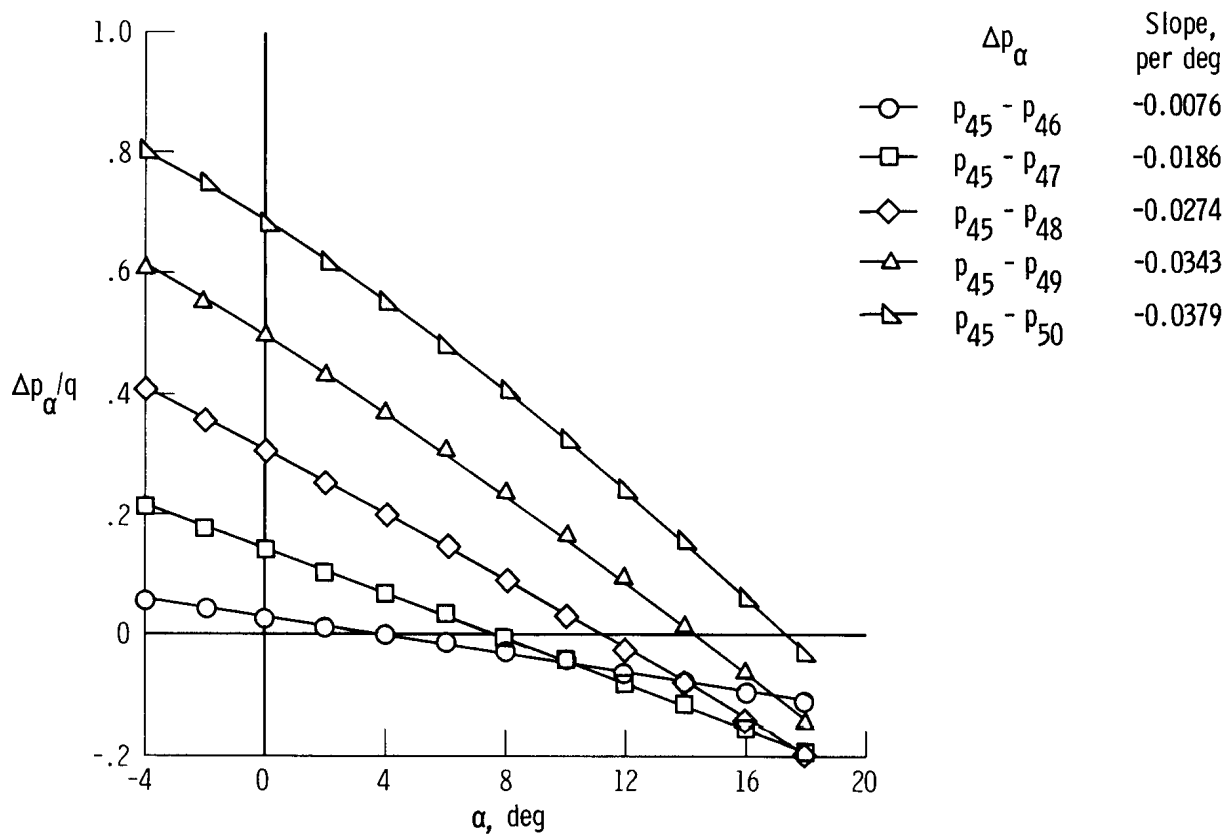
(f) $M = 0.90$.

Figure 8. Continued.



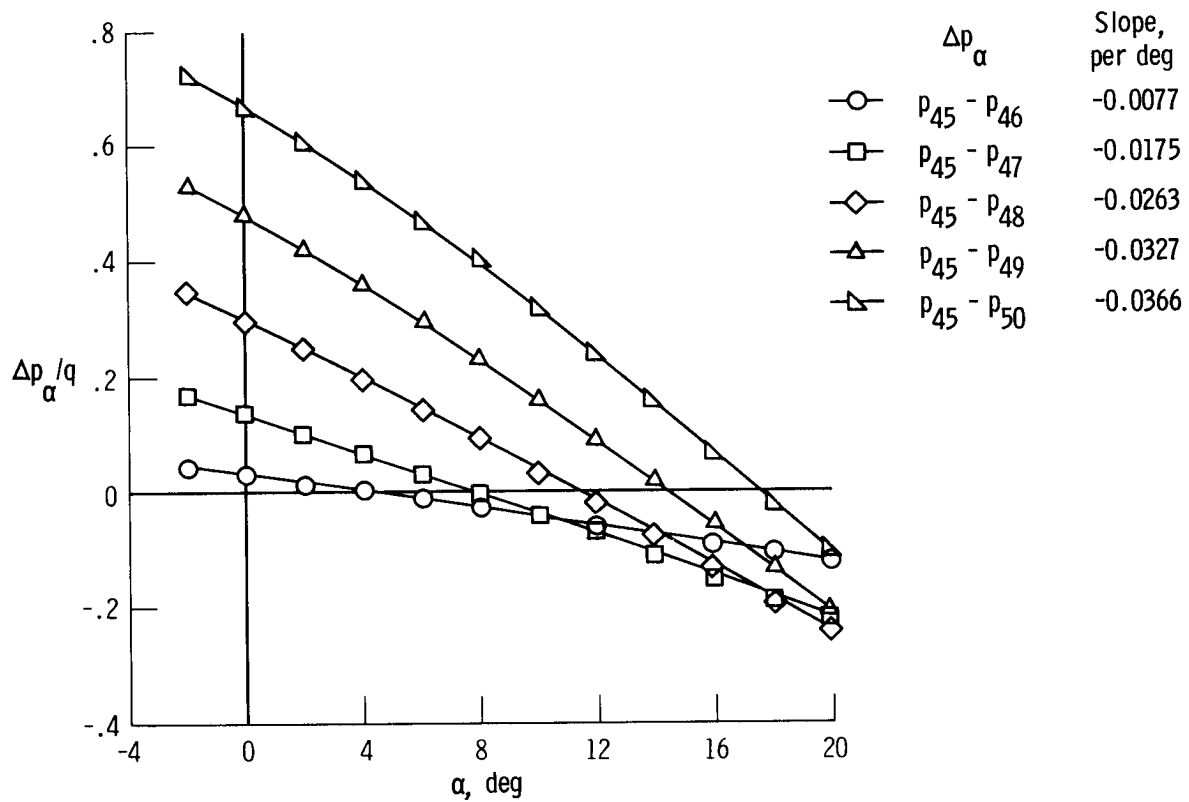
(g) $M = 0.95$.

Figure 8. Continued.



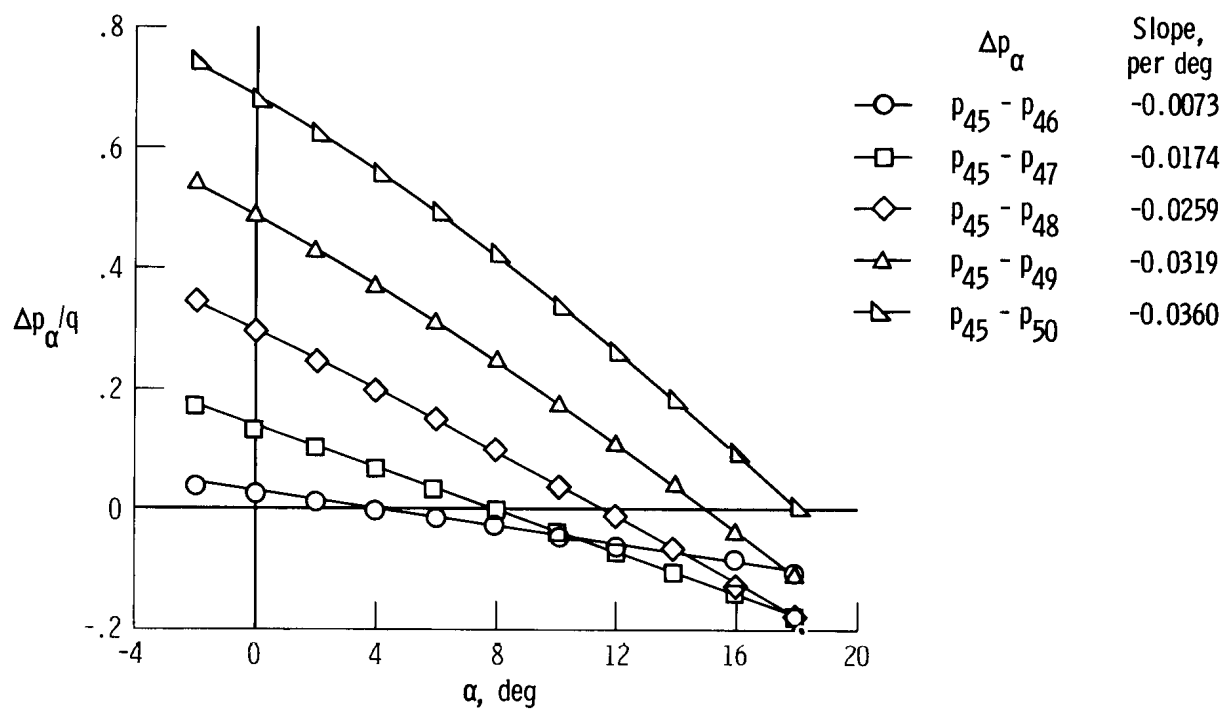
(h) $M = 1.05$.

Figure 8. Continued.



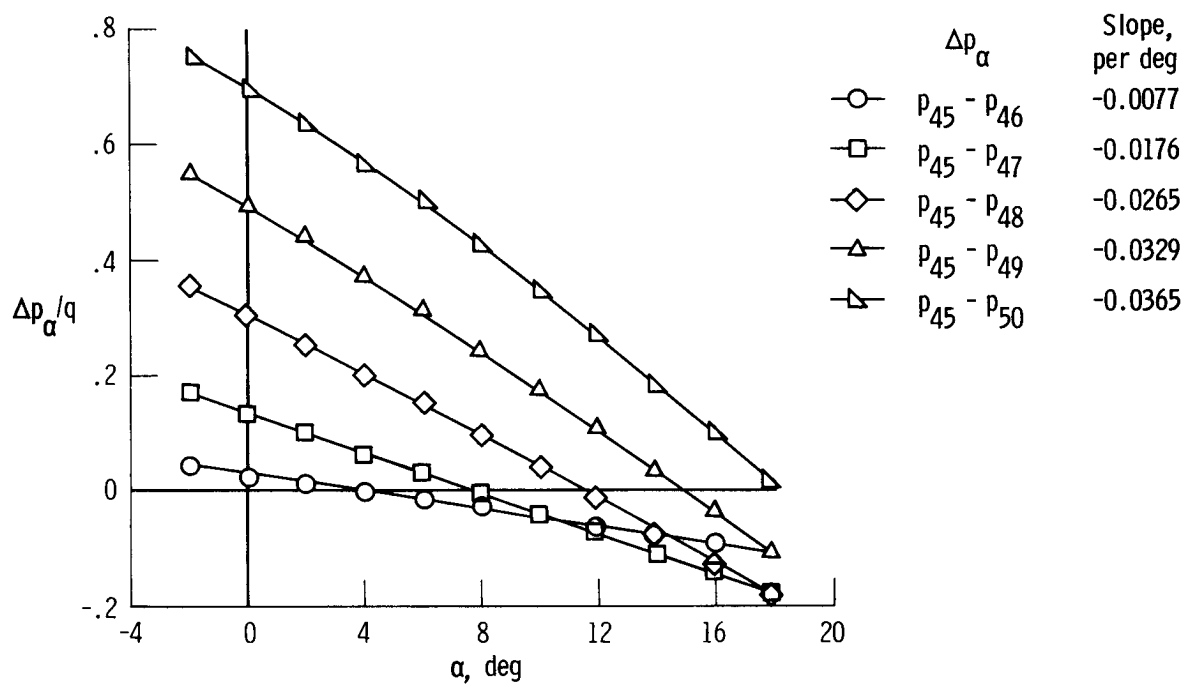
(i) $M = 1.10$.

Figure 8. Continued.



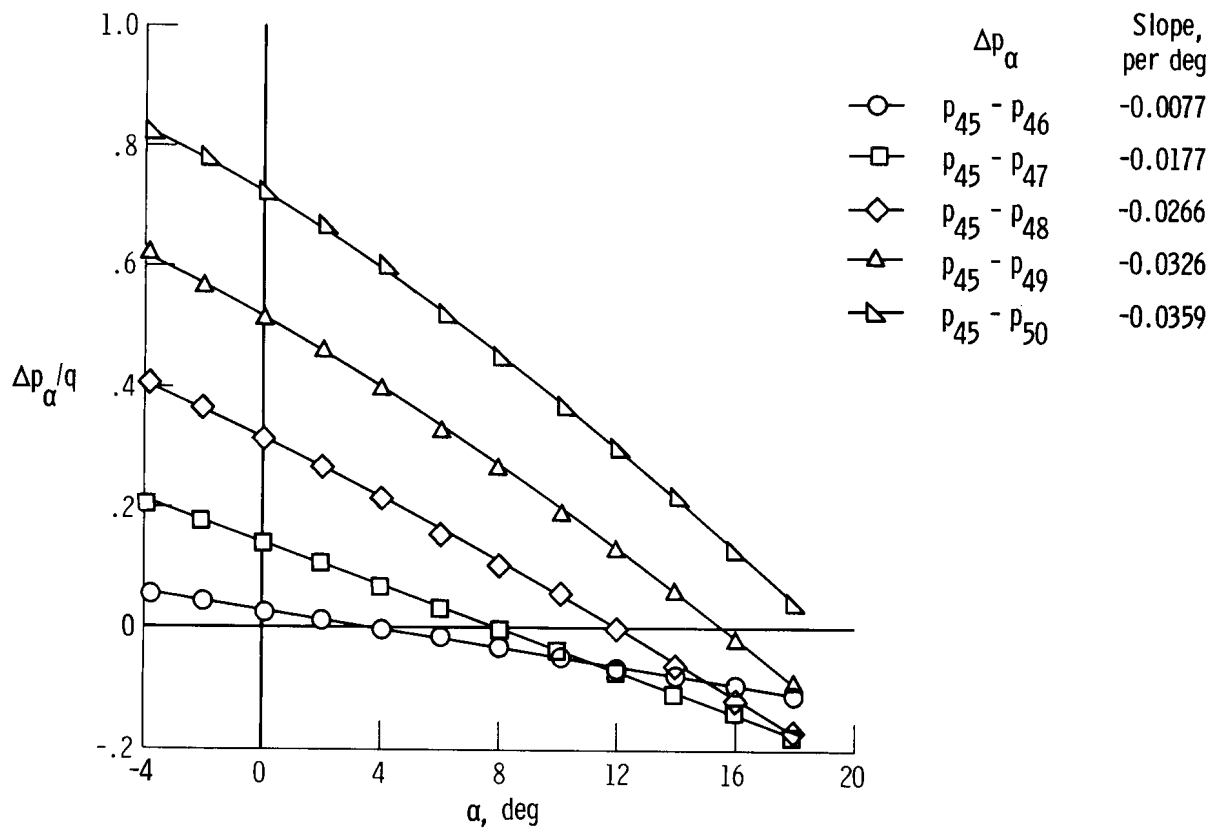
(j) $M = 1.20$.

Figure 8. Continued.



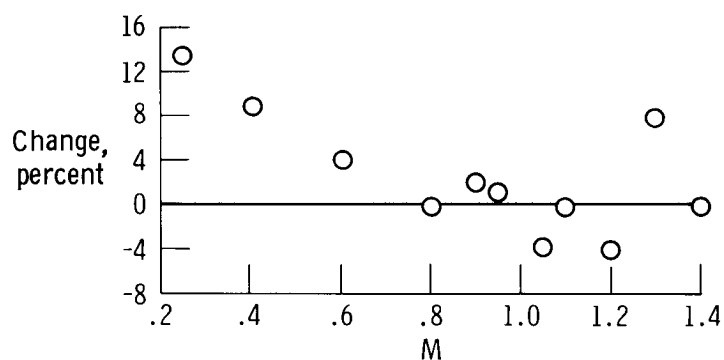
(k) $M = 1.30$.

Figure 8. Continued.

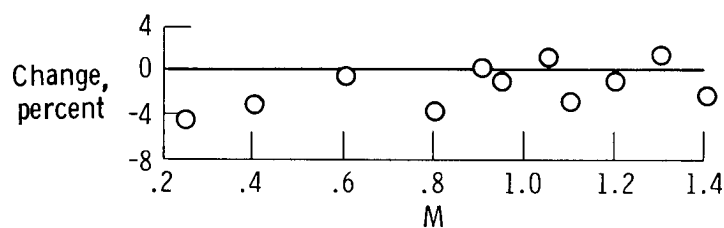


(1) $M = 1.40$.

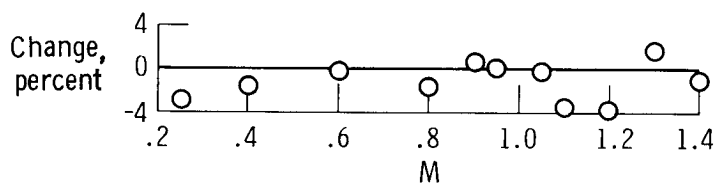
Figure 8. Concluded.



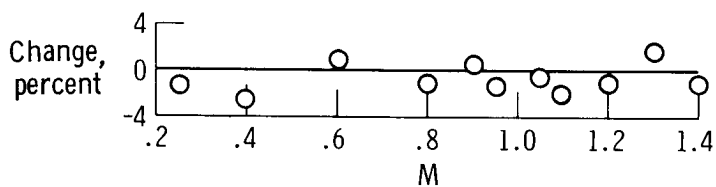
(a) $p_{45} - p_{46}$.



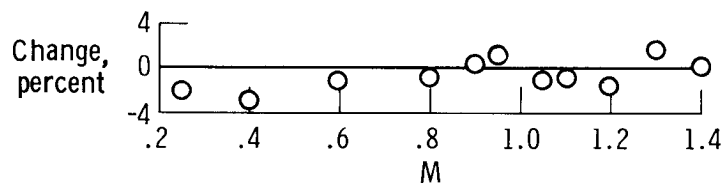
(b) $p_{45} - p_{47}$.



(c) $p_{45} - p_{48}$.



(d) $p_{45} - p_{49}$.



(e) $p_{45} - p_{50}$.

Figure 9. Percentage of change in angle of attack sensitivity as angle of sideslip increases from 0° to 2° .

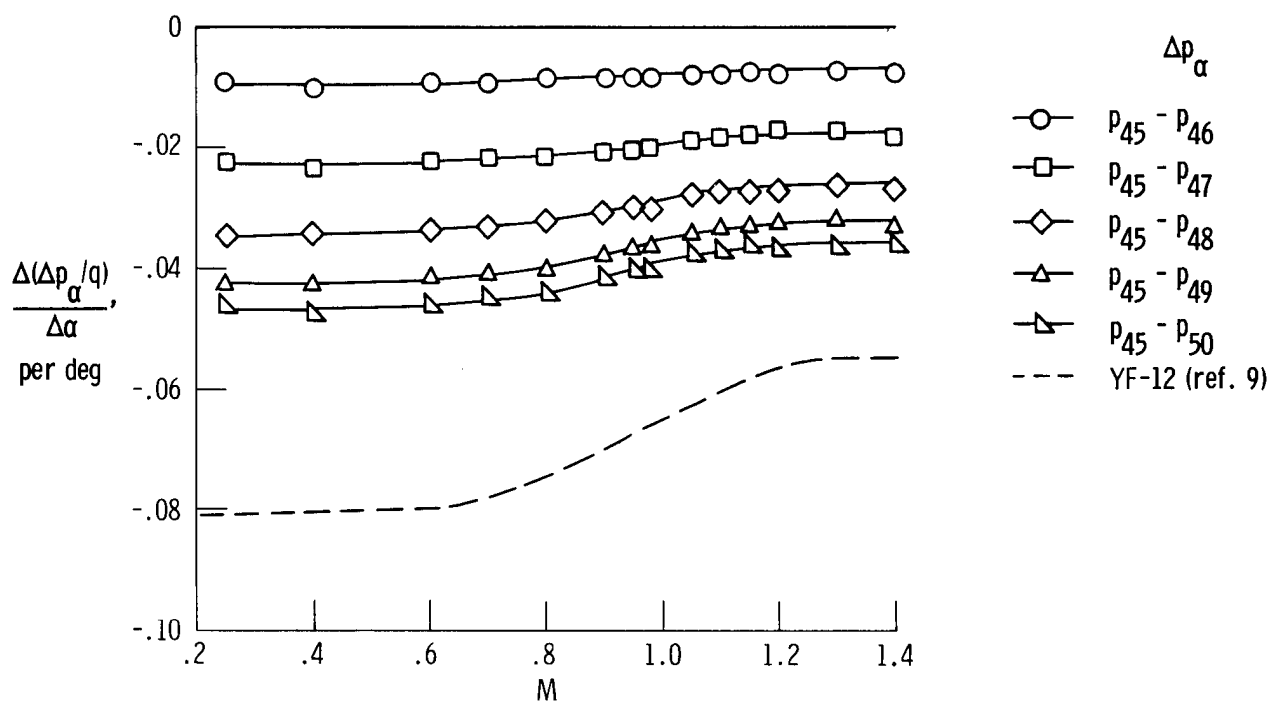


Figure 10. Sensitivity of nose cap orifices to angle of attack when plotted against Mach number. $\beta = 0^\circ$.

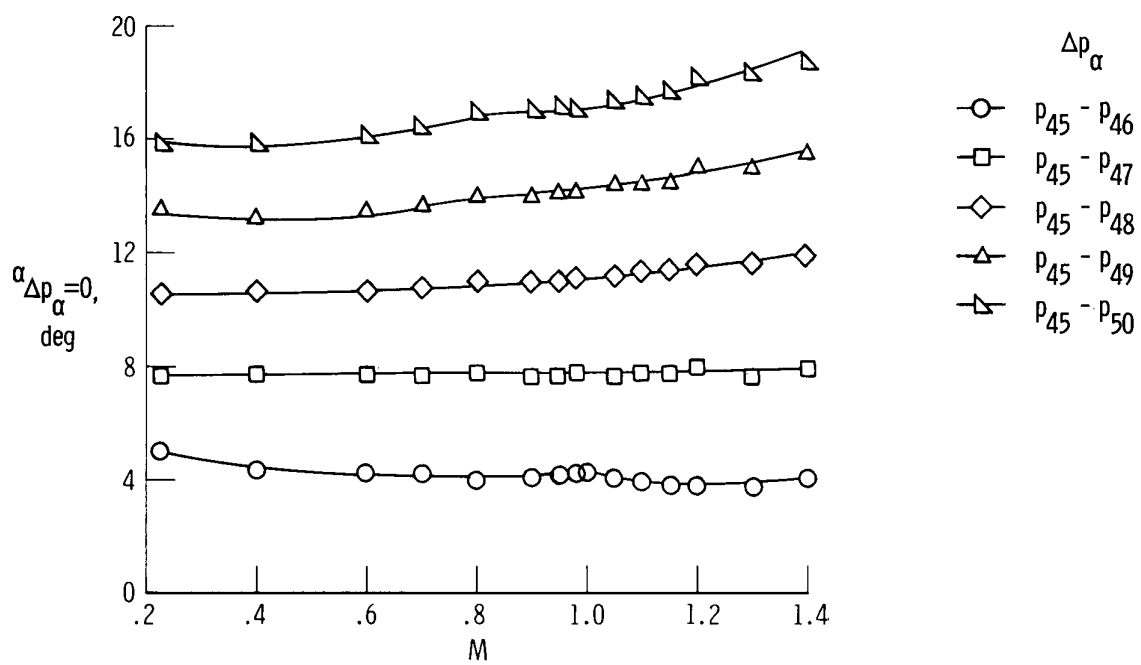
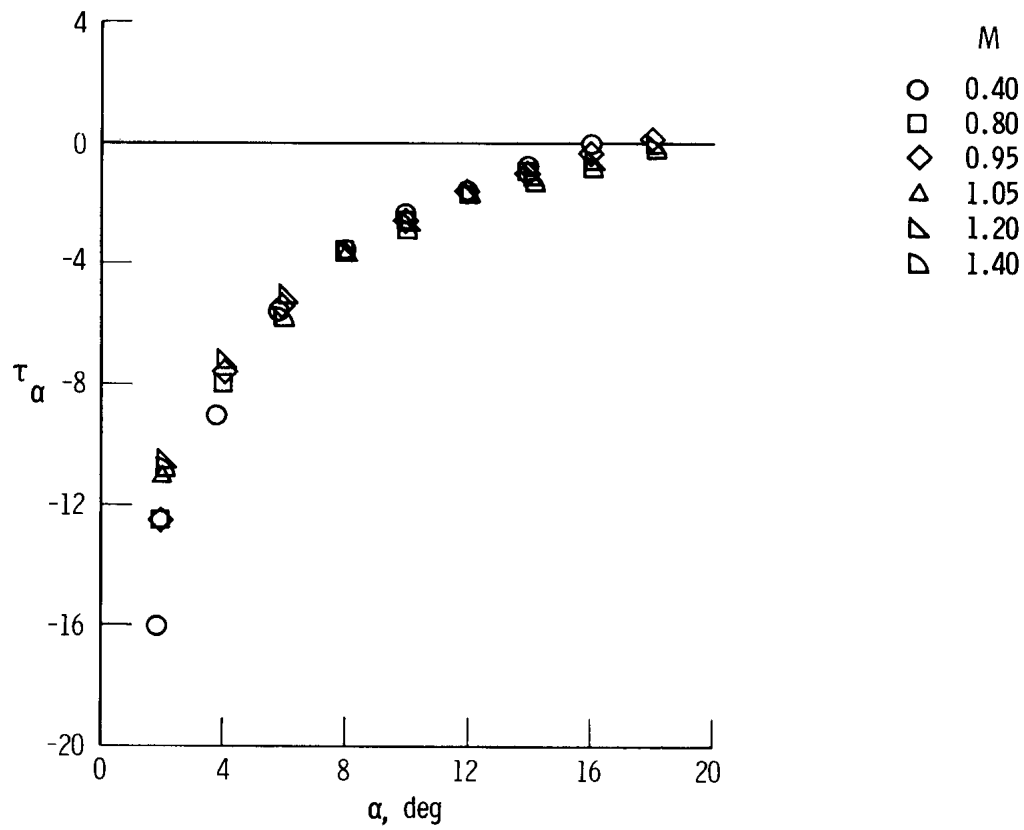
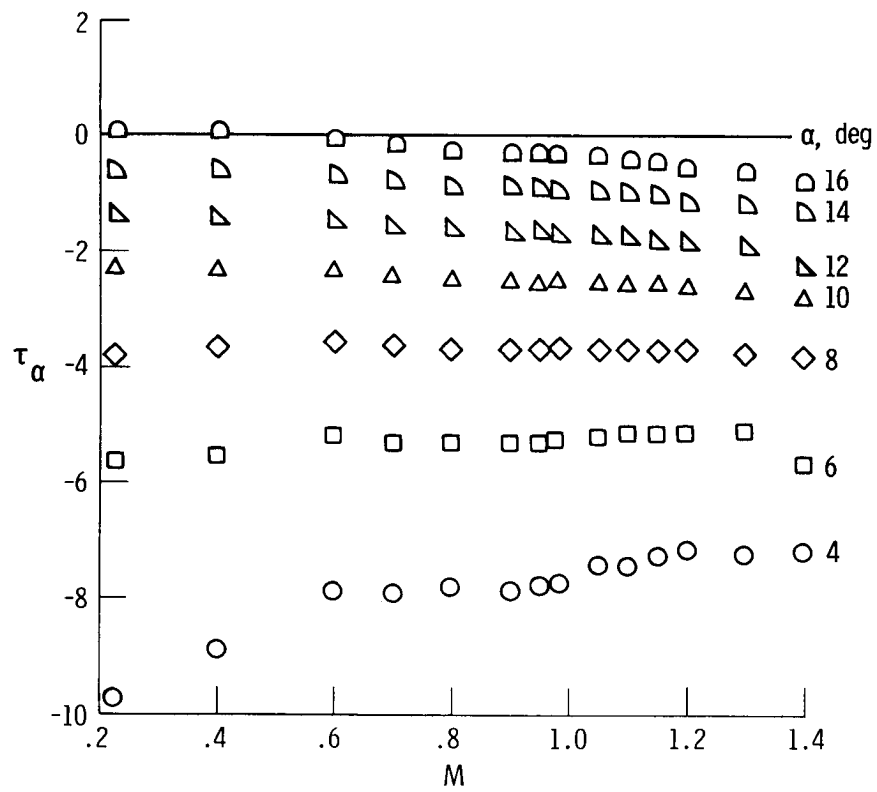


Figure 11. Angle of attack for which $\frac{\Delta p_\alpha}{q}$ equals zero as a function of Mach number. $\beta = 0^\circ$.



(a) τ_α versus angle of attack.

Figure 12. τ_α pressure parameter plotted against angle of attack and Mach number. $\beta = 0^\circ$.



(b) τ_α versus Mach number.

Figure 12. Concluded.

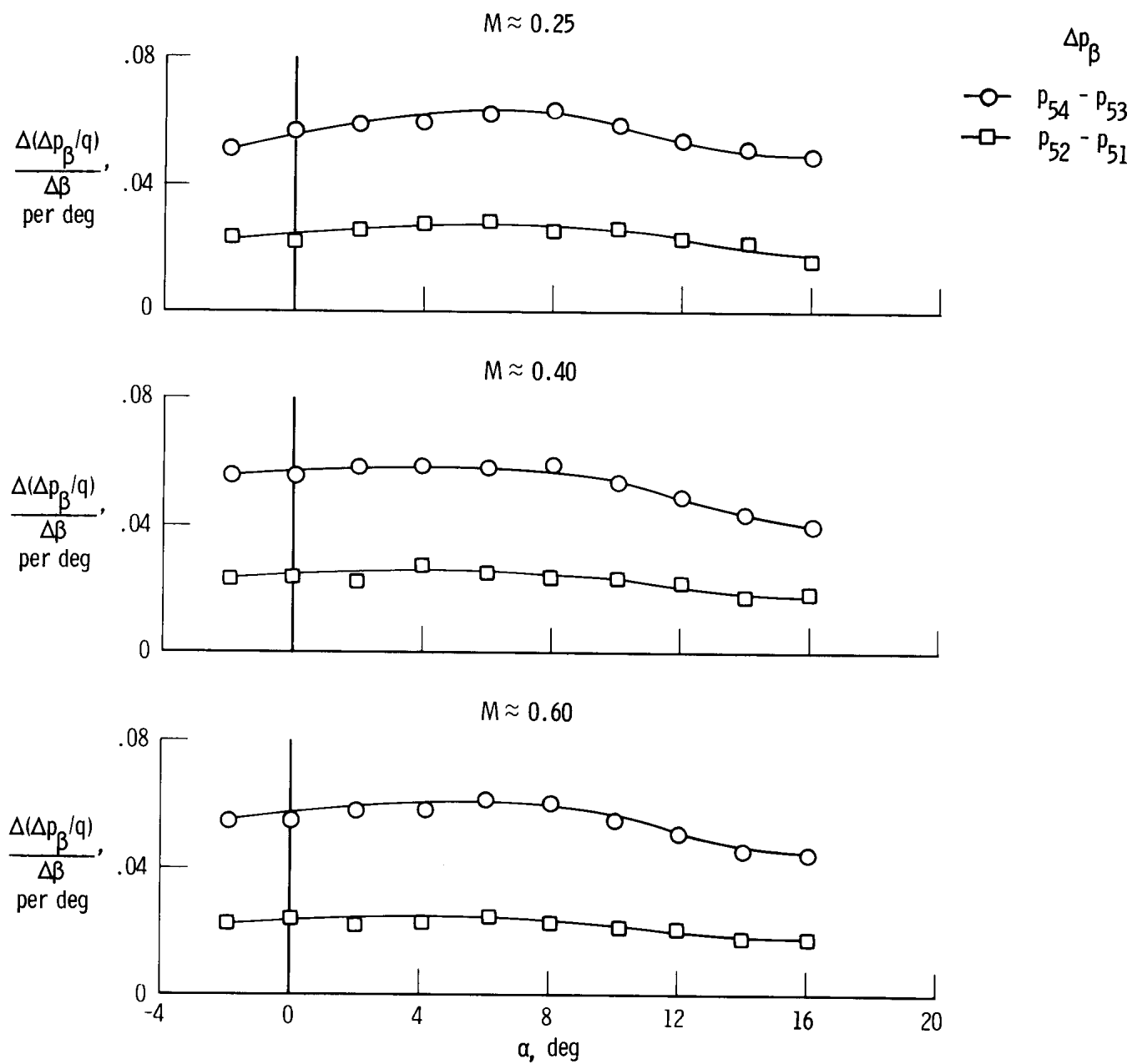


Figure 13. Angle of sideslip sensitivity for two pairs of nose cap orifices plotted against angle of attack.

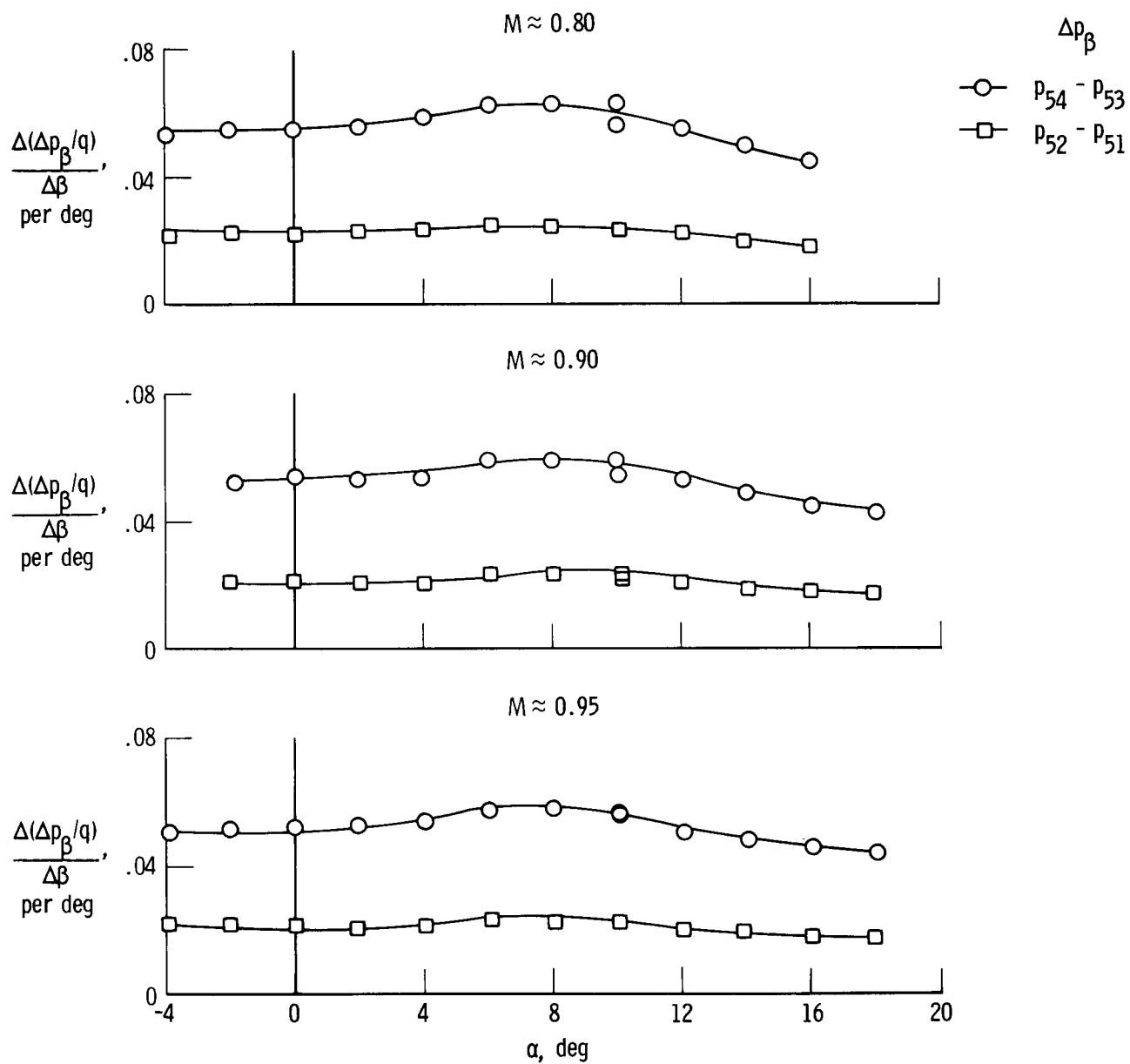


Figure 13. Continued.

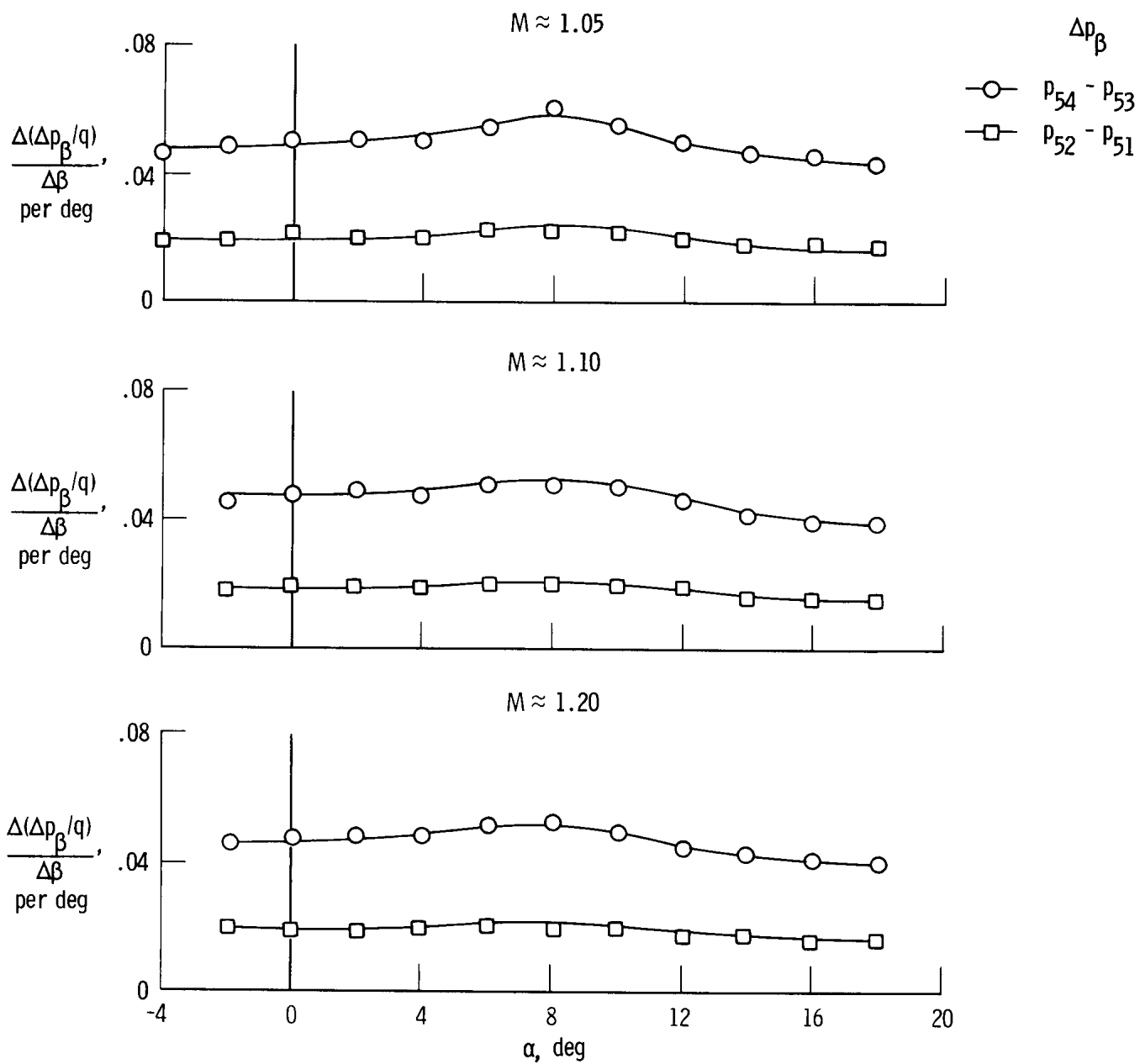


Figure 13. Continued.

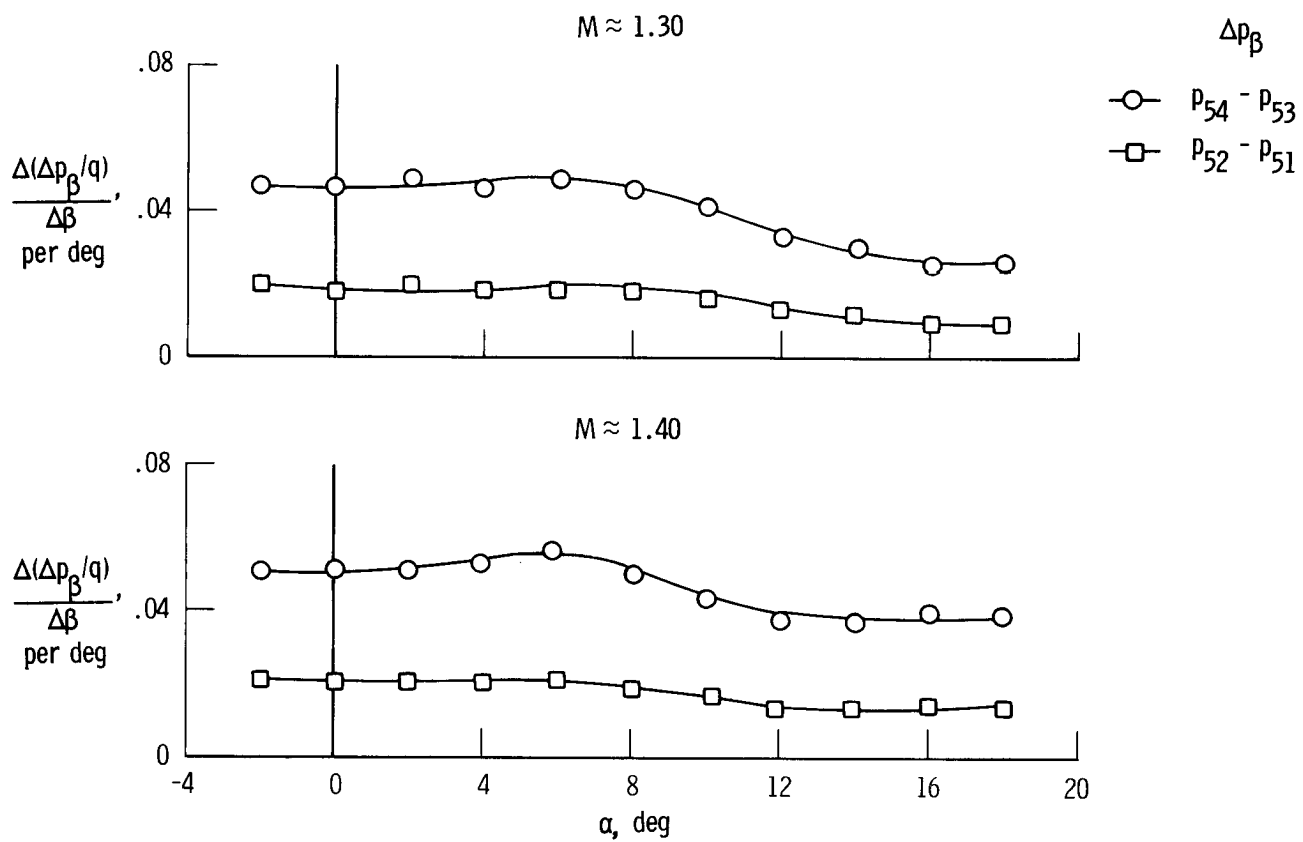


Figure 13. Concluded.

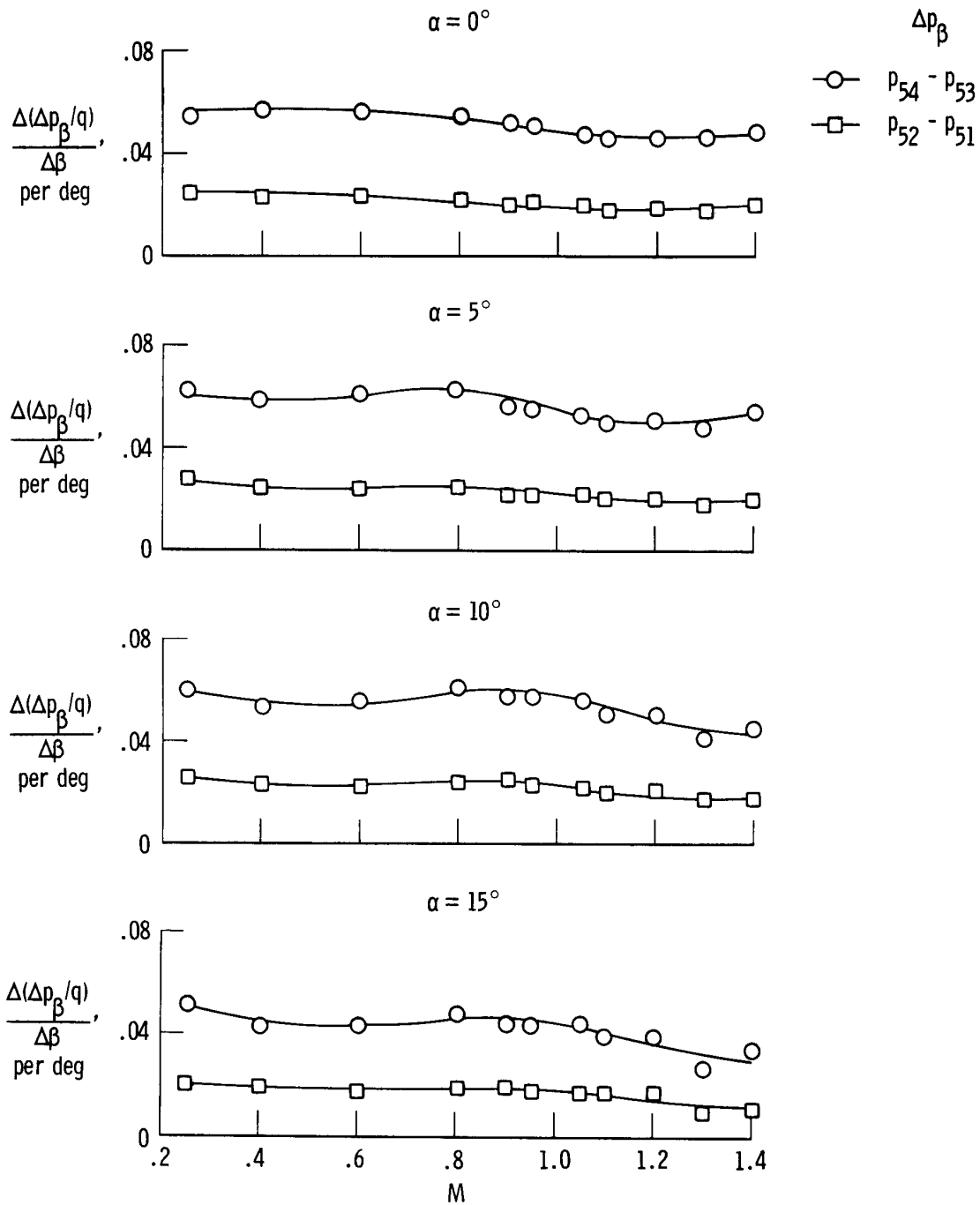


Figure 14. Angle of sideslip sensitivity values for selected nose cap orifices plotted against Mach number.

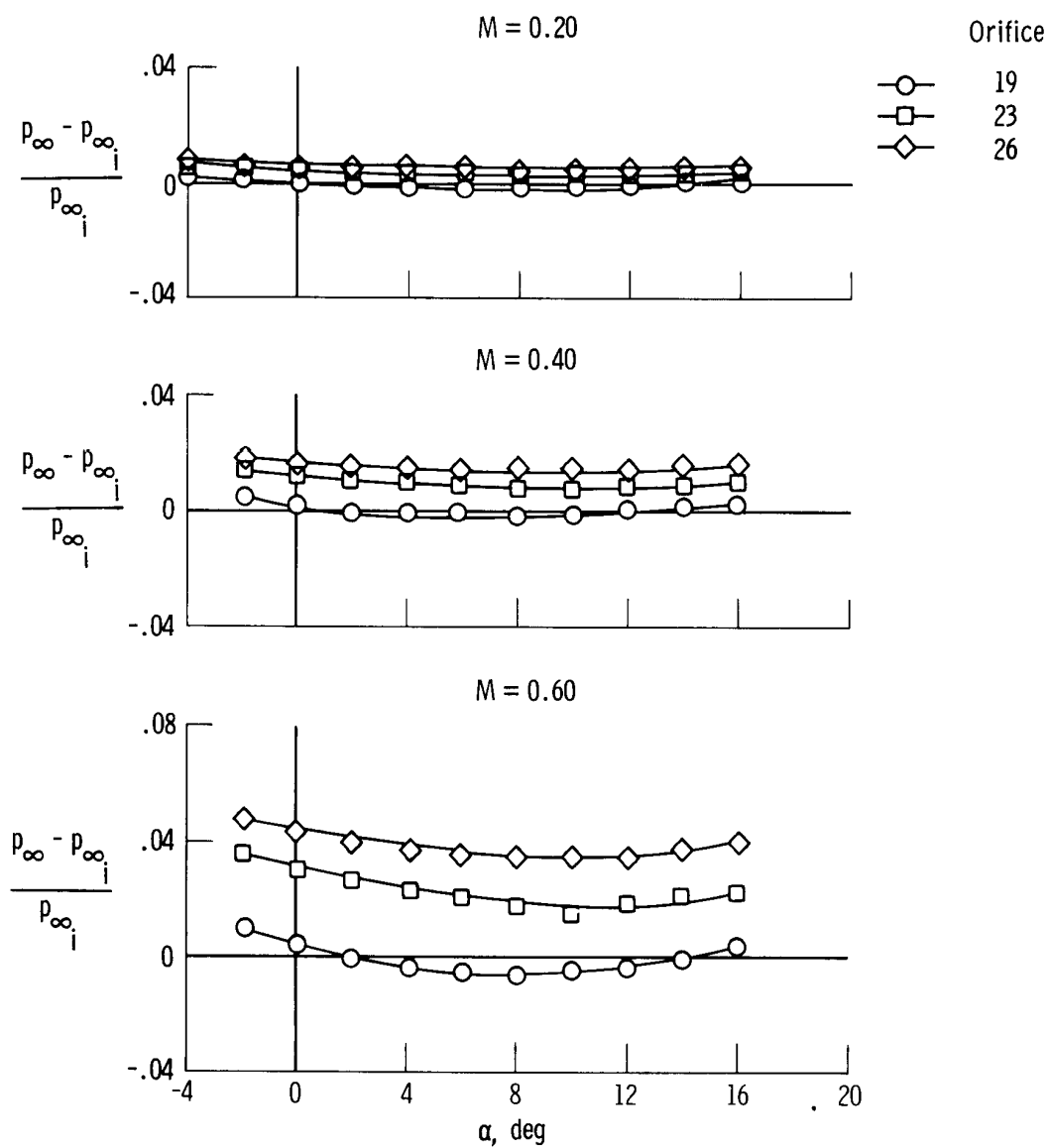


Figure 15. Correction for static pressure position error for auxiliary pressure orifices on forward fuselage plotted against angle of attack. $\beta = 0^\circ$.

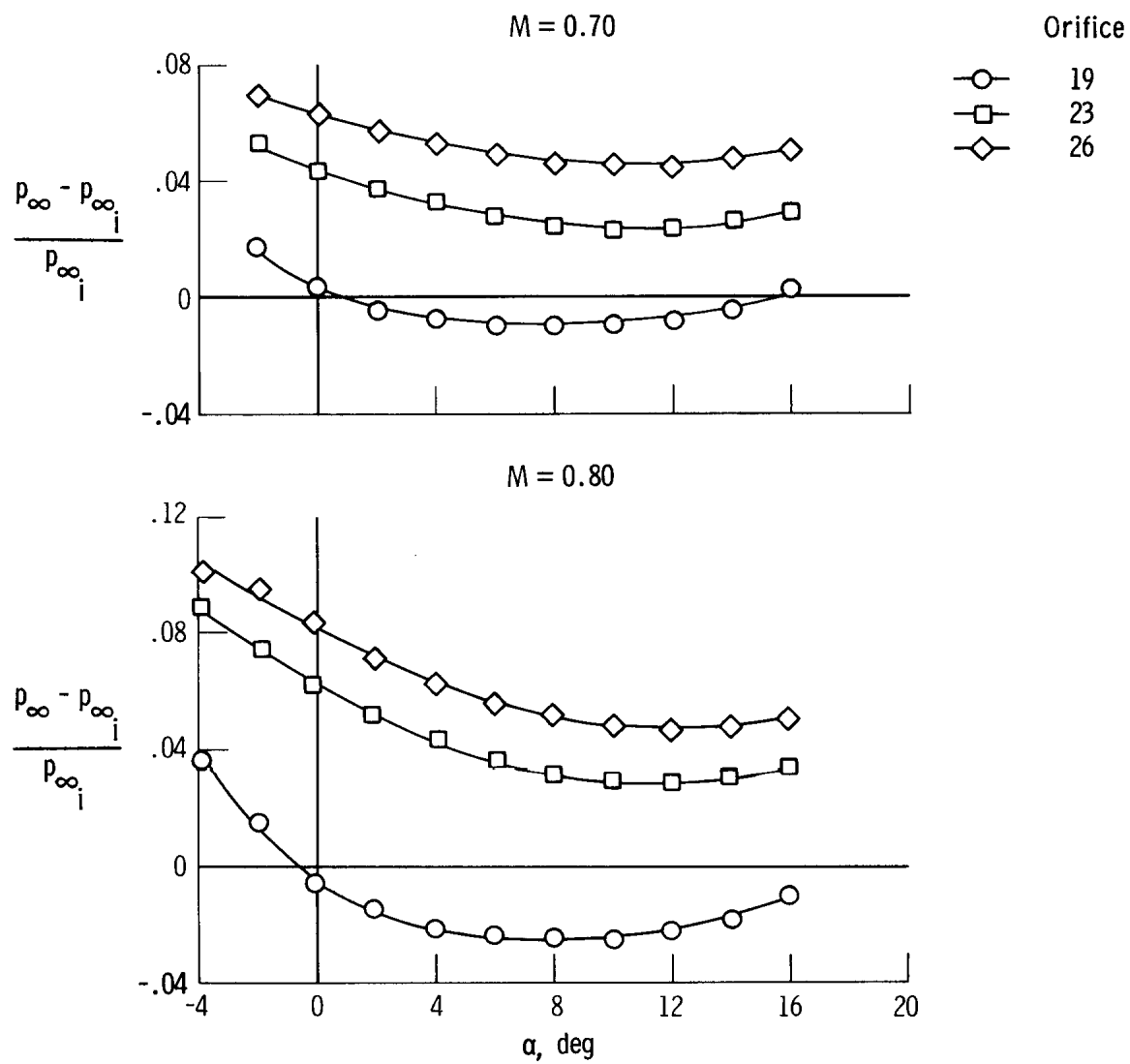


Figure 15. Continued.

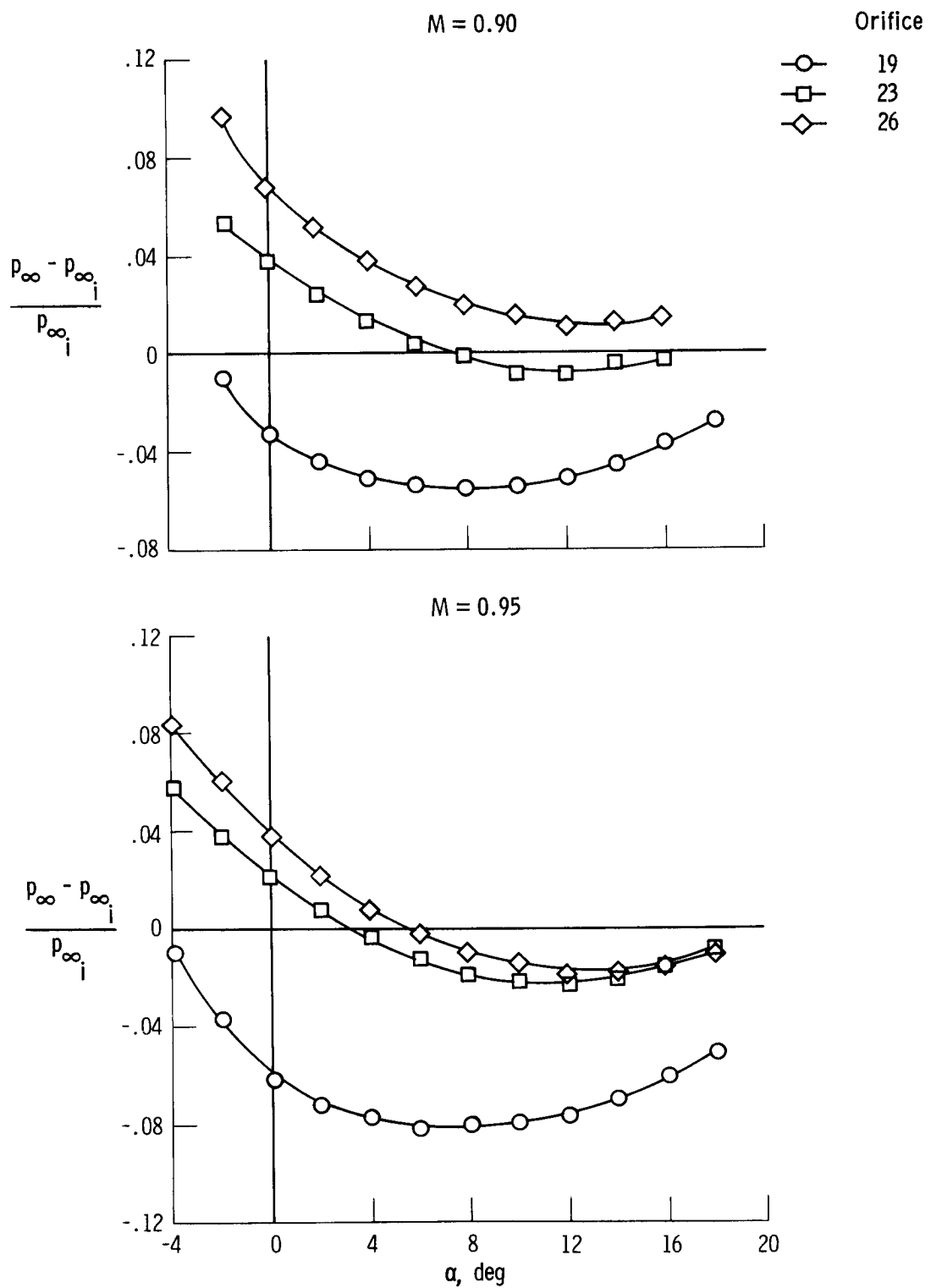


Figure 15. Continued.

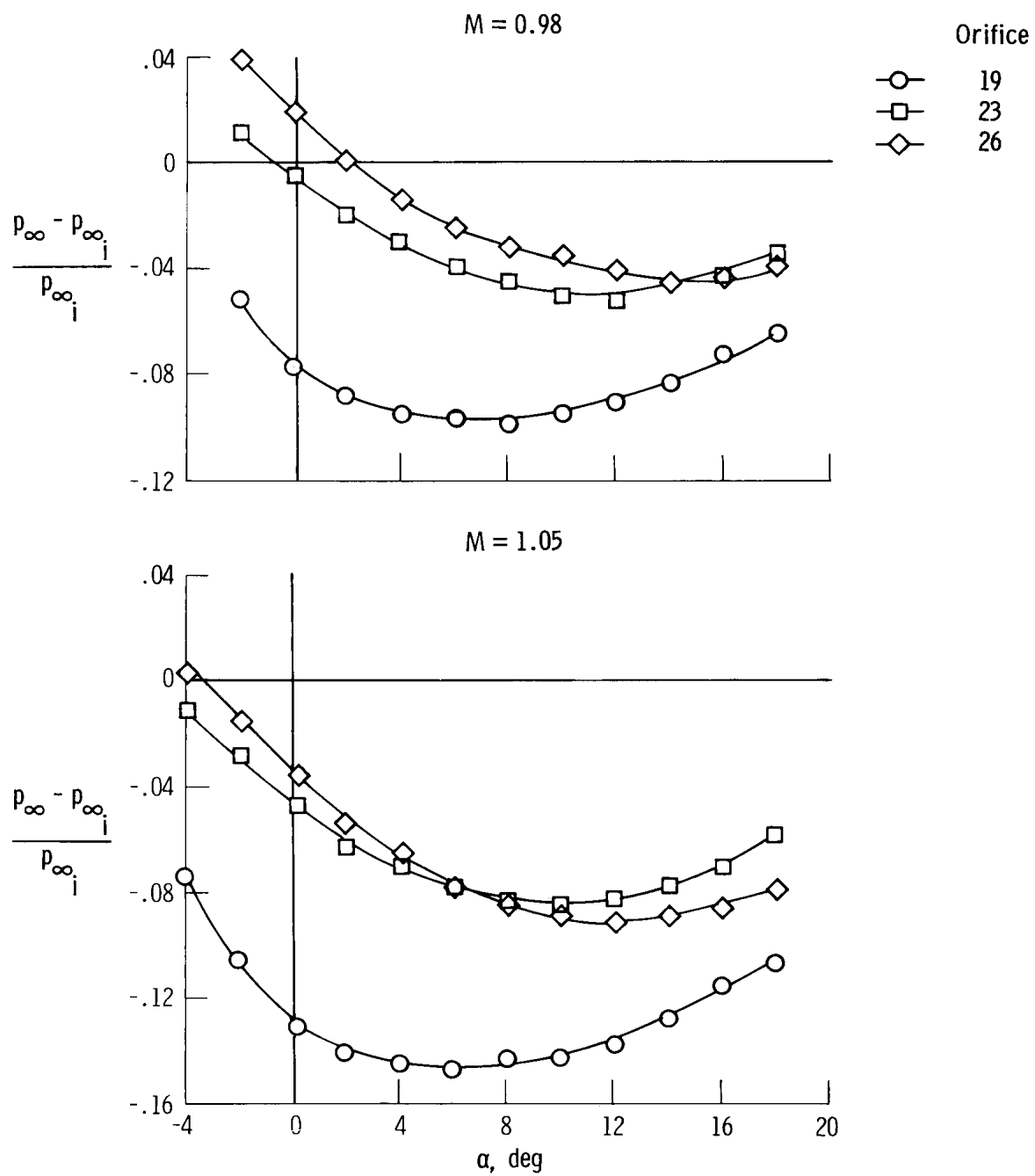


Figure 15. Continued.

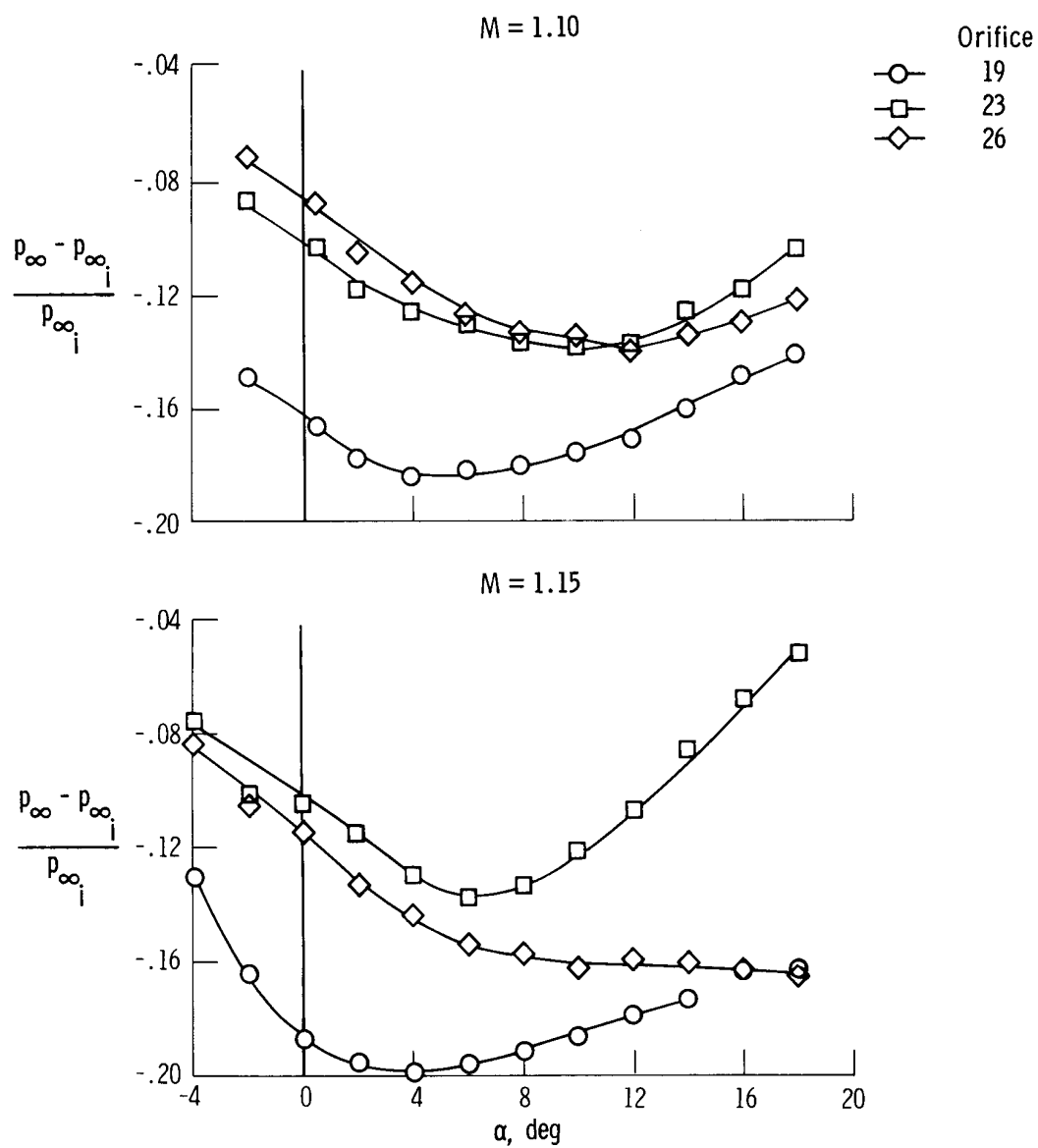


Figure 15. Continued.

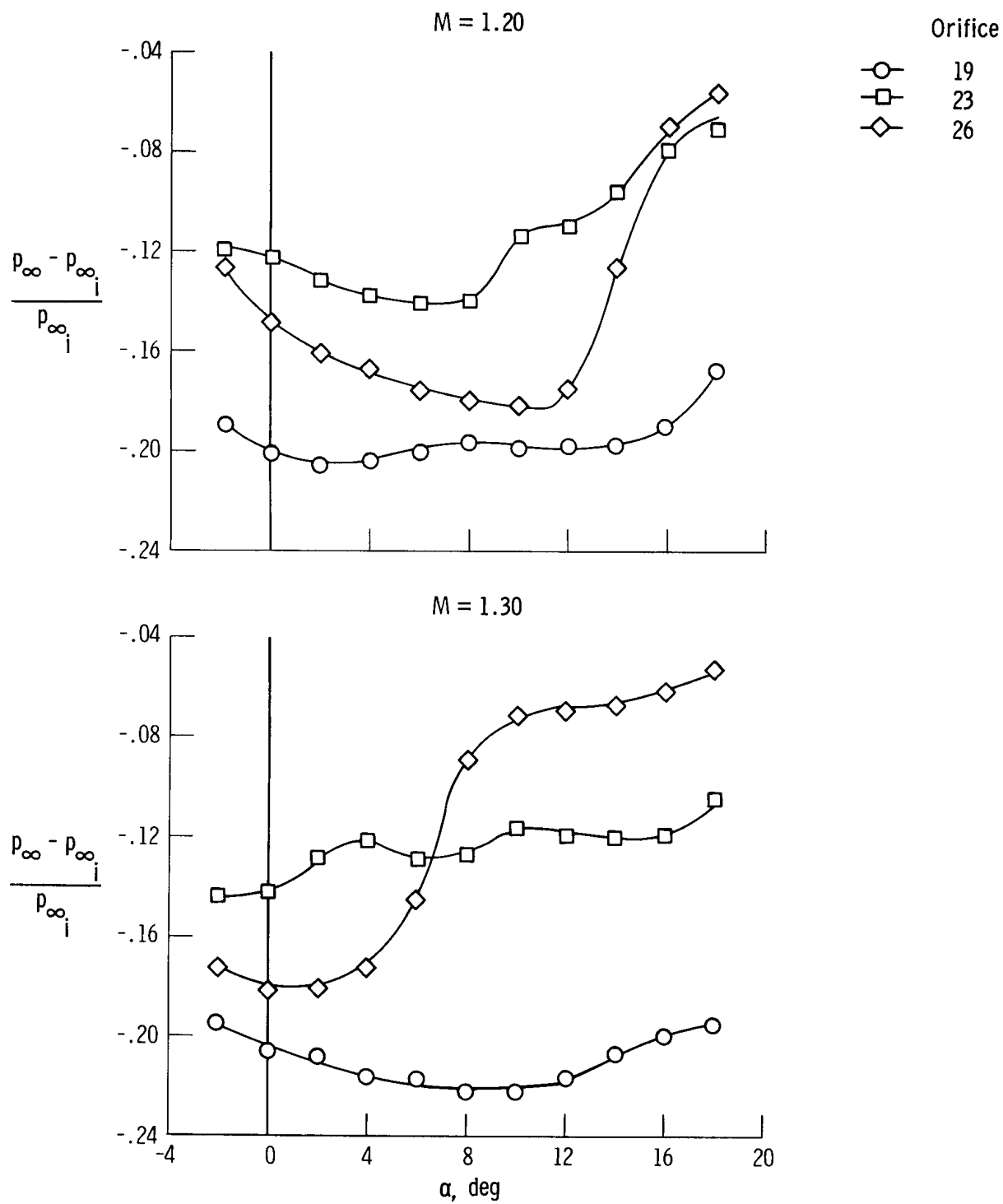


Figure 15. Continued.

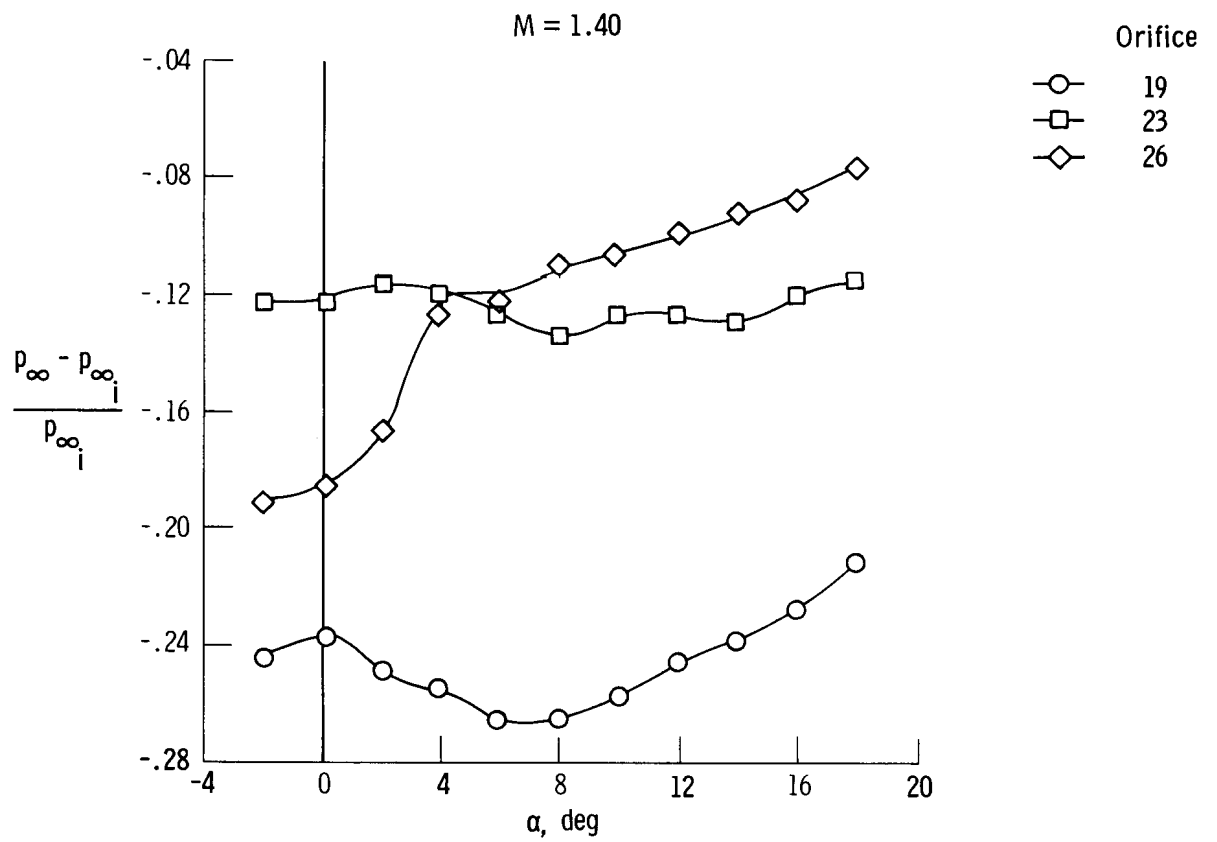


Figure 15. Concluded.

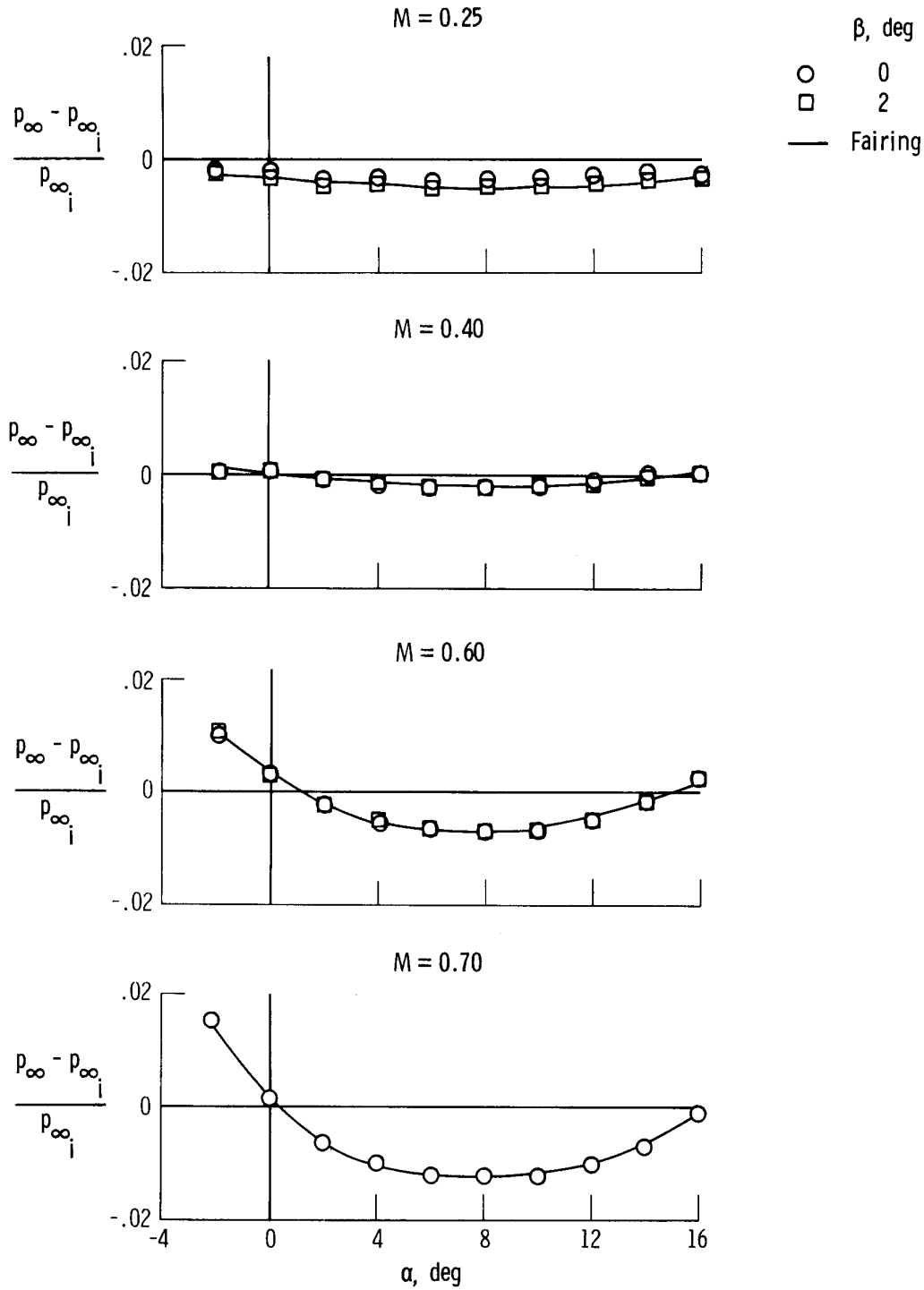


Figure 16. Correction to static pressure position error for orifices 19 and 20 when averaged and plotted against angle of attack for sideslips of 0° and 2° . Data were not acquired for 2° sideslip at all Mach numbers.

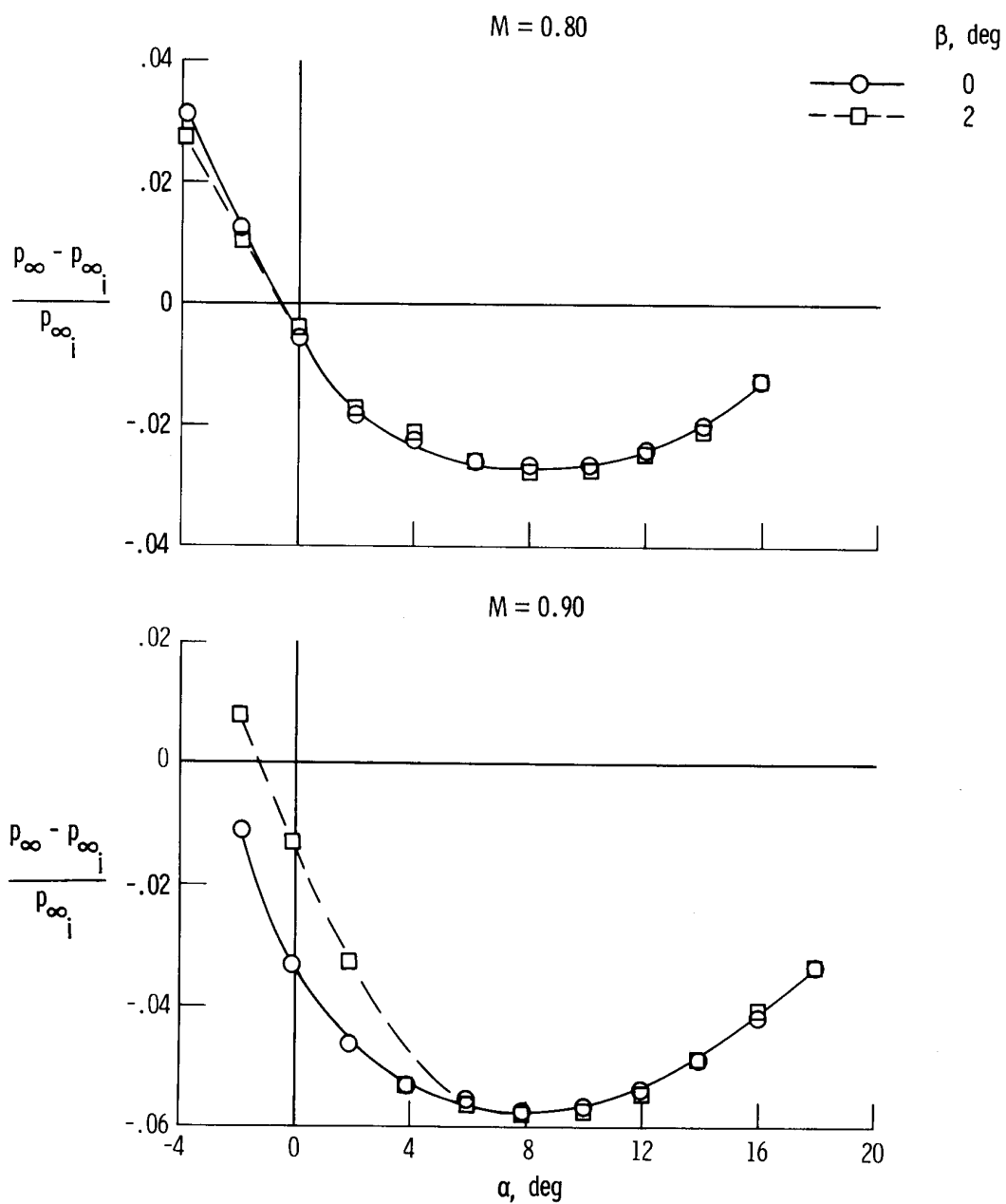


Figure 16. Continued.

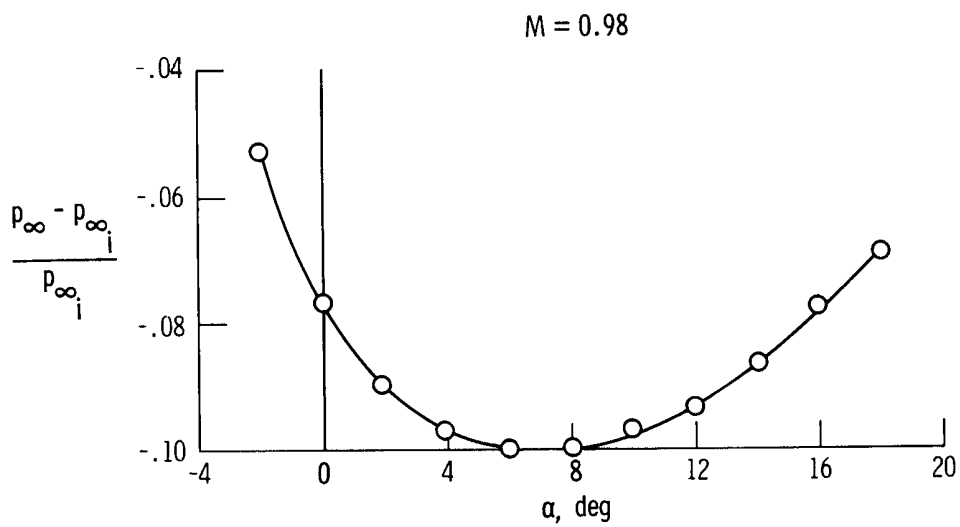
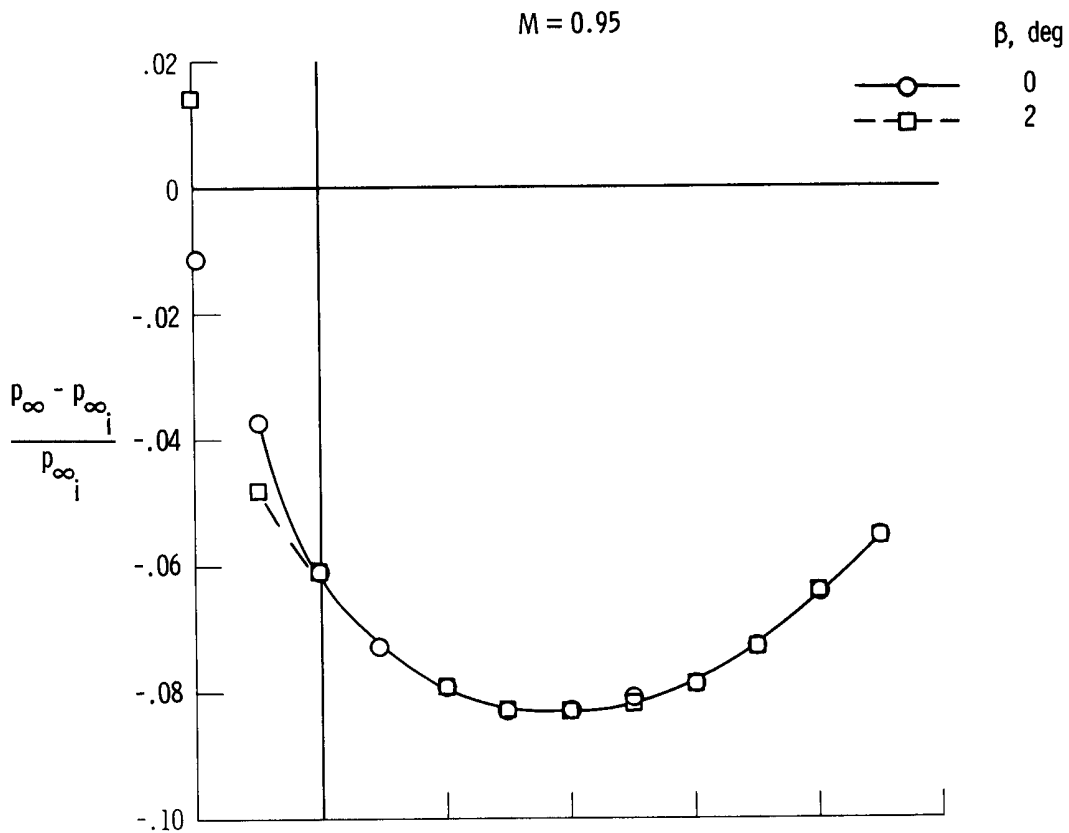


Figure 16. Continued.

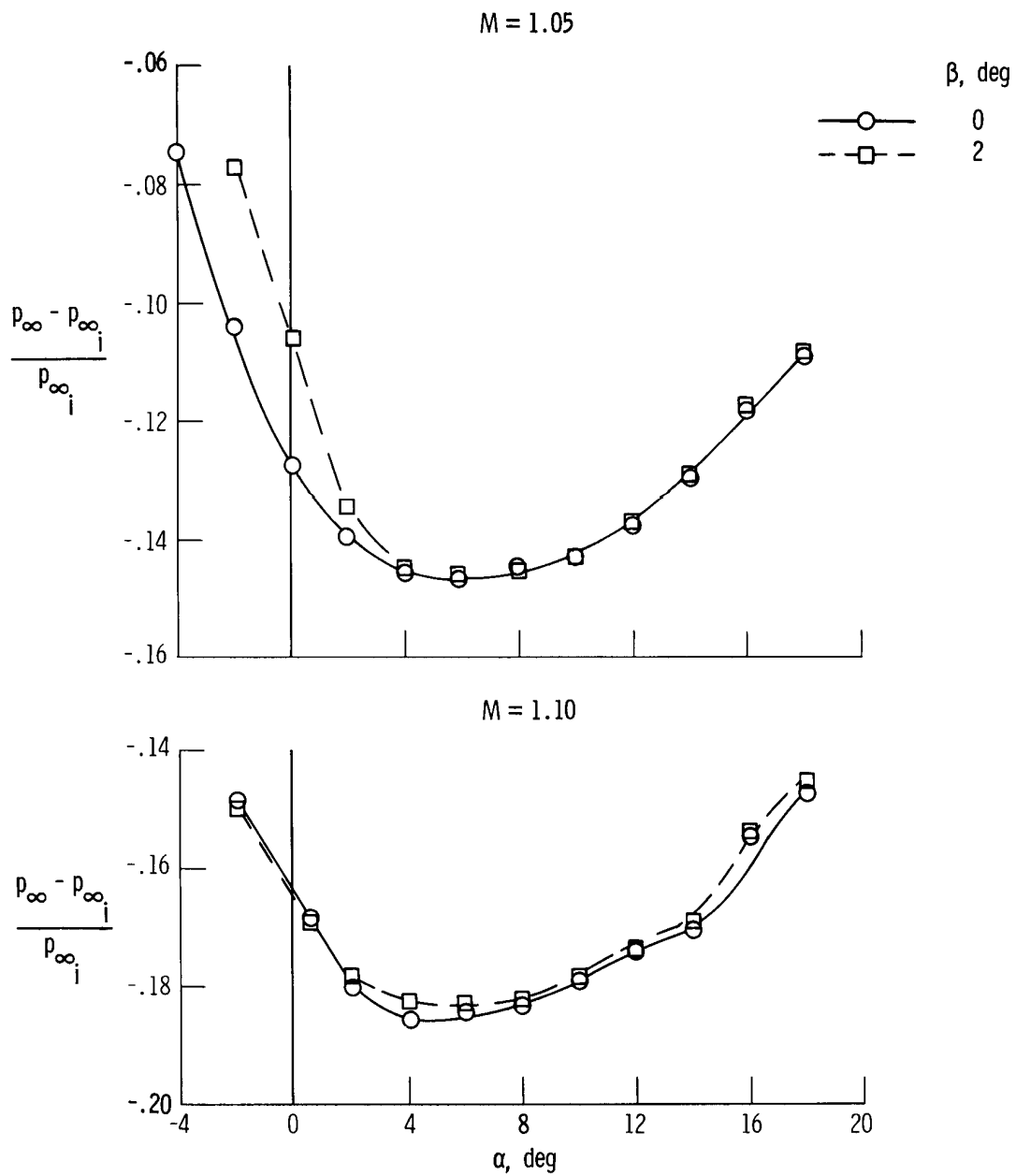


Figure 16. Continued.

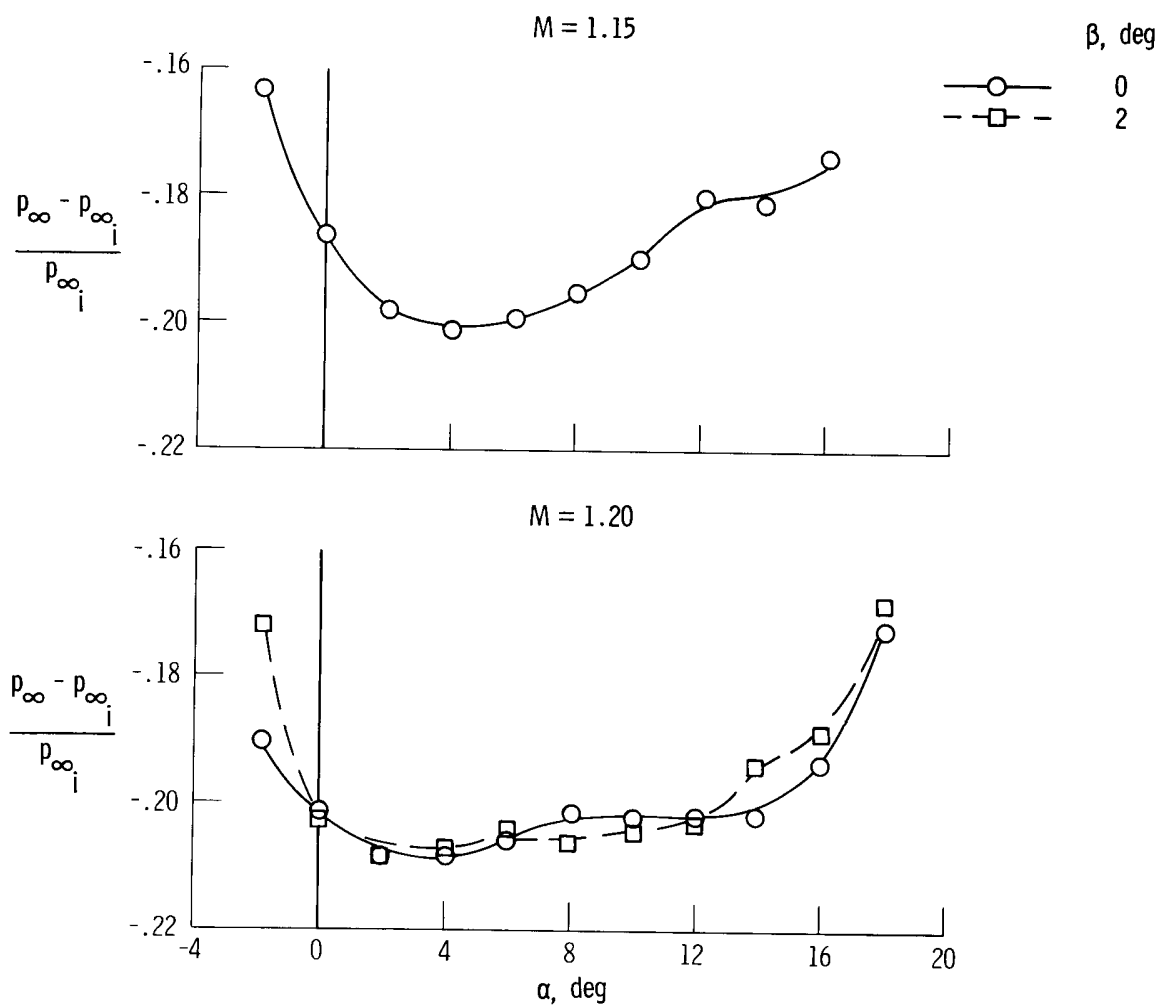


Figure 16. Continued.

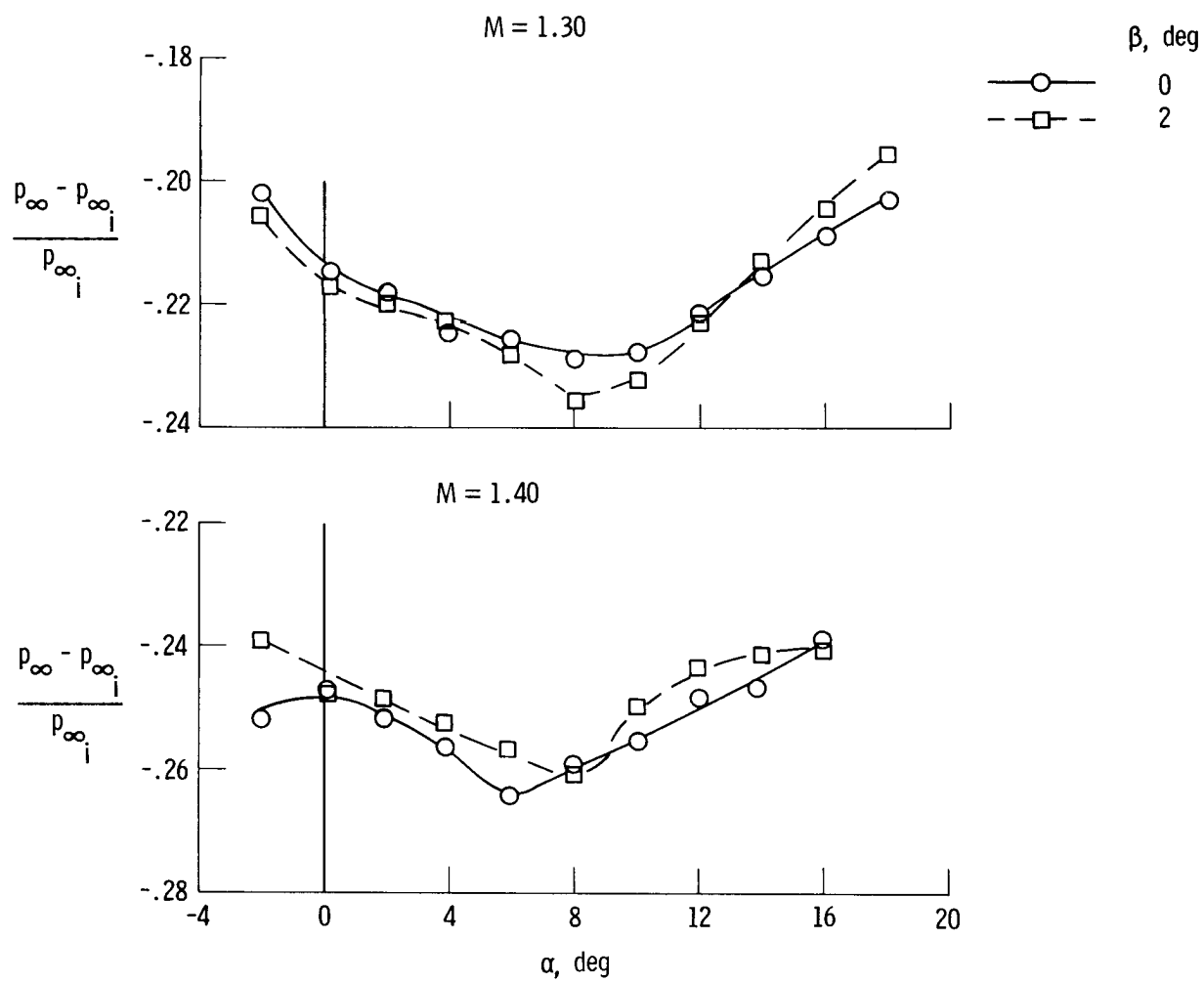


Figure 16. Concluded.

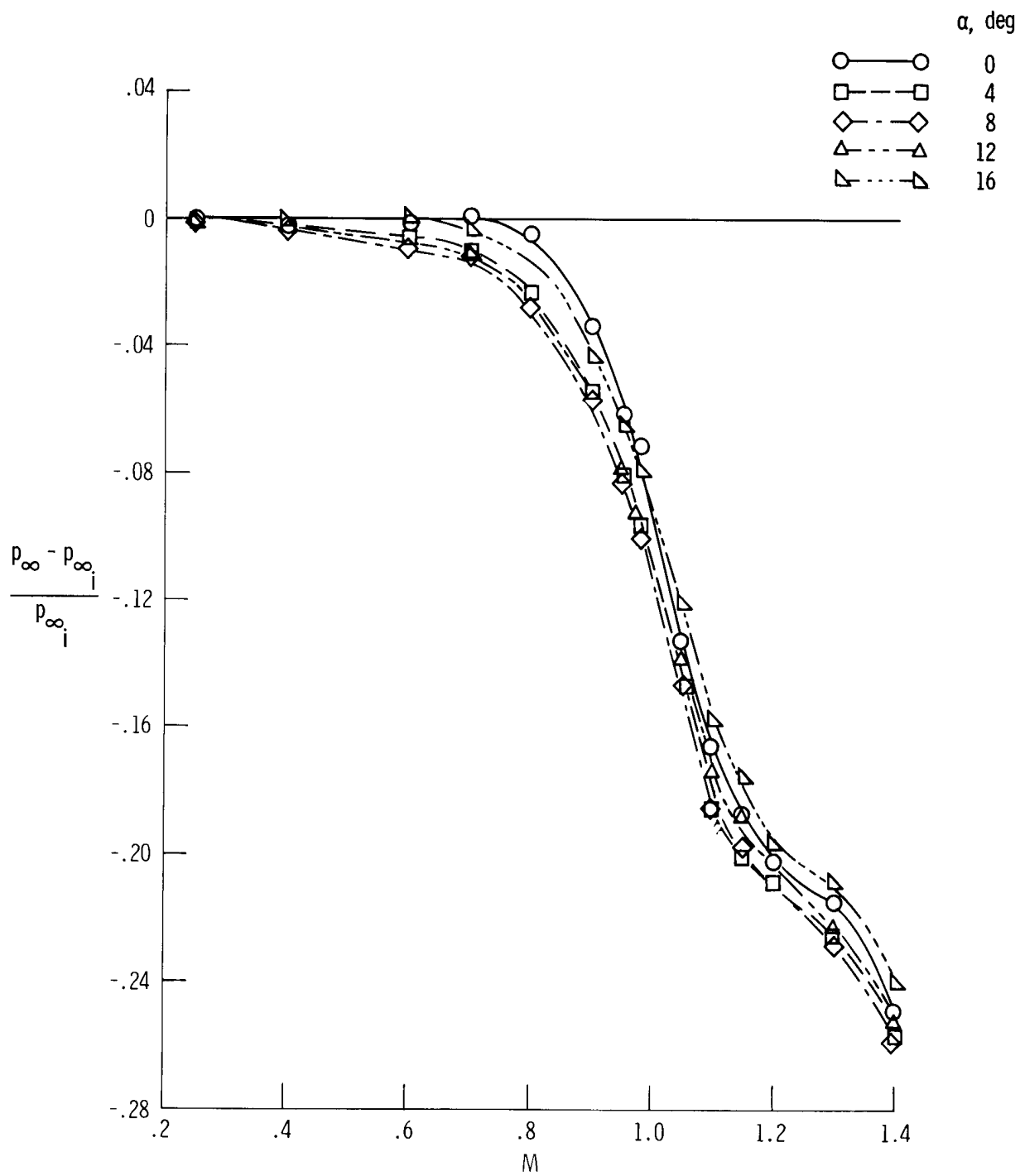


Figure 17. Correction for static pressure position error for orifices 19 and 20 when averaged and plotted against Mach number. $\beta = 0^\circ$.

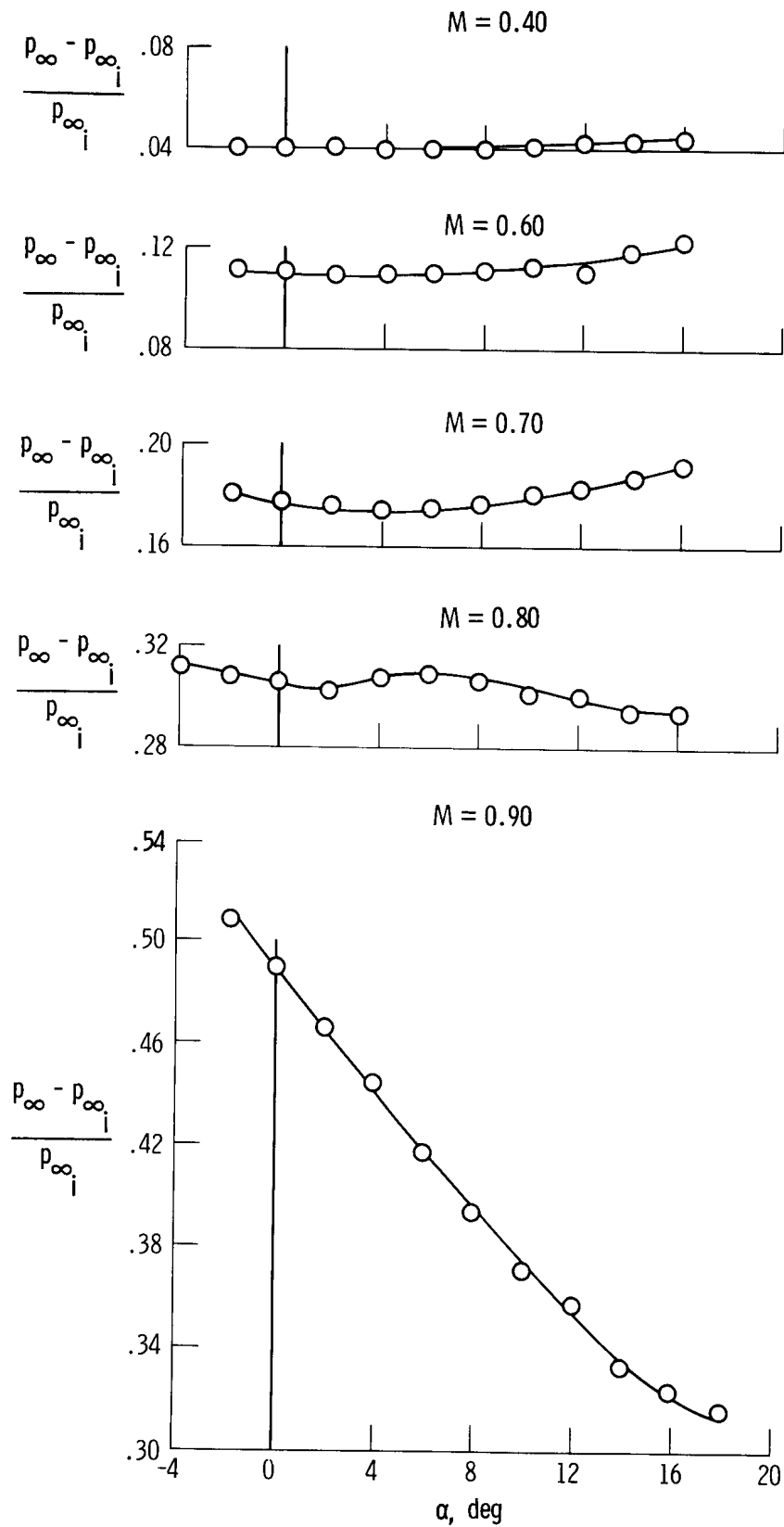


Figure 18. Correction for static pressure position error for orifice 112 plotted against angle of attack.

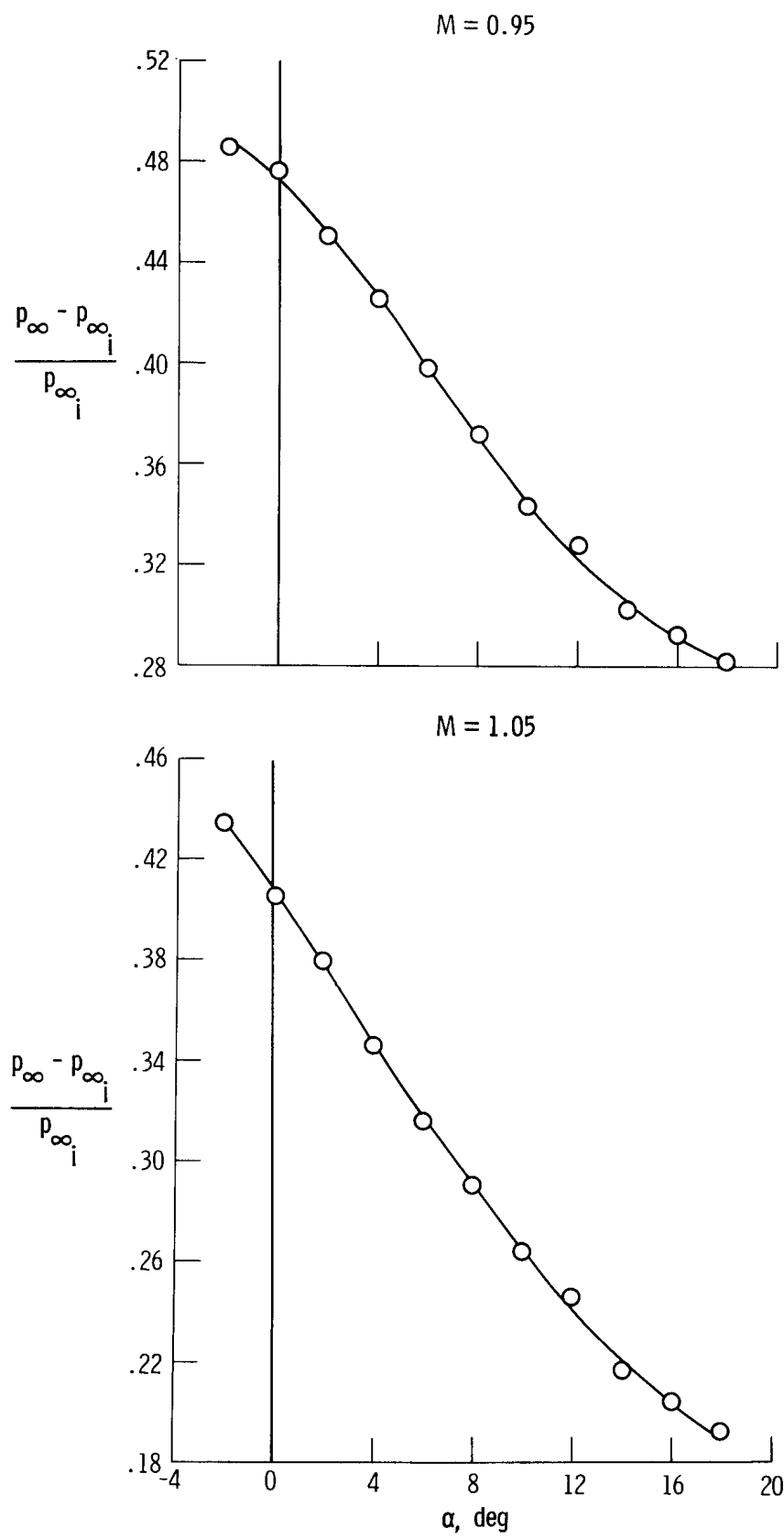


Figure 18. Continued.

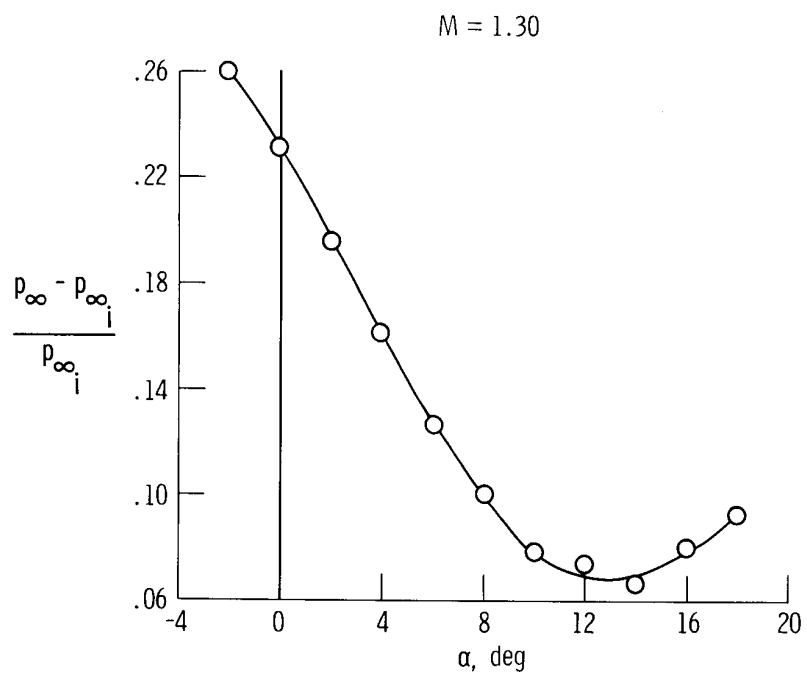
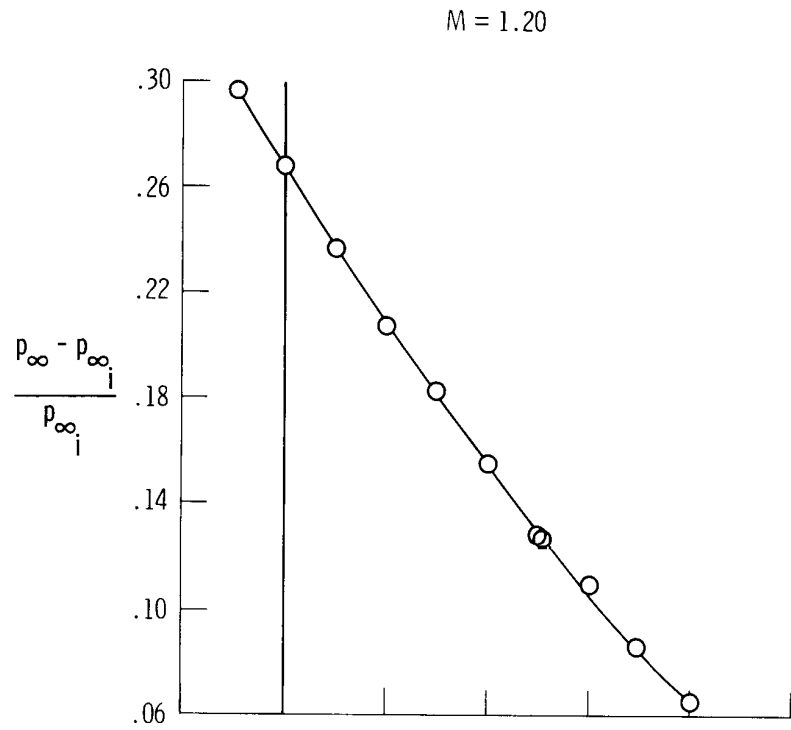


Figure 18. Continued.

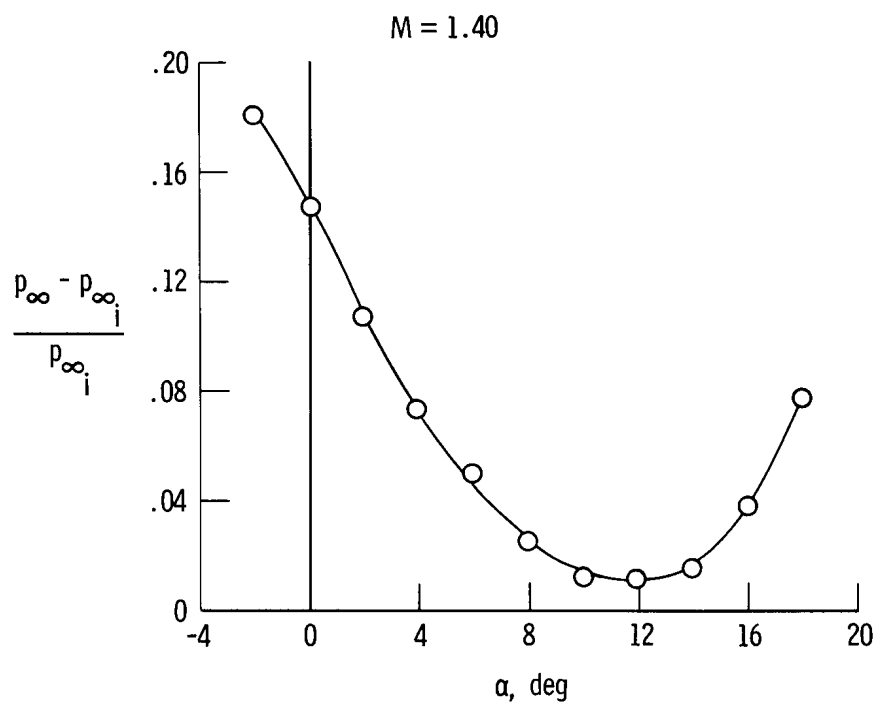


Figure 18. Concluded.

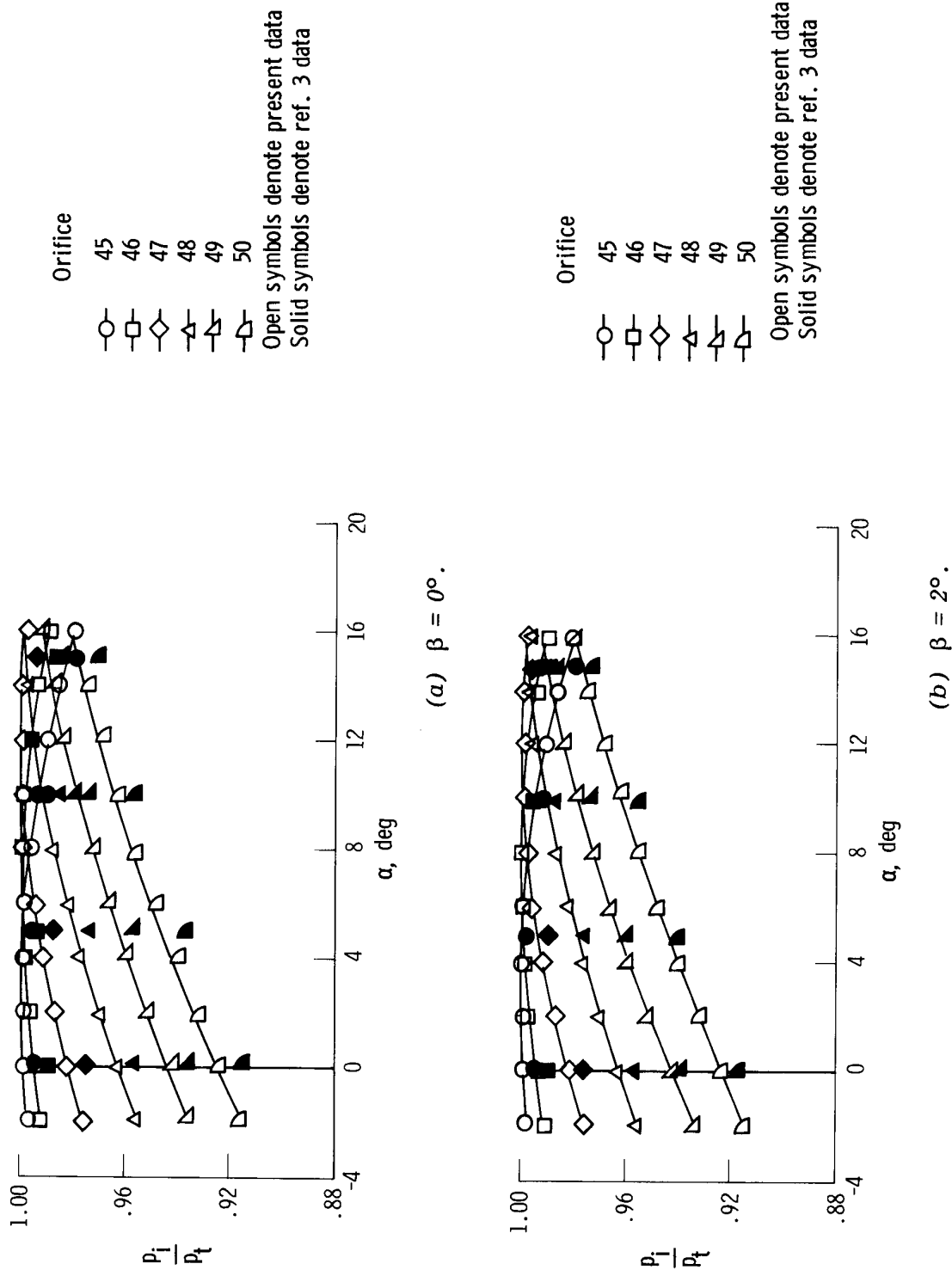


Figure 19. Comparisons of ratios of nose cap pressures to reference total pressure as measured by two wind tunnel facilities. $M = 0.40$.

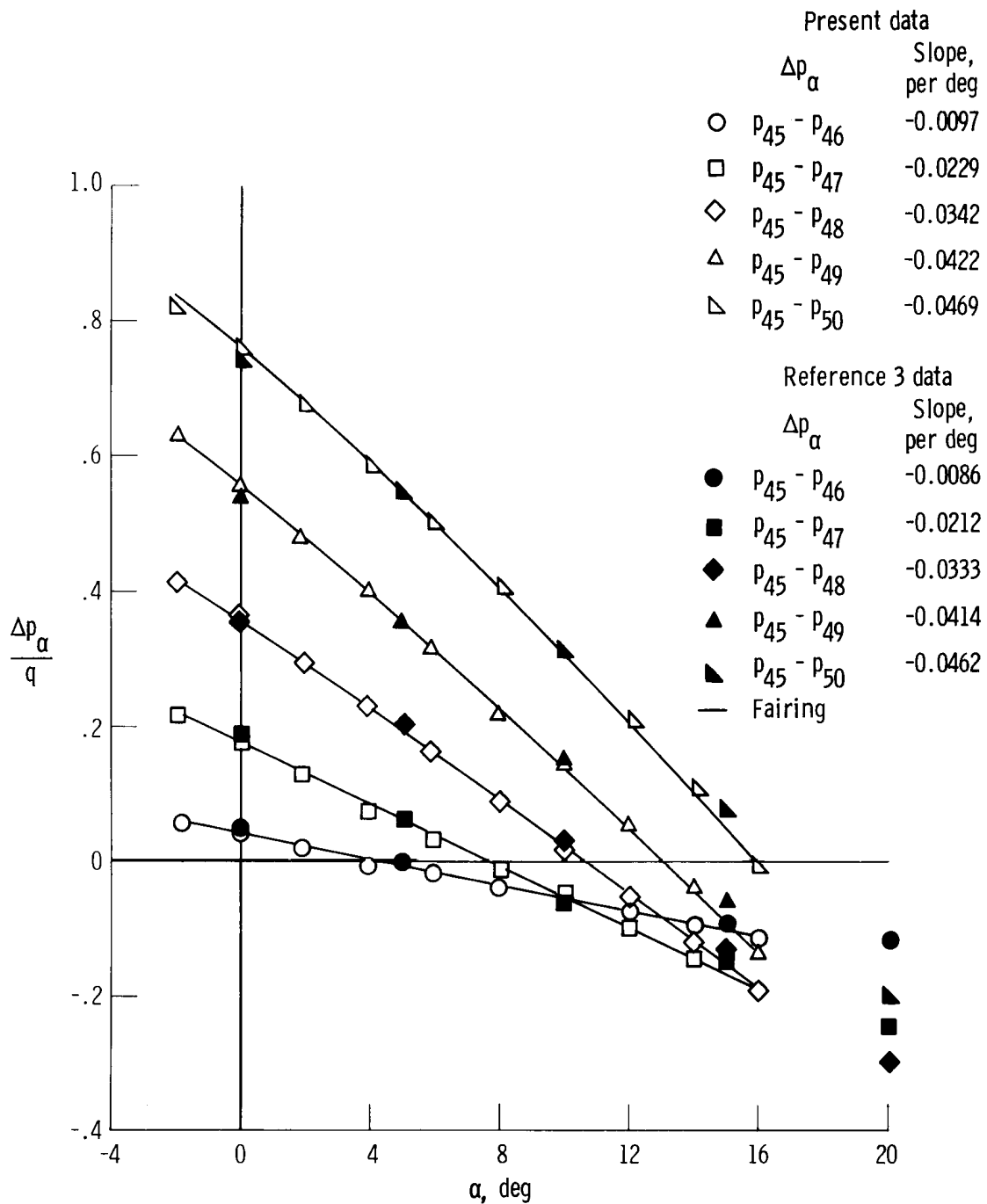
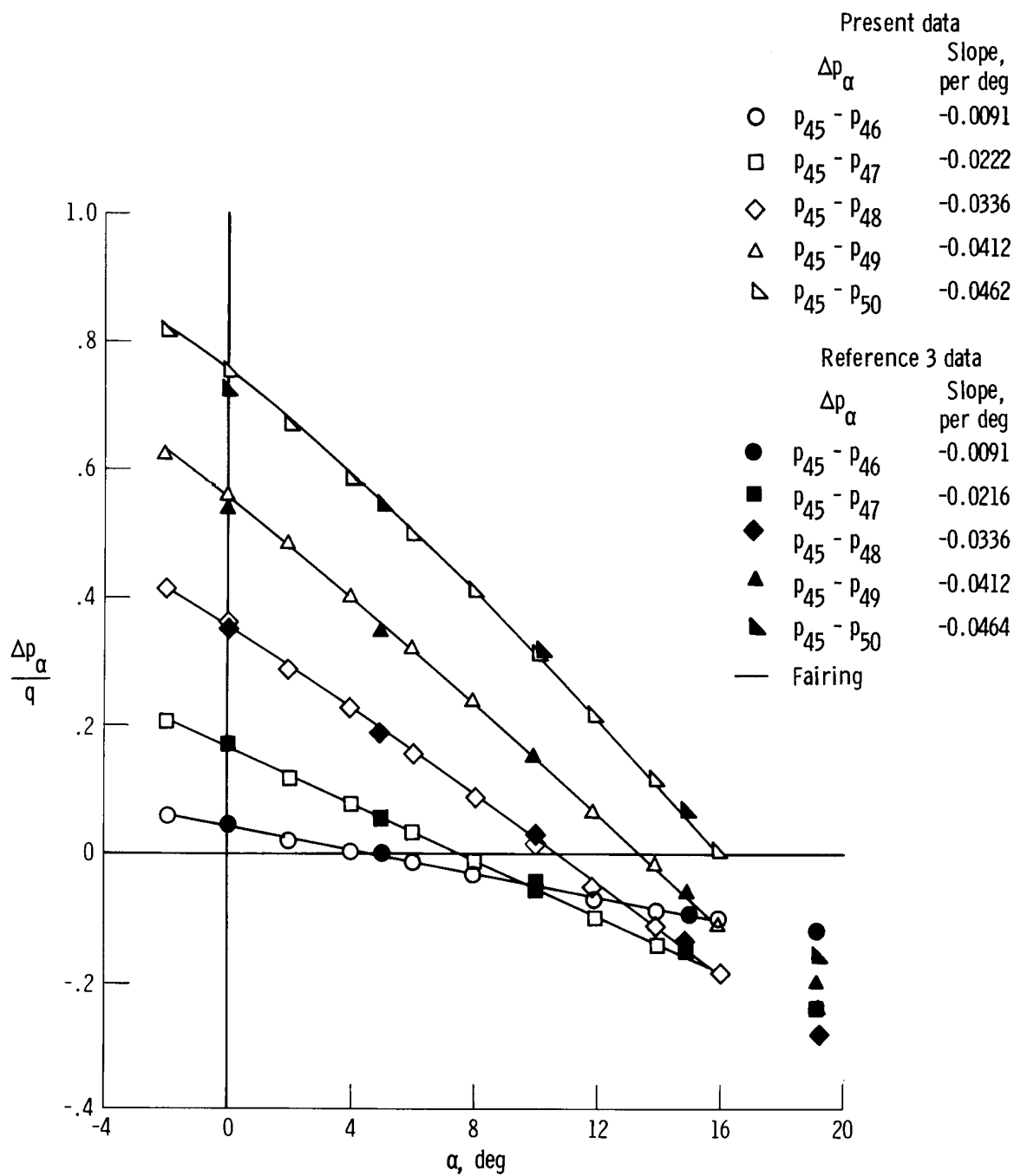
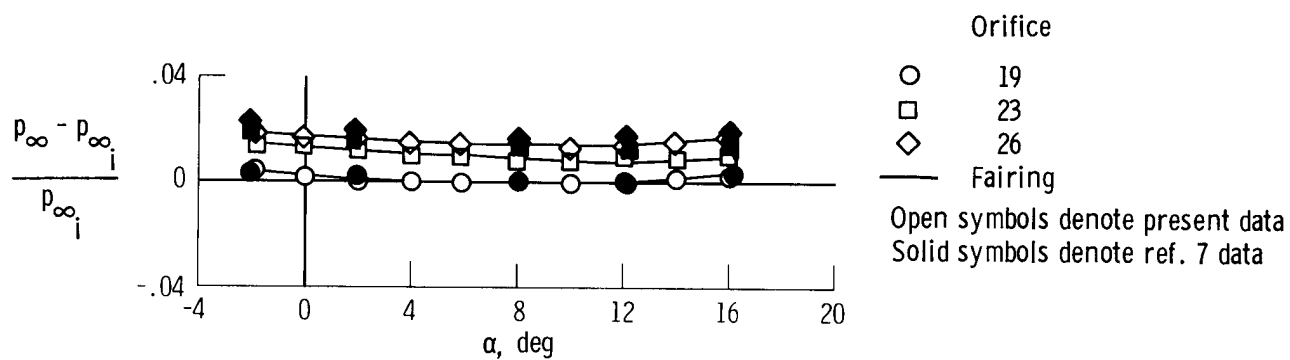


Figure 20. Comparisons of angle of attack pressure parameters for nose cap orifices as measured from two wind tunnel facilities. $M = 0.40$.

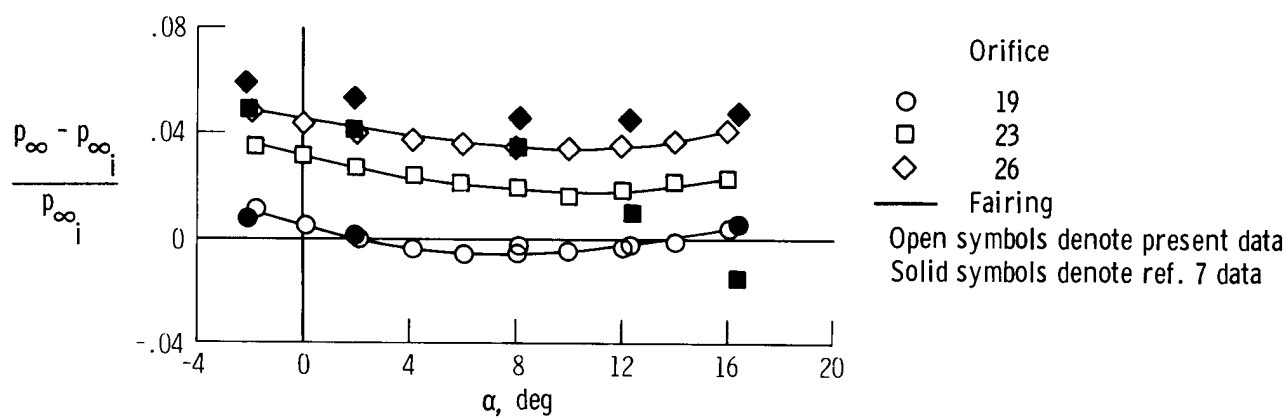


(b) $\beta = 2^\circ$.

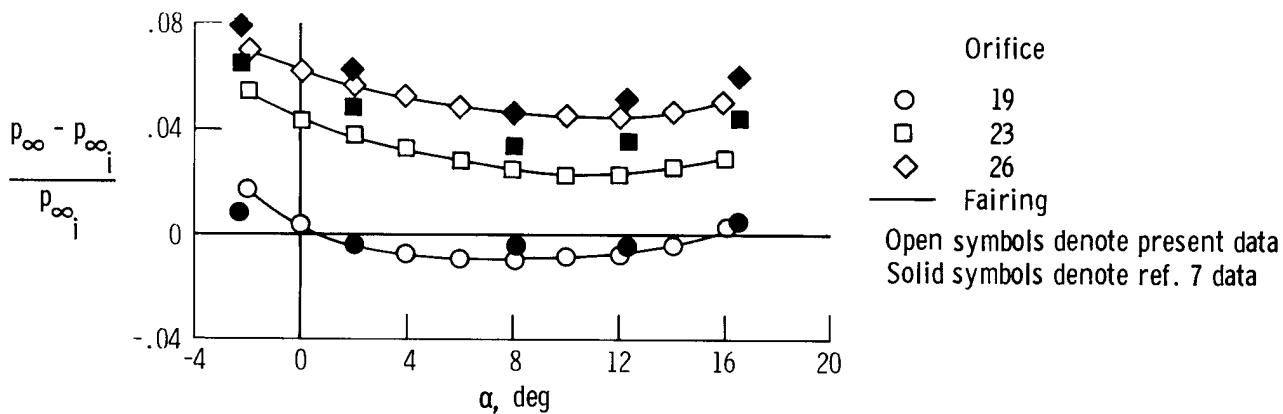
Figure 20. Concluded.



(a) $M = 0.40$.

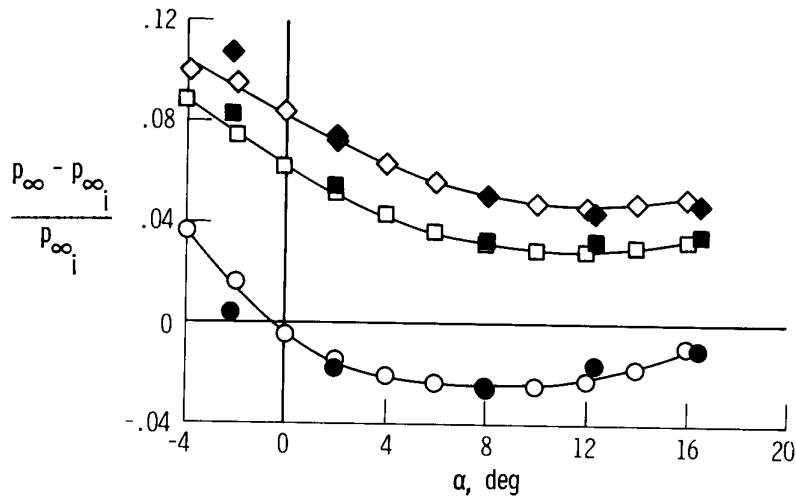


(b) $M = 0.60$.

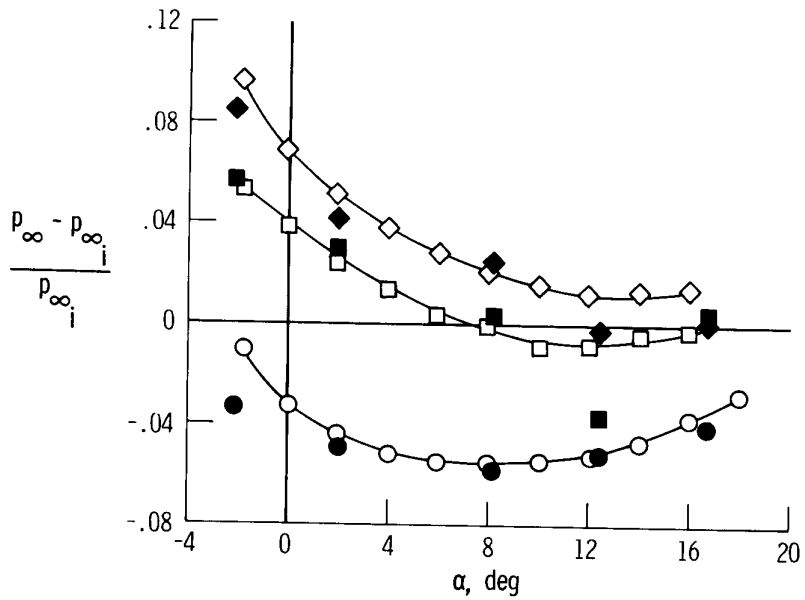


(c) $M = 0.70$.

Figure 21. Comparisons of static pressure position error corrections for auxiliary pressure orifices as measured from two wind tunnel facilities. $\beta = 0^\circ$.

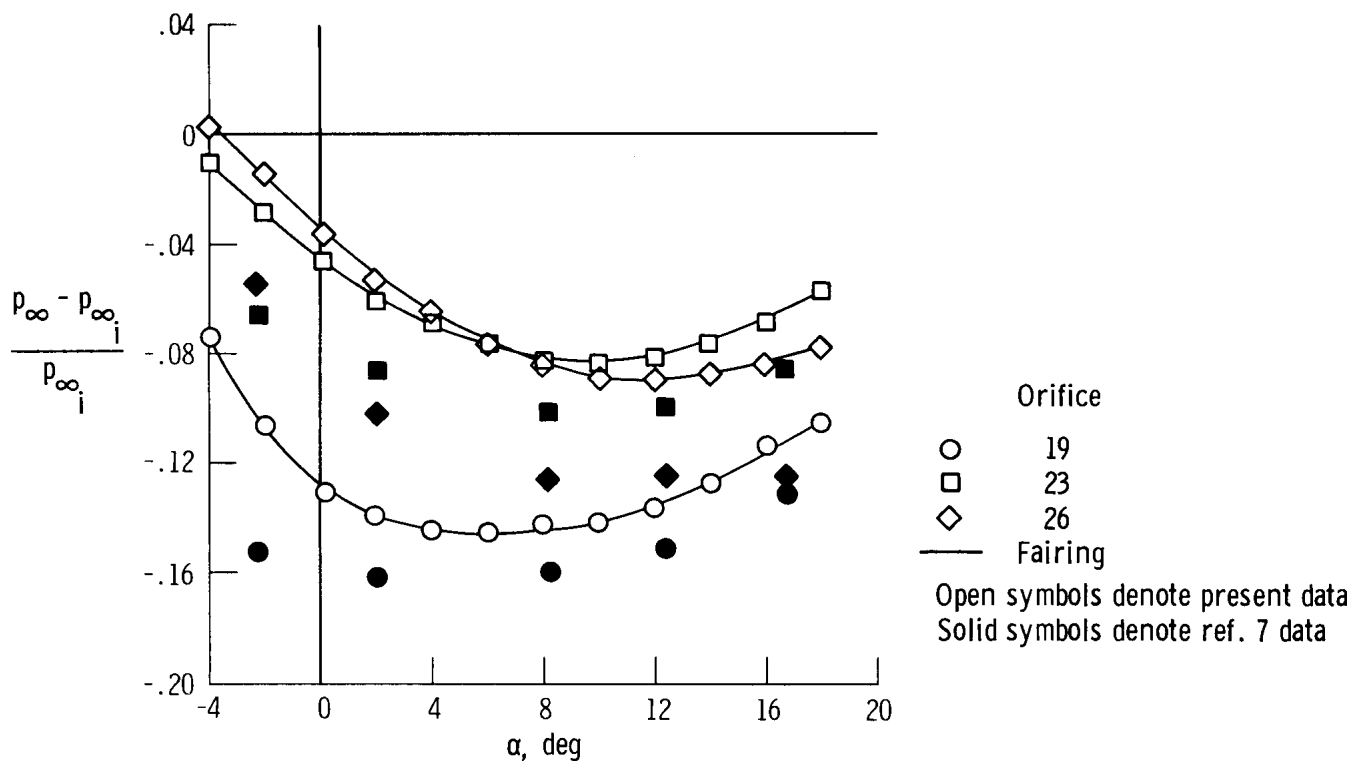


(d) $M = 0.80$.

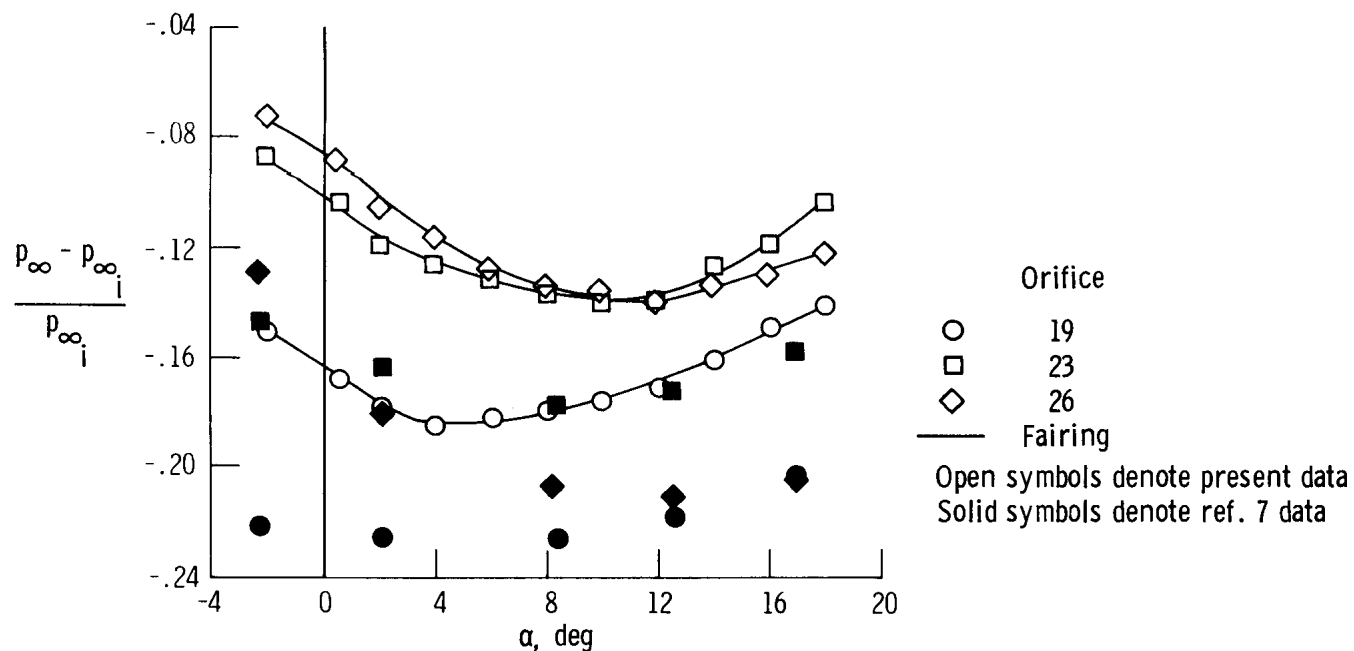


(e) $M = 0.90$.

Figure 21. Continued.

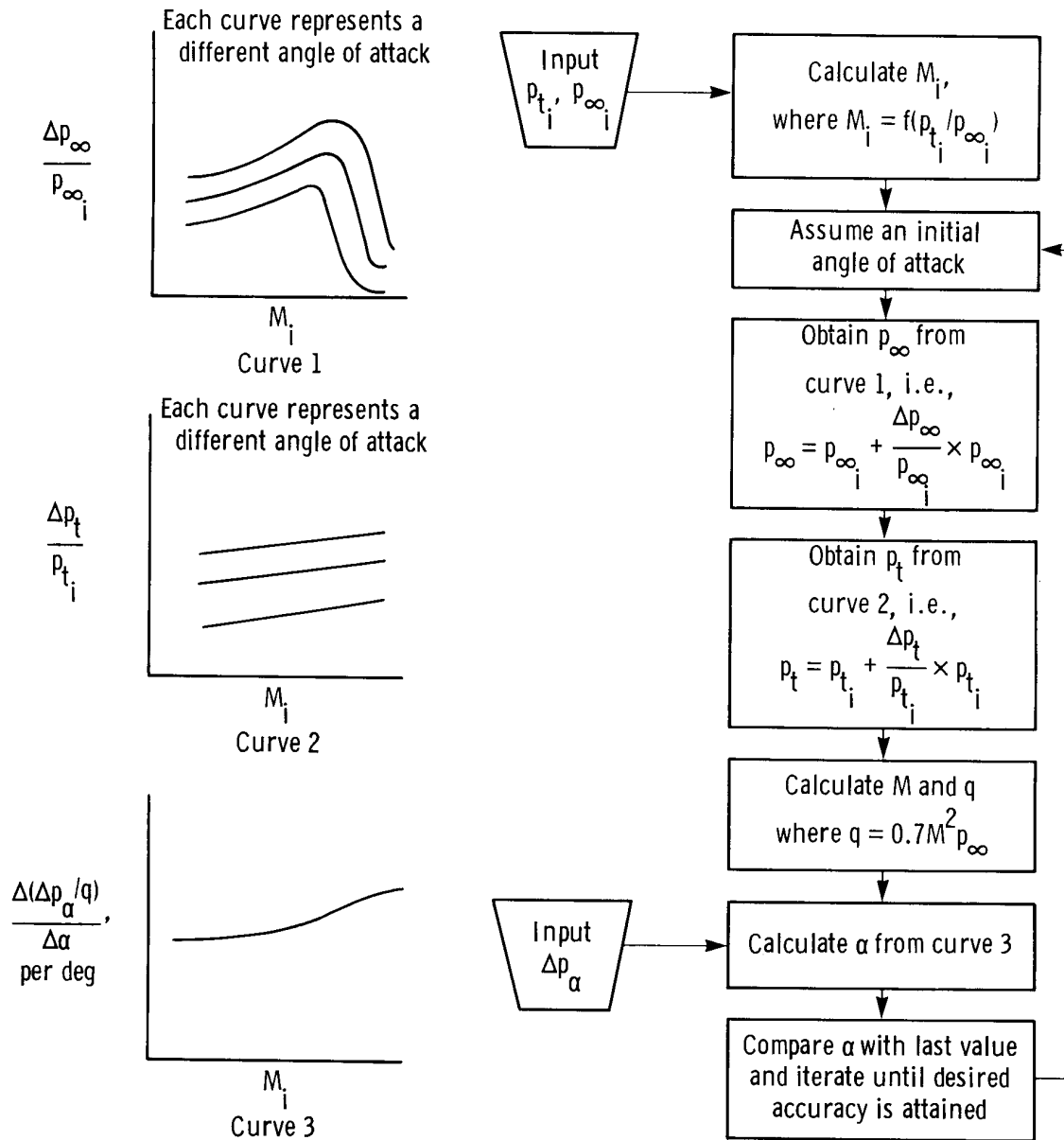


(f) $M \approx 1.05$.



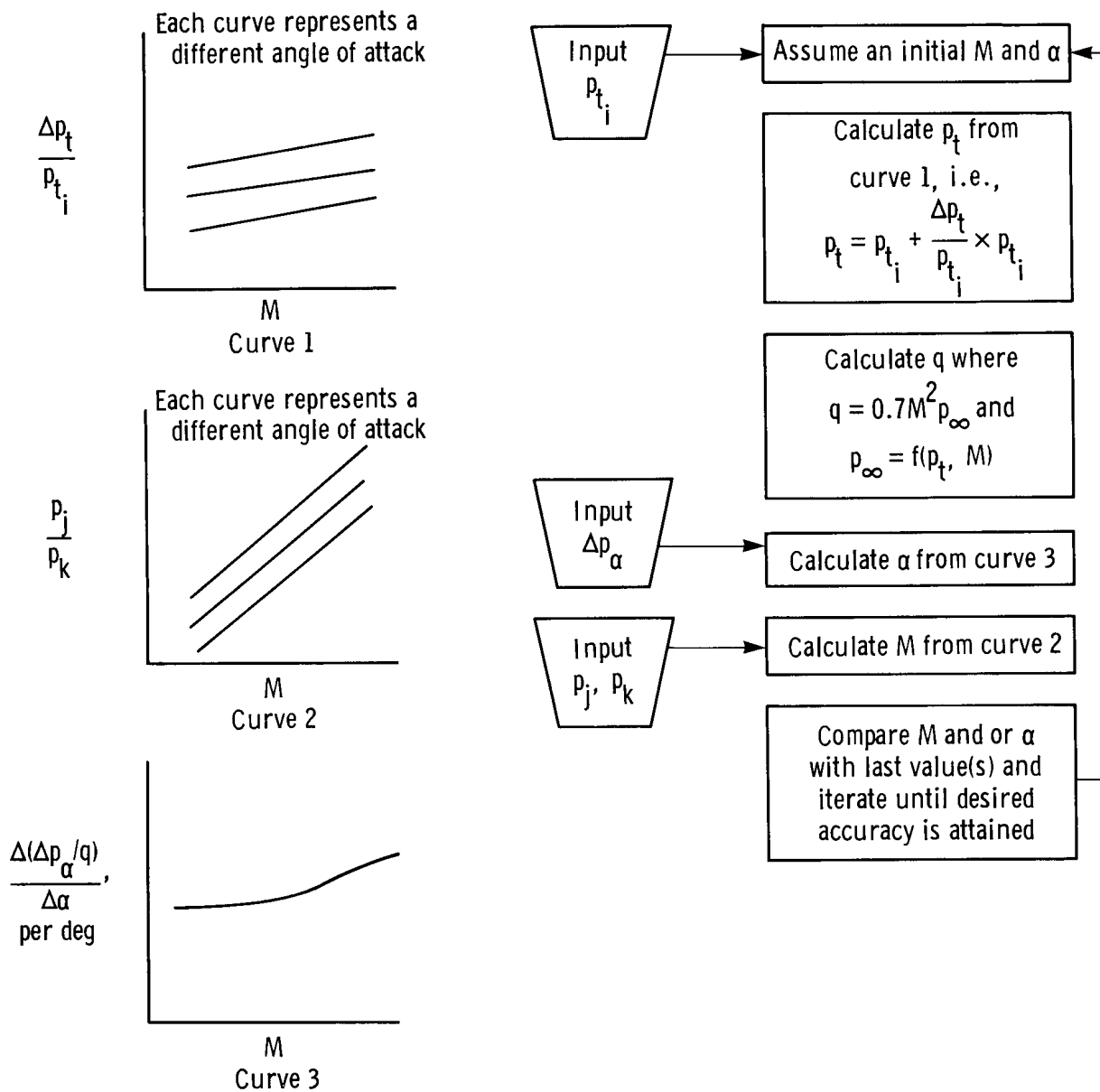
(g) $M \approx 1.10$.

Figure 21. Concluded.



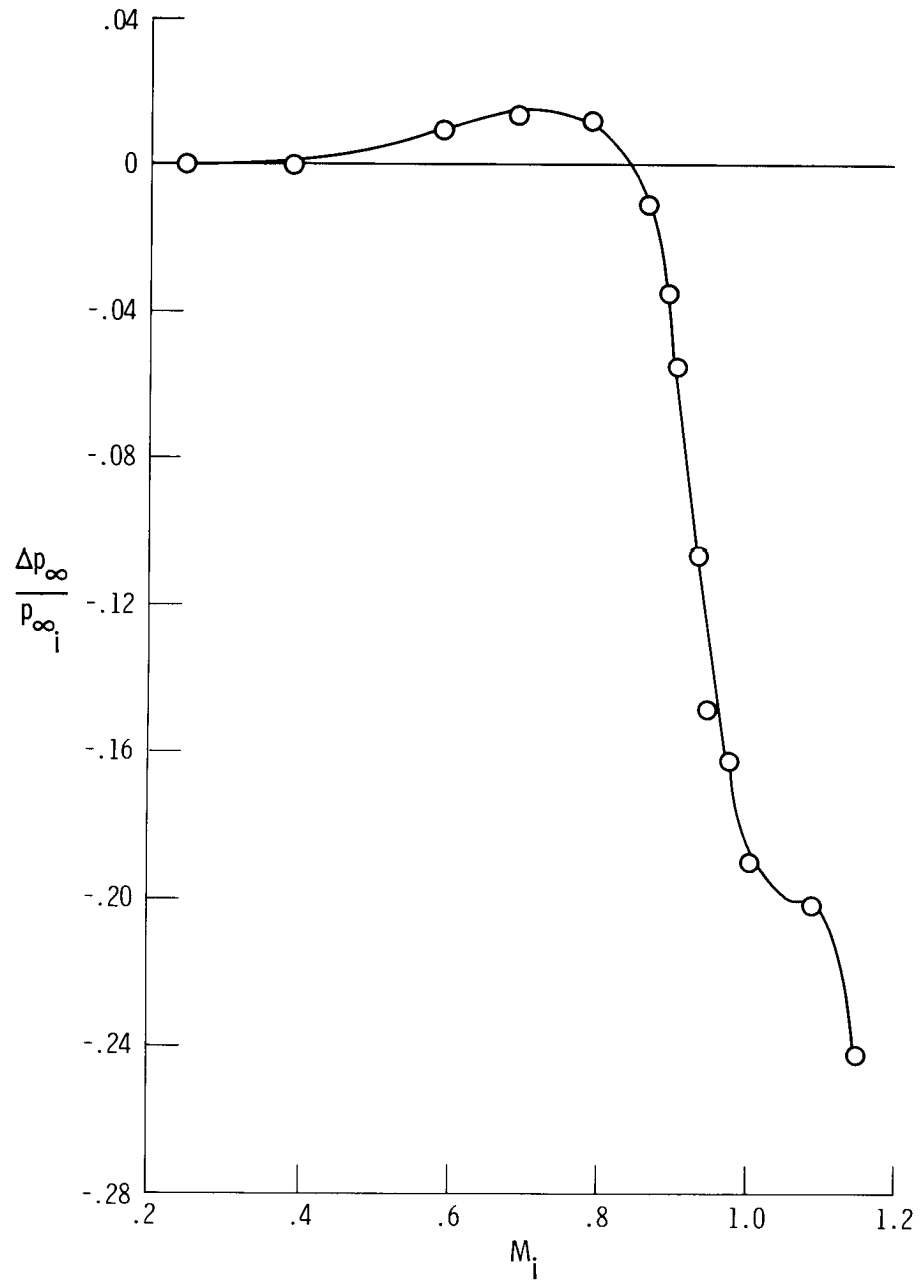
(a) Method I.

Figure 22. Calibration curves and calculation steps required of the two air data reduction methods. $\Delta p_t = p_t - p_{t_i}$.



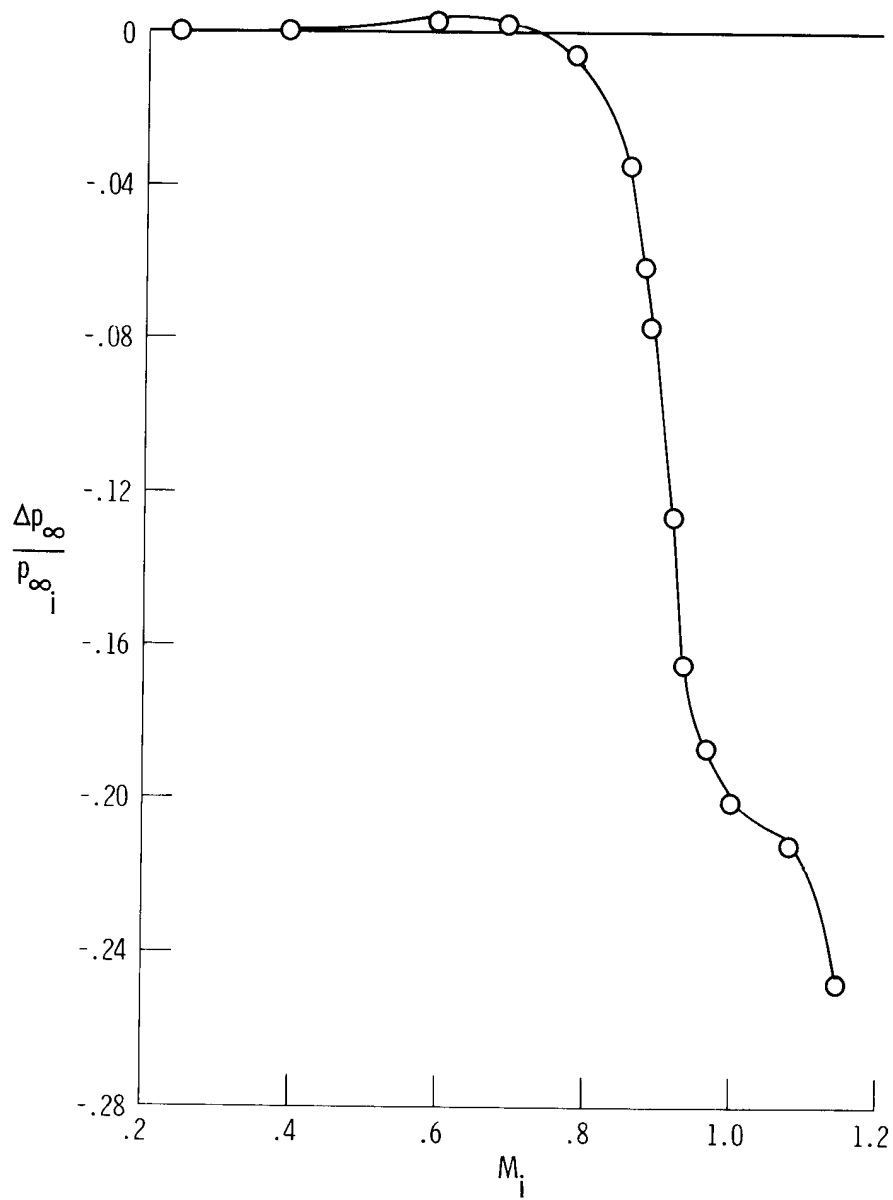
(b) Method II.

Figure 22. Concluded.



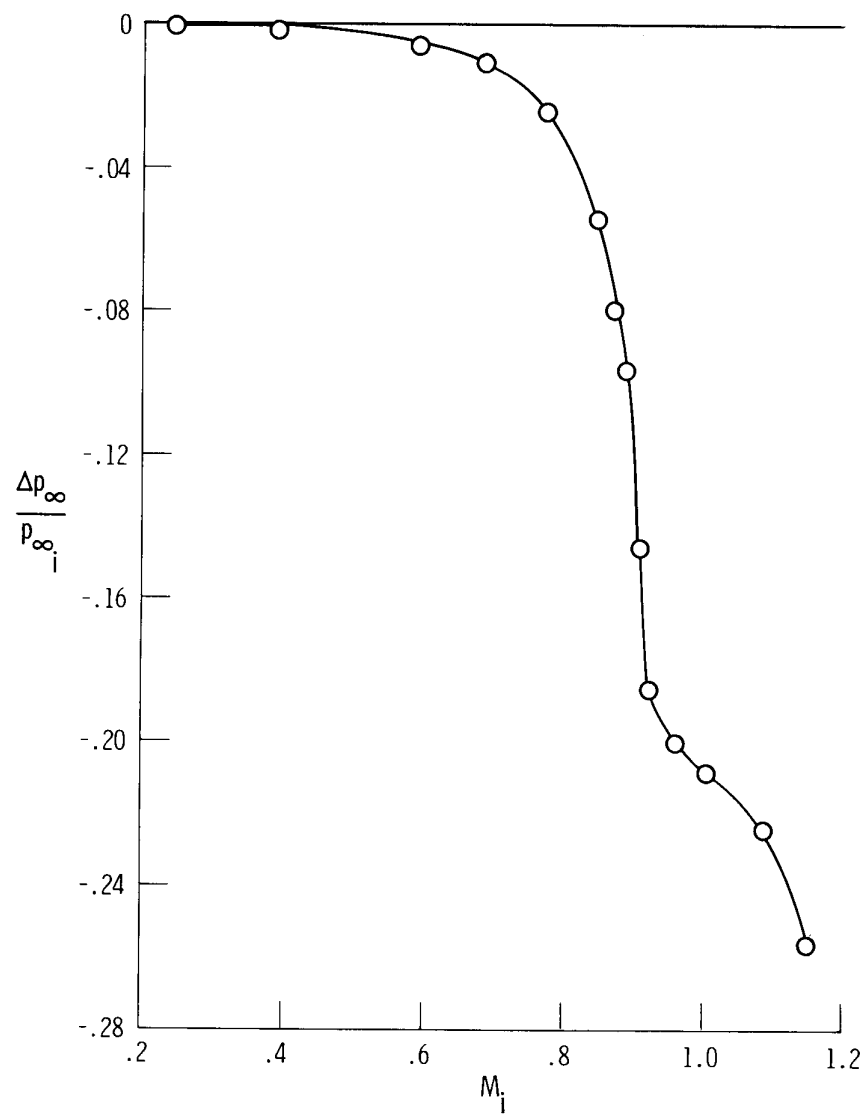
(a) $\alpha = -2.0^\circ$.

Figure 23. Static pressure position error correction curves for data reduction method I. $\beta = 0^\circ$; array A; $\Delta p_\infty = p_\infty - p_{\infty_i}$.



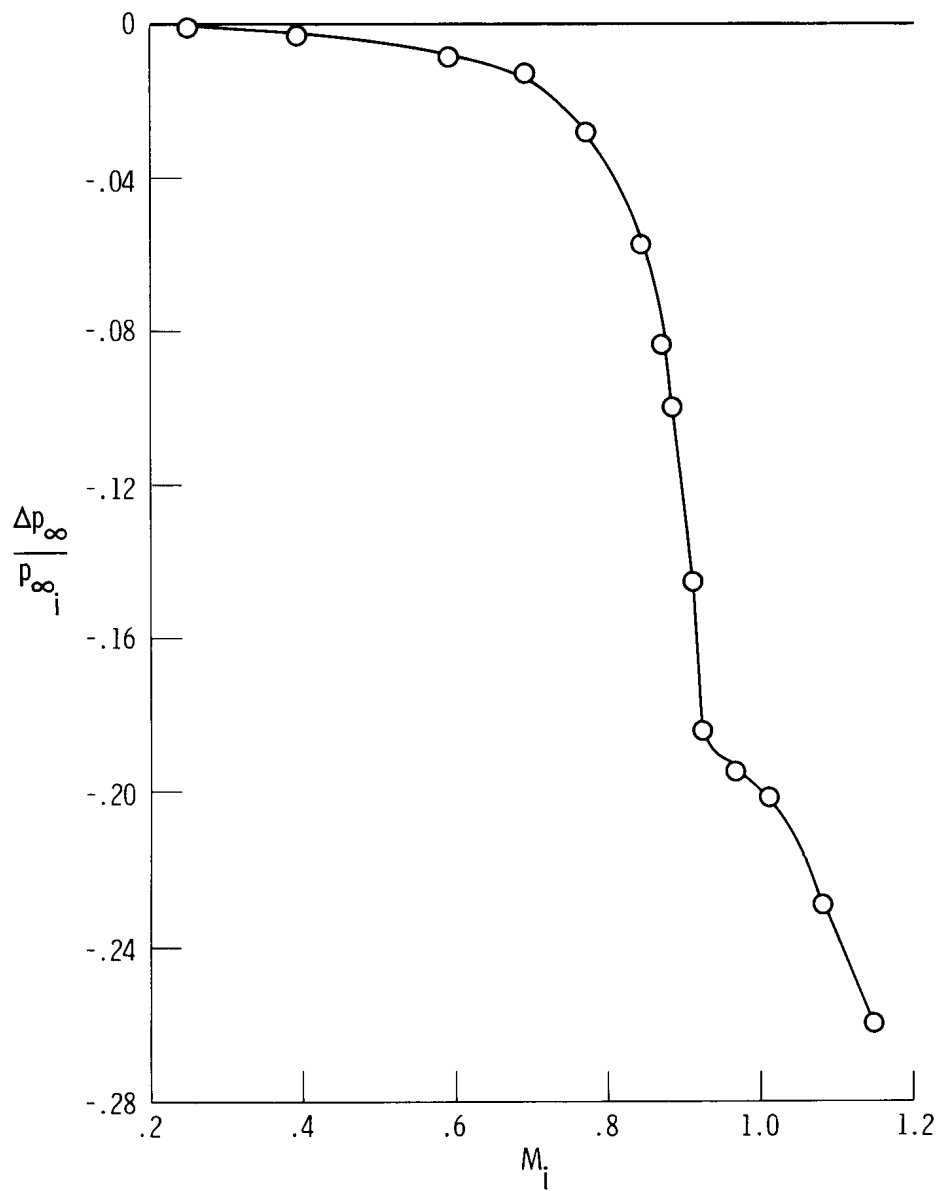
(b) $\alpha = 0^\circ$.

Figure 23. Continued.



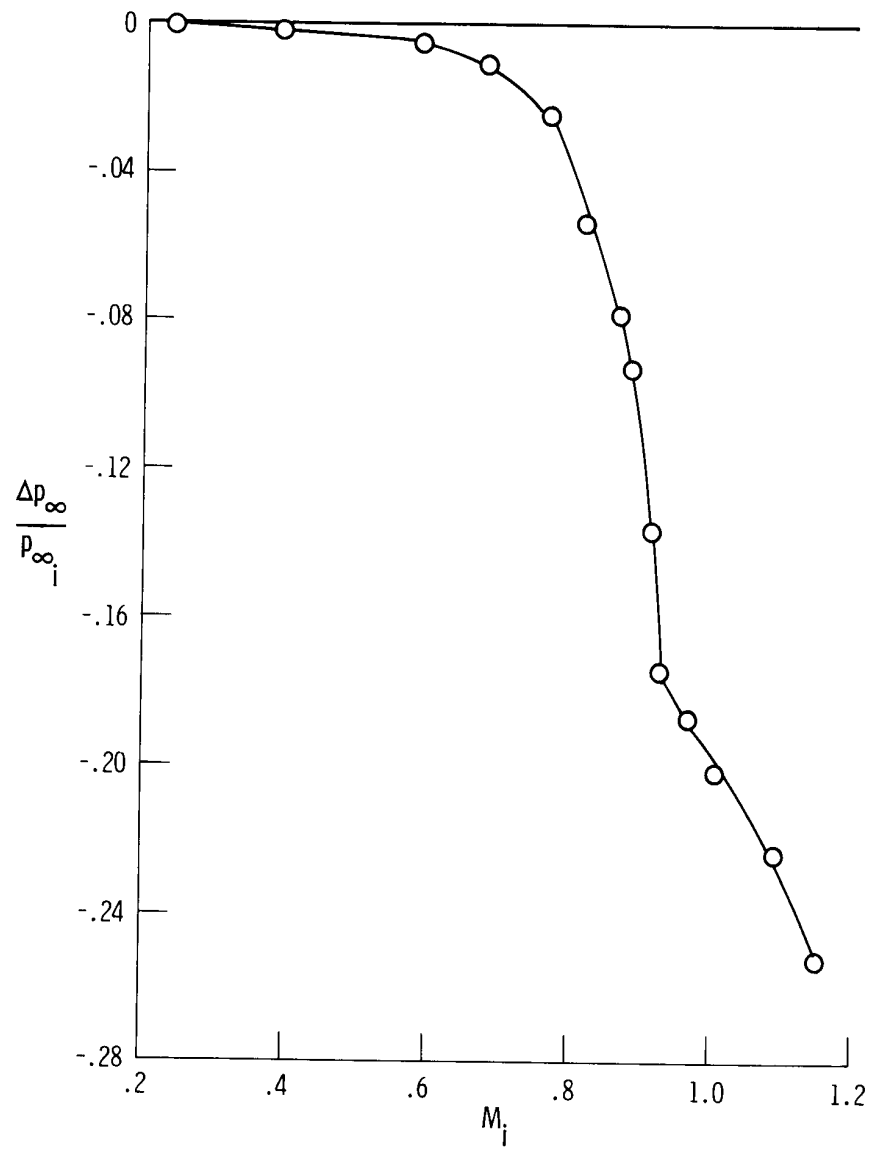
(c) $\alpha = 4^\circ$.

Figure 23. Continued.



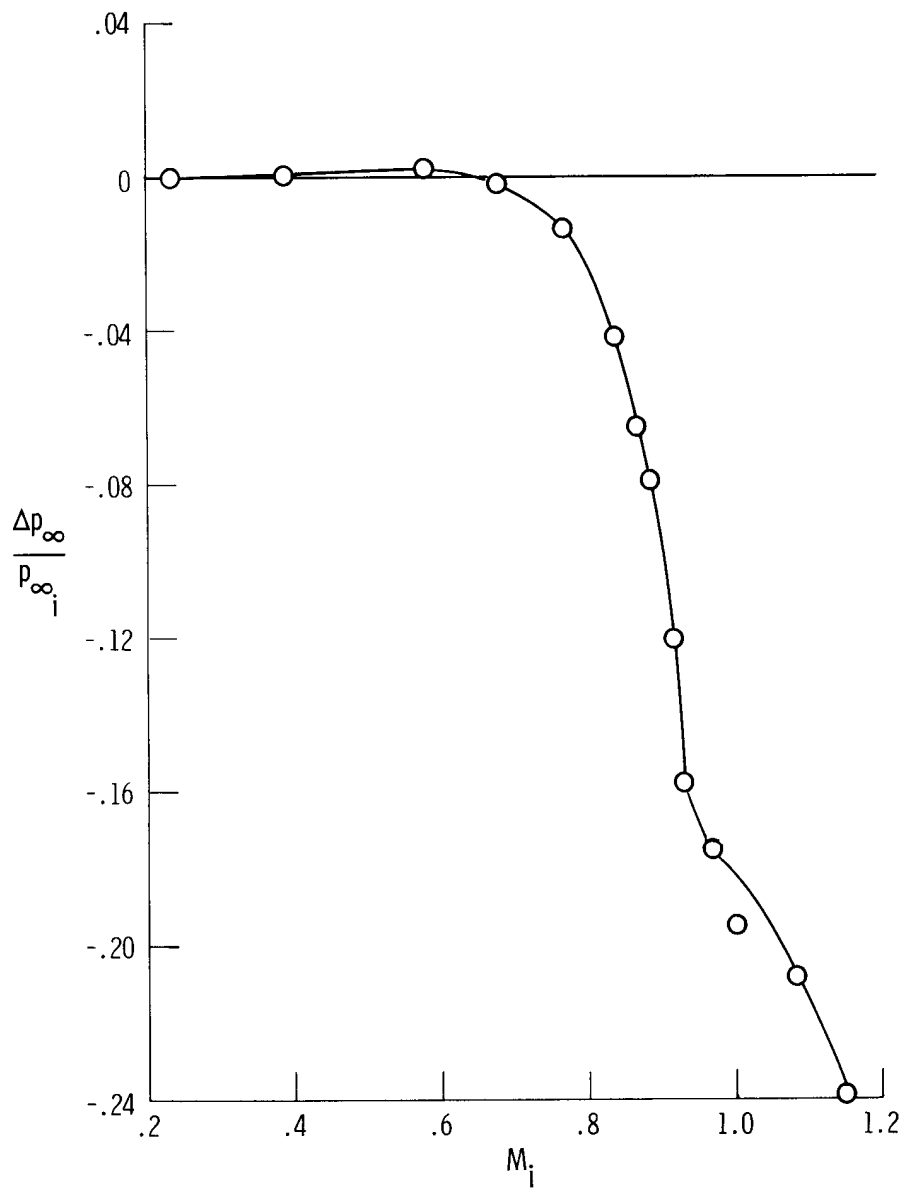
(d) $\alpha = 8^\circ$.

Figure 23. Continued.



(e) $\alpha = 12^\circ$.

Figure 23. Continued.



(f) $\alpha = 16^\circ$.

Figure 23. Concluded.

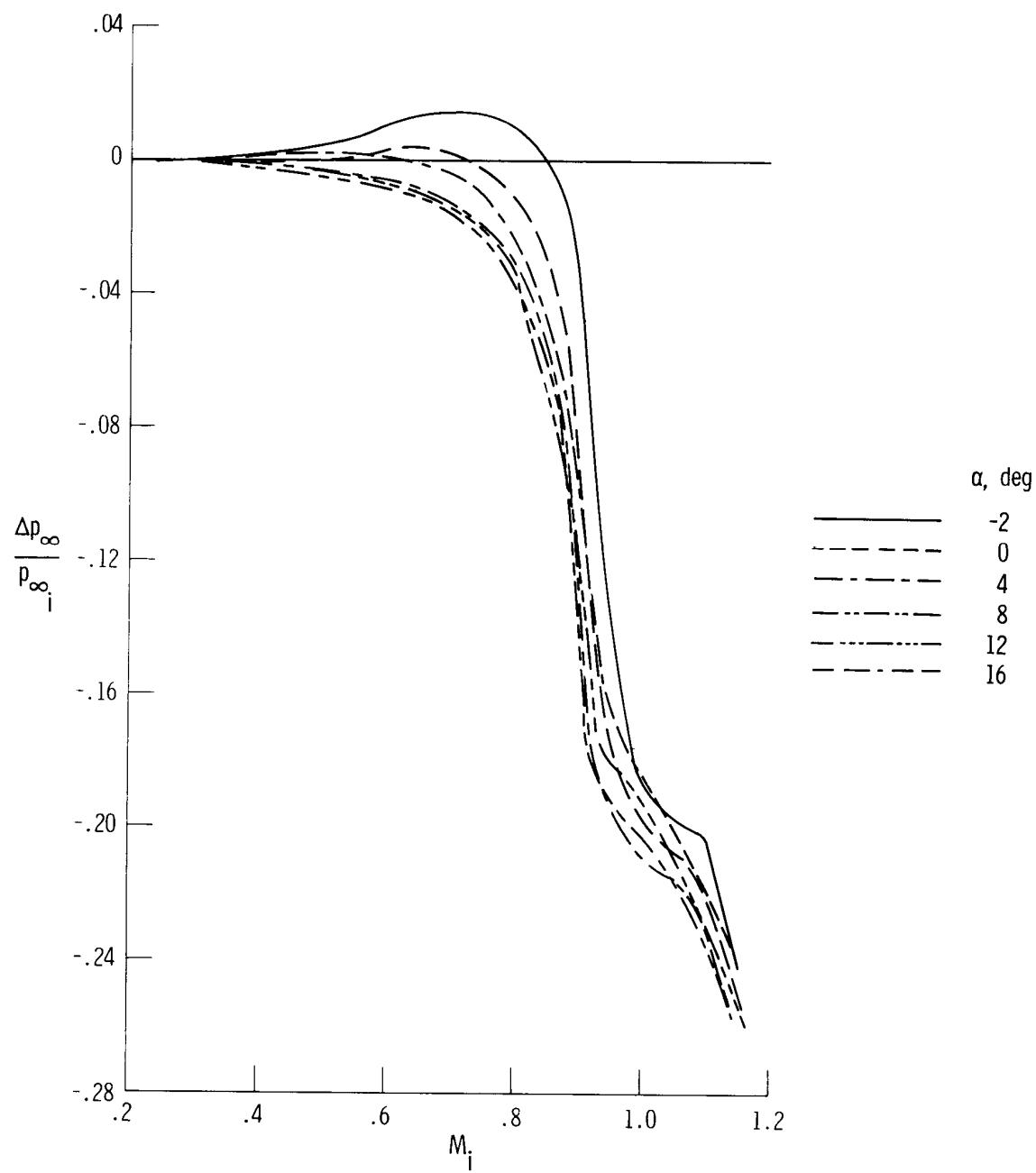
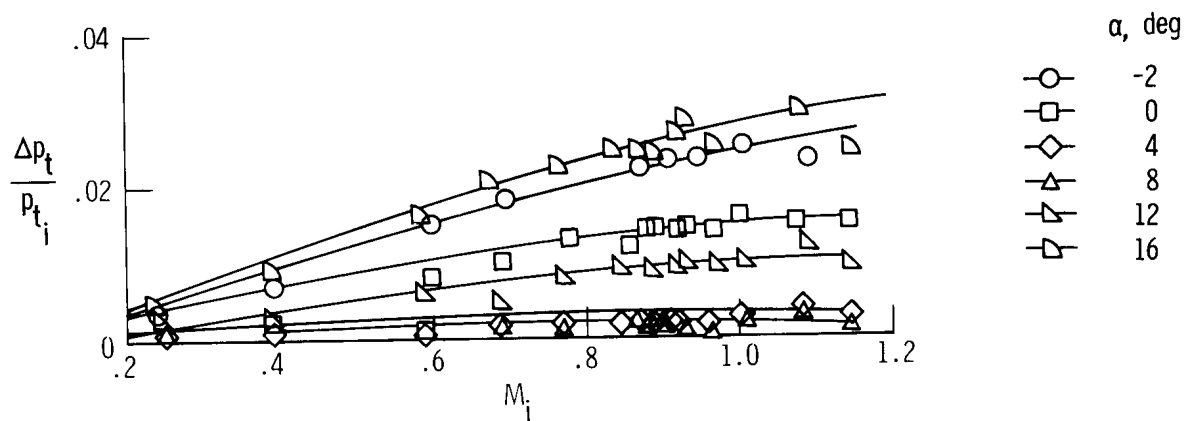
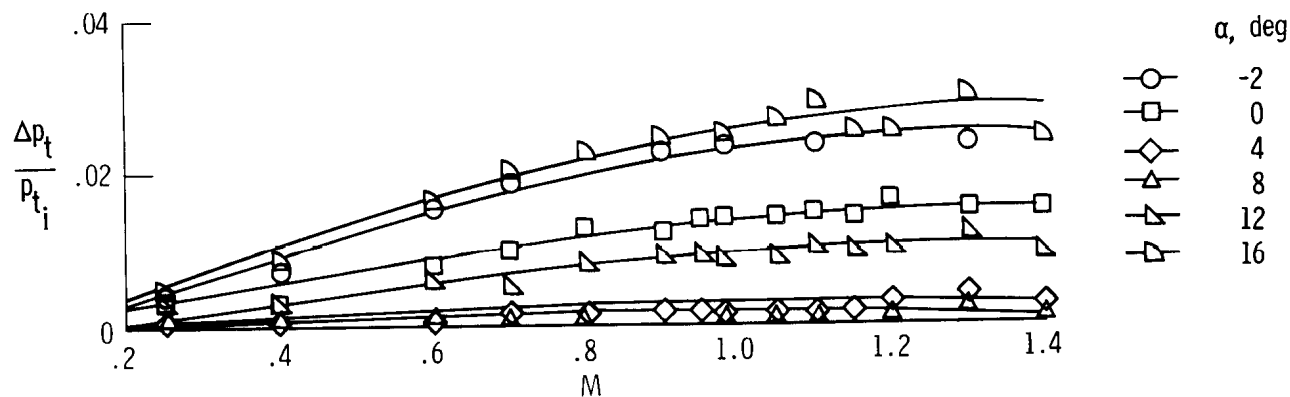


Figure 24. Comparison of figure 23 curves.



(a) Method I.



(b) Method II.

Figure 25. Stagnation pressure correction curves for data reduction methods I and II
 $\beta = 0^\circ$; orifice 46 reference.

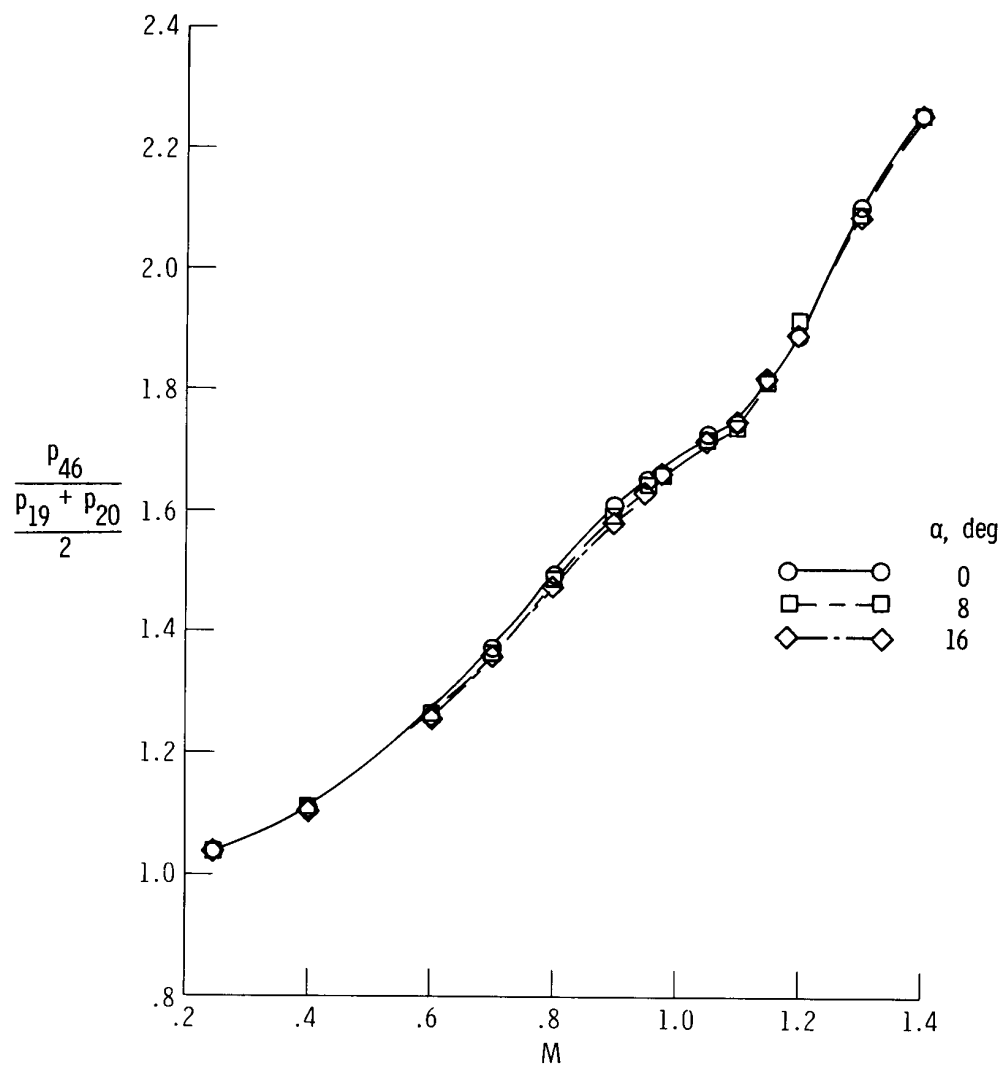
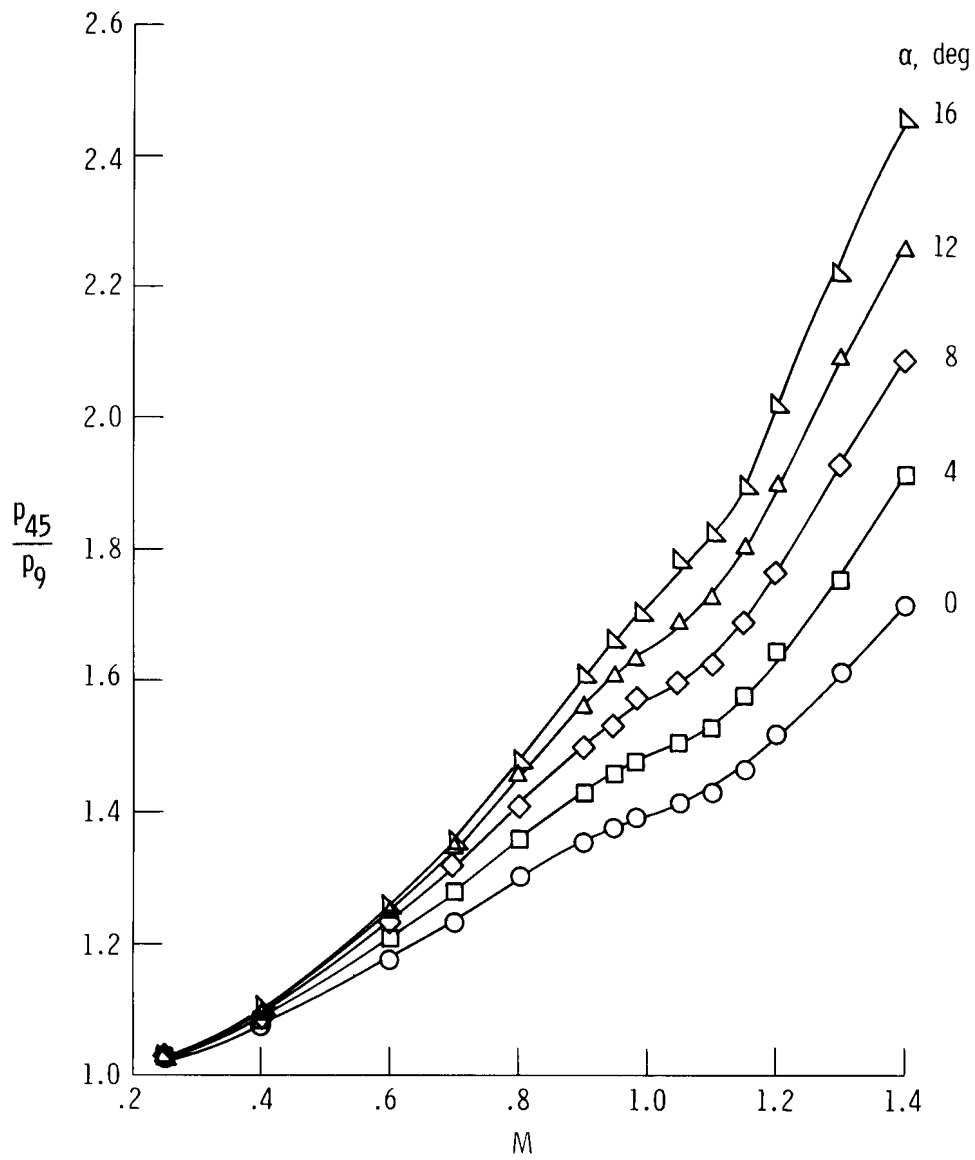
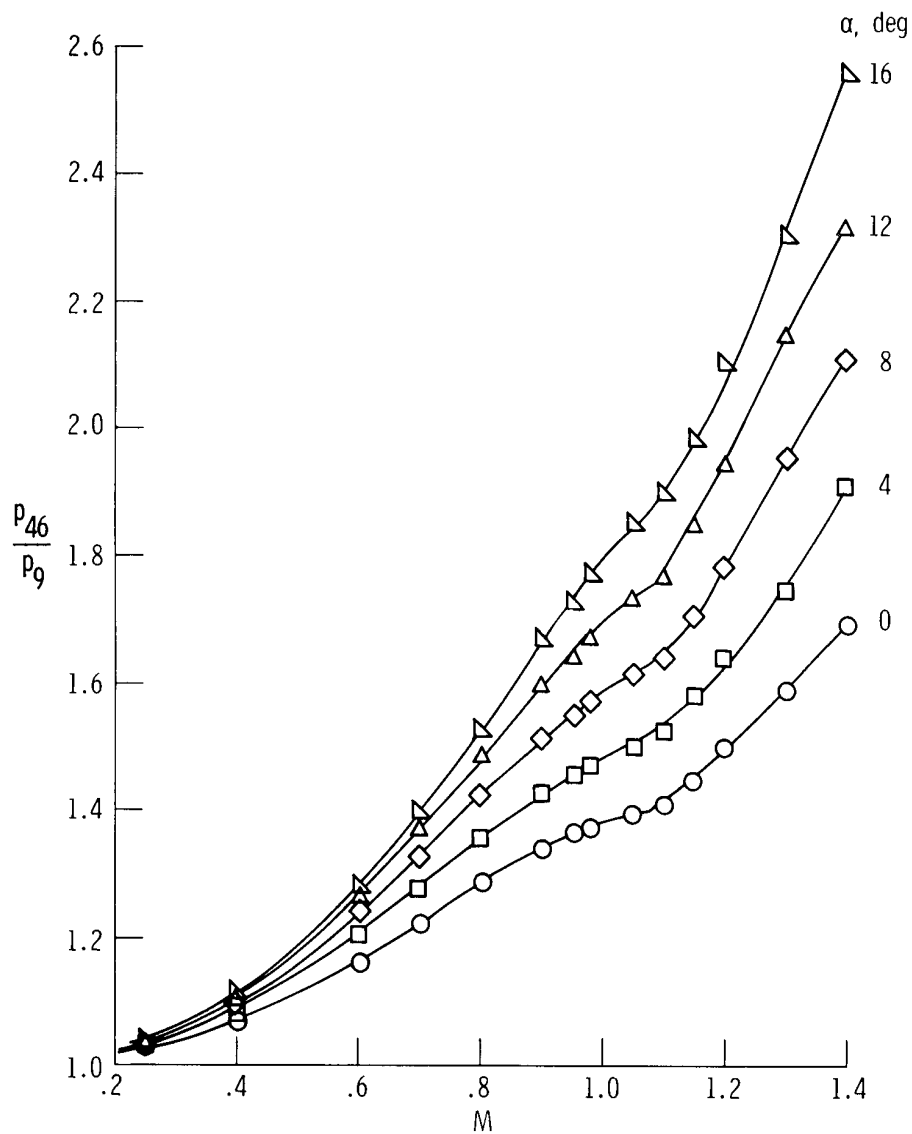


Figure 26. Calibration curve 2 for data reduction method II.
 $\beta = 0^\circ$; array A.



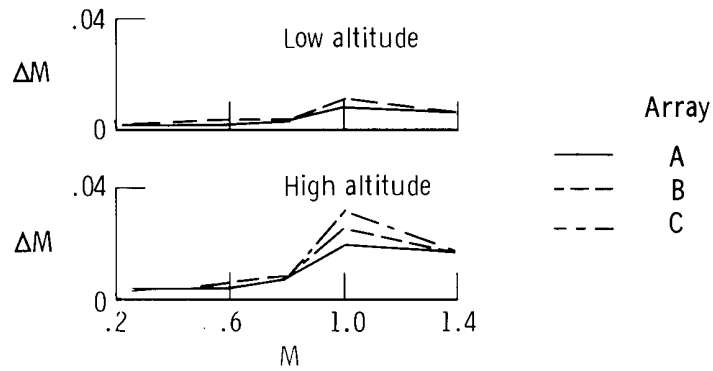
(a) Array B.

Figure 27. Calibration curve 2 for data reduction method II. $\beta = 0^\circ$.

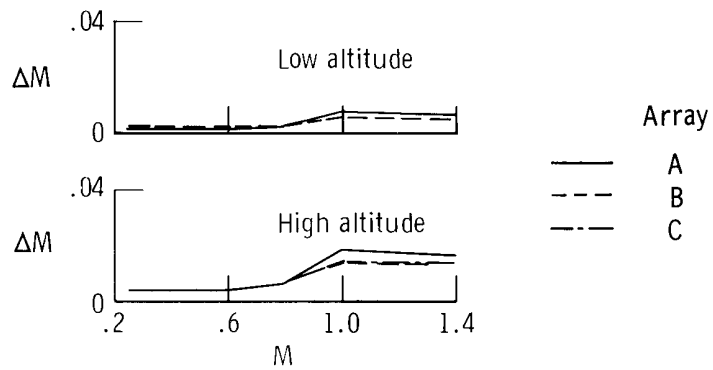


(b) Array C.

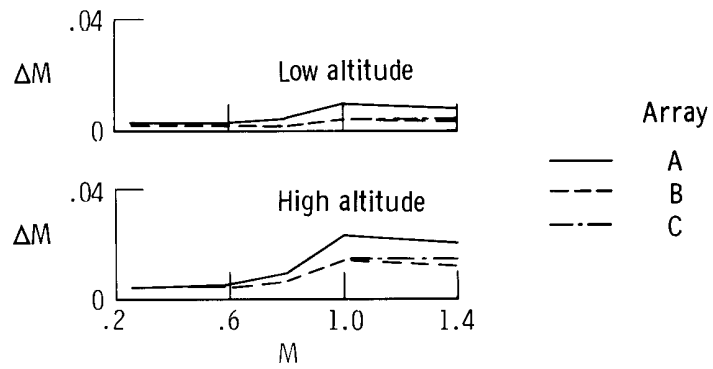
Figure 27. Concluded.



(a) $\alpha = 0^\circ$.

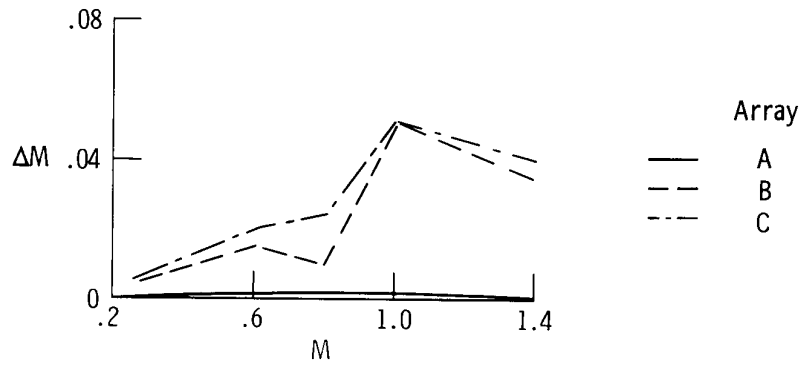


(b) $\alpha = 8^\circ$.

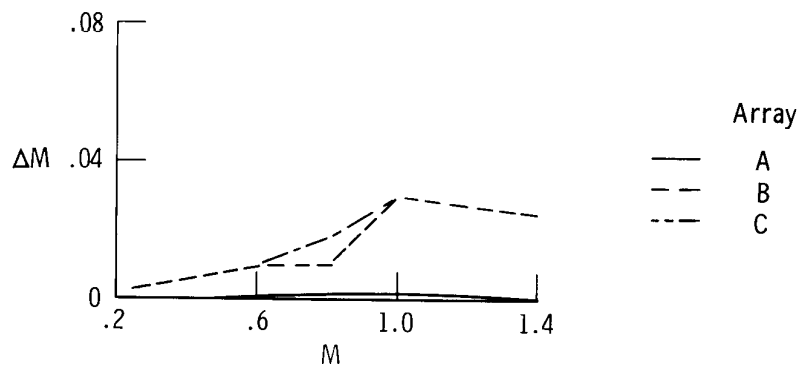


(c) $\alpha = 16^\circ$.

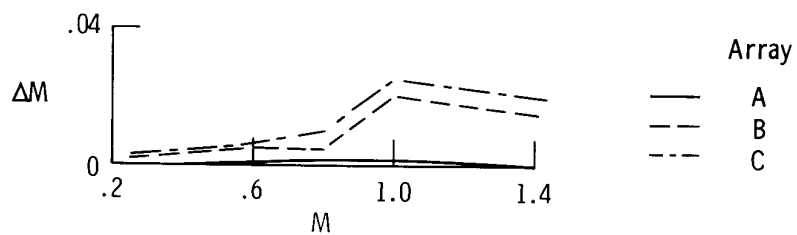
Figure 28. Errors in Mach number due to an instrumentation error of ± 0.005 kPa. Signs of errors selected to maximize error in Mach number.



(a) $\alpha = 0^\circ$.

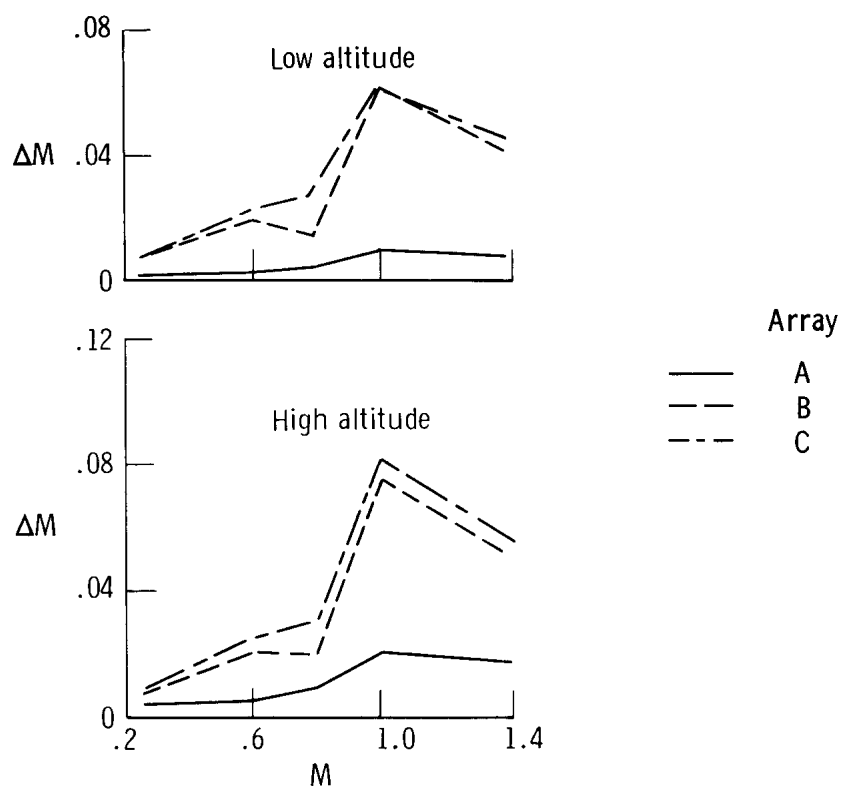


(b) $\alpha = 8^\circ$.

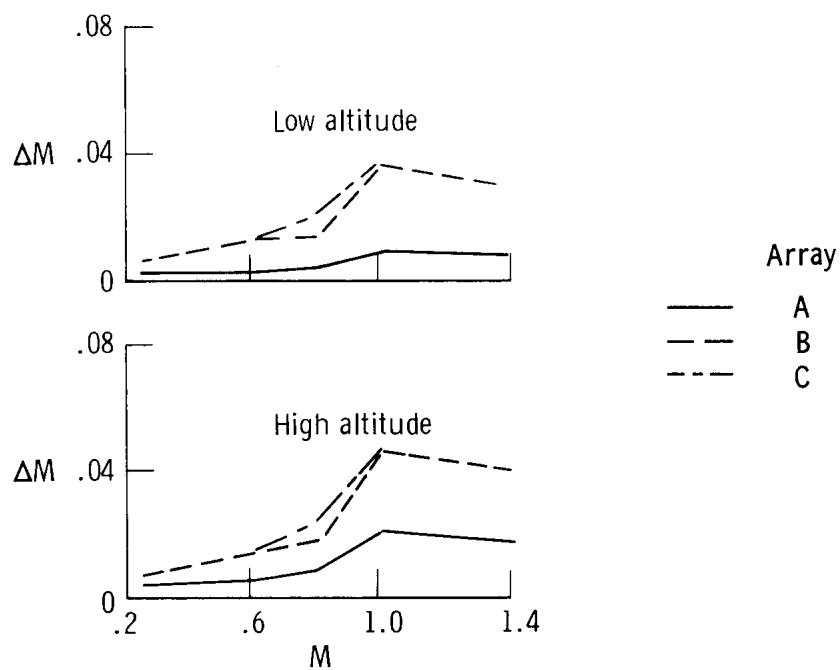


(c) $\alpha = 16^\circ$.

Figure 29. Errors in Mach number due to an angle of attack error of 1° .

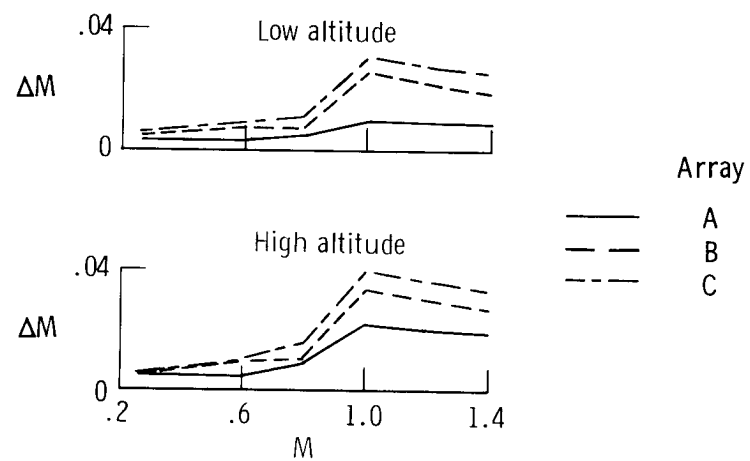


(a) $\alpha = 0^\circ$.



(b) $\alpha = 8^\circ$.

Figure 30. Total Mach number errors.



(c) $\alpha = 16^\circ$.

Figure 30. Concluded.

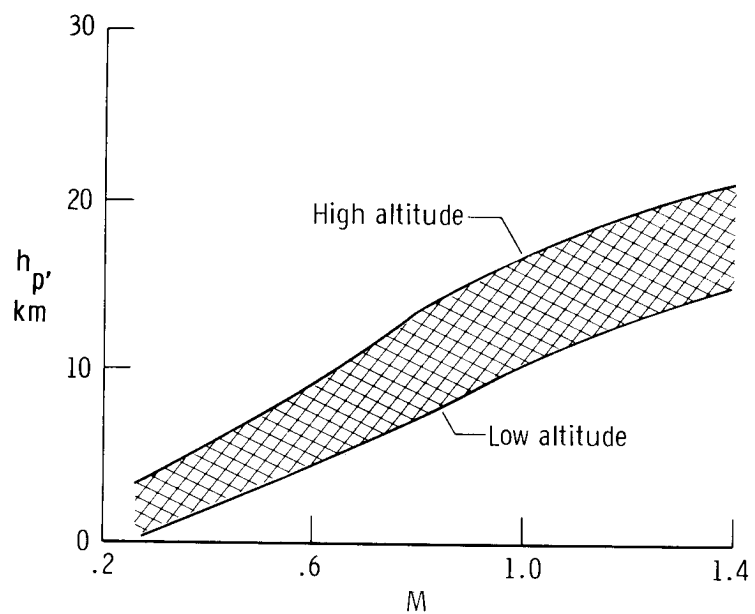


Figure 31. Tentative shuttle trajectory profiles on entry.

1. Report No. NASA TP-1643		2. Government Accession No.		3. Recipient's Catalog No.	
4. Title and Subtitle USE OF NOSE CAP AND FUSELAGE PRESSURE ORIFICES FOR DETERMINATION OF AIR DATA FOR SPACE SHUTTLE ORBITER BELOW SUPERSONIC SPEEDS				5. Report Date September 1980	
				6. Performing Organization Code	
7. Author(s) Terry J. Larson and Paul M. Siemers III				8. Performing Organization Report No. H-1096	
9. Performing Organization Name and Address NASA Dryden Flight Research Center P.O Box 273 Edwards, California 93523				10. Work Unit No. 506-51-34	
				11. Contract or Grant No.	
				13. Type of Report and Period Covered Technical Paper	
12. Sponsoring Agency Name and Address National Aeronautics and Space Administration Washington, D.C. 20546				14. Sponsoring Agency Code	
15. Supplementary Notes Terry J. Larson: Dryden Flight Research Center. Paul M. Siemers III: NASA Langley Research Center, Hampton, Virginia.					
16. Abstract <p>Wind tunnel pressure measurements were acquired from orifices on a 0.1 scale forebody model of the space shuttle orbiter that were arranged in a preliminary configuration of the shuttle entry air data system (SEADS). Pressures from those and auxiliary orifices were evaluated for their ability to provide air data at subsonic and transonic speeds. The orifices were on the vehicle's nose cap and on the sides of the forebody forward of the cabin. The investigation covered a Mach number range of 0.25 to 1.40 and an angle of attack range from -4° to 18°.</p> <p>The study shows that an air data system consisting of nose cap and forebody fuselage orifices constitutes a complete and accurate air data system at subsonic and transonic speeds. For Mach numbers less than 0.80, the data indicate that orifices confined to the nose cap could be used as a complete and accurate air data system.</p> <p>The study also suggests that air data systems that use only flush pressure orifices could be used to determine basic air data on other aircraft at subsonic and transonic speeds.</p>					
17. Key Words (Suggested by Author(s)) Air data Airspeed and altitude measurements Flow angularity measurements				18. Distribution Statement Unclassified - Unlimited STAR category 06	
19. Security Classif. (of this report) Unclassified		20. Security Classif. (of this page) Unclassified		21. No. of Pages 129	
				22. Price* A07	

*For sale by the National Technical Information Service, Springfield, Virginia 22161